October 2013

Hurricane Surge Risk Reduction For Galveston Bay

MSc. Thesis
by
K.J. Stoeten

Royal HaskoningDHV
Enhancing Society Together

TU Delft

Iv-Groep

Hurricane Surge Risk Reduction For Galveston Bay

MSc Thesis

by

Kasper J. Stoeten

Faculty of Civil Engineering and Geosciences

Hydraulic Engineering

In collaboration with:

Graduation Committee:

Prof.dr.ir. S.N. Jonkman, Delft University of Technology

Prof.dr. S. Brody, Texas A&M University

Dr.ir. R.J. Labeur, Delft University of Technology

Dr.ir. M. van Ledden, Royal HaskoningDHV

Ir. A. Willems, Iv-Groep

I Preface

This thesis is presented in partial fulfilment of the requirements for the degree of MSc. in Hydraulic Engineering and has been completed at the Delft University of Technology. This report covers the development and preliminary application of a rapid-scan method to assess hurricane surge probability within the Galveston Bay, Texas. This study has been performed in collaboration with Iv-Infra and Royal HaskoningDHV.

I would like to express sincere gratitude to the members of my graduation committee and in particular to my daily supervisors Arno Willems and Mathijs van Ledden. Their kind guidance and assistance proved invaluable. Furthermore, I would like extend my thanks to my colleagues at Iv-Infra and Royal HaskoningDHV. Finally yet importantly, I would like to thank those who contributed to my internship at Texas A&M University. It is with great pleasure that I look back at my internship, which would not have been possible without the opportunities granted.

Kasper Stoeten

Delft, October 2013

II Abstract

More than five years after Hurricane Ike devastated the Galveston Bay Area, the most critical challenge remains; reducing flood vulnerability. In response to Hurricane Ike's disastrous impact, several structural flood risk reduction strategies have been proposed. Some advocating local solutions, others advocating system-wide coastal barriers. The relationship between storm surge within Galveston Bay and storm surge at the open coast may profoundly affect the performance of these local or system-wide solutions. Limited understanding of bay behavior under hurricane forcing limits the ability to select the optimal solution.

To assess the bay behavior under hurricane forcing, a probabilistic behavior-oriented storm surge model has been developed. The model couples meteorological forcing with hydrodynamic response and provides a first-estimate of storm surge within simplified semi-enclosed bays. A large suite of synthetic parametric hurricane wind fields provides input for the storm surge model. Storm surge at the open coast is obtained by solving the one-dimensional depth integrated shallow water equations. Storm surge within the semi-enclosed bay relies on a parametric relation between wind set-up and storm surge at the open-coast. Hindcasts of historic storms show that the model provides a reasonable estimate of storm surge within the bay, with a typical error of ± 0.5 meter.

Storm surge within Galveston Bay is a delicate balance between inflow and local wind set-up. Simulations show that local wind set-up contributes up to 50% to the surge within the bay, depending on landfall location and storm intensity. Results indicate that the 1/1,000 yr^{-1} surge at the northern bay end exceeds the 1/1,000 yr^{-1} surge at the open coast by about 0.5 meter. The 1/10,000 yr^{-1} surge at the northern bay end exceeds the 1/10,000 yr^{-1} surge at the open coast by about 1.0 meter. Although significant, obtained results do not indicate that the difference in surge elevation plays a crucial role in strategy selection.

To assess the benefits of a coastal spine, ship channel gate or Texas City levee upgrade, a preliminary flood risk assessment has been performed. For each strategy, the benefits in terms of risk reduction are estimated by relating simulated surge probabilities to residential exposure, industrial exposure and surface elevation. Comparing the estimated investment cost and benefits of each strategy allows an informed monetary comparison of the individual risk reduction strategies.

The flood risk assessment confirms that the Galveston Bay Area is highly vulnerable to storm surge. Existing regulations solely require industrial complexes to protect up to the 100-year flood level. Consequently, residential exposure significantly exceeds industrial exposure for return periods of up to once per 100 years. Industrial exposure outweighs residential exposure for less frequent events. Considerable benefits can be achieved by protecting both residential property and industrial assets.

Preliminary results indicate that a coastal spine significantly reduces storm surge within the bay and yields the highest benefits in terms of risk reduction. The ship channel gate and the Texas City Levee Upgrade yield a similar rate of return but achieve considerably less benefits.

III Table of Contents

Chapter 1. Introduction

Galveston Bay is a large semi-enclosed estuary located on the Upper Texas Coast in the United States of America (Appendix A). Galveston Bay is one of the most important drivers of the economy of the Greater Houston Metropolitan. Among its most valuable industrial assets are the second largest port in the United States and several large refineries, all located within close proximity of the Bay. The Greater Houston Metropolitan is one of the fastest growing metropolitan areas in the United States. The population density on the west end of Galveston Bay is relatively high and increasing at an above average rate (Census, 2010). Over 900.000 citizens reside between sea level and the 2-meter elevation contour (Schiller, 2010).

The abundance of economic activities within close proximity of the bay shore combined with strong population growth, local geography and climate hints at a high vulnerability to coastal flooding. On average, one major hurricane makes landfall on the upper Texas shore every 15 years (Parisi & Lund, 2008). According to SurgeDAT, a storm surge database (Needham & Keim, 2012), the Upper Texas Coast is among the most surge prone areas in the United States. Historic events indicate that the Port of Houston may be subject to higher storm surges than Galveston Island. Hurricane Ike (2008) resulted in an estimated $29.4 billion dollars in damage (Perry, et al., 2008).

In the aftermath of Hurricane Ike several flood risk reduction strategies were proposed. The proposed strategies range from localized solutions to large-scale engineering projects. Among the proposed strategies are the Ike Dike (Merrell, 2010) and the Centennial Gate (SSPEED, 2011). To date it is unknown whether a localized or a system wide strategy offers the greatest benefits, or highest rate of return.

One of the most important parameters is the recurrence interval of surge within a Bay. Existing studies (Resio et al., 2009; Irish et al., 2011) often focus at the open coast. Few studies investigate storm surge within semi-enclosed bays, although the relationship between surge within the bay and surge at the open coast may profoundly affect selection of the optimal risk reduction strategy.

Weisberg and Zheng (2006) investigated the sensitivity of storm surge to landfall location for Tampa Bay. They conclude that the worst-case scenario encompasses maximum winds at the mouth of the estuary. Crawford (1979) applied a storm surge model to coastal Southern Louisiana and found a distinct track dependent “sloshing” behavior in Lake Pontchartrain. Rego and Li (2010) simulated the “sloshing” behavior of Galveston Bay during hurricane Ike and identified a “fast-reversing cross bay gradient” with a gradient of about 0.08m/km that reversed in just under 5 hours. Valle-Levinson et al. (2002) and Shen et al. (2006) both describe the response of the Chesapeake Bay to hurricane forcing. They find that surge within the Chesapeake Bay is a superposition of open-coast surge propagating into the bay, and local wind forcing. Most of the abovementioned authors solely treat bay behavior while some indicate additional research is required to include the probability of occurrence.

1.1 Problem Statement

The past decade's most of the US flood hazard policies focused on prediction and mediating effects once they occurred, which suggests that flooding is accepted (Bijker, 2007). Recent developments within the Galveston Bay Area (Merrell, 2010; SSPEED, 2011) indicate that a policy change towards prevention is gaining momentum.

While some research has examined individual risk reduction strategies within Galveston Bay, there is little to no system wide review of the available strategies. Often, the approach focusses on one particular solution motivated by the personal preferences of the initiators. The relationship between surge return periods within semi-enclosed bays and surge return periods at the open coast may profoundly affect the selection of the optimal risk reduction strategy. Limited understanding of the combination of storm parameters, risk reduction strategies and surge return periods within the bay and at the open coast limits the ability to select the optimal solution.

This study utilizes an integral and system wide approach to derive the preferred flood risk reduction strategy for Galveston Bay. Its goal is to (i) gain insight into the behavior of Galveston Bay under hurricane conditions, (ii) obtain an order-of-magnitude estimate of return periods of surge at the open coast and within the bay and (iii) derive the order-of-magnitude dependent optimal risk reduction strategy for Galveston Bay.

1.2 Research Question

The central question of this study is;

<u>How can the performance of flood risk reduction strategies for Galveston Bay be assessed and to what degree does hydrodynamic bay behavior impact selection of the optimal solution?</u>

With the above question in mind the following objectives are addressed;

Objective 1: To develop a simplified model and subsequently assess flood probabilities at the open coast and within the bay.

Objective 2: To determine the optimal strategy by establishing a preliminary cost and benefit analysis of the flood risk reduction strategies.

1.3 Methodology

Hurricane storm surge within semi-enclosed estuary systems is hard to comprehend because of the complex interaction between inflow, overflow, wind set-up and wave set-up. In order to obtain global understanding of the system we simplify a complex system into a system that solely relies on the utmost important processes.

A statistical analysis of local storm climatology provides the required range of storm parameters. The results from the statistical analysis are used to construct a large suite of synthetic storms that might happen in the future. Subsequent application of the suite of storms to the storm surge model provides a range of potential storm surge events (Figure 1-1). A statistical analysis of the simulated storm surge events provides the required return period estimates of storm surge within a semi-enclosed bay.

Hindcasting historical storms allows validation of the storm surge model. Altering system parameters including depth, inlet surface area and initial water levels allows one to assess the influence of human intervention on surge return periods. The proposed methodology allows an objective assessment of the joint probability of all parameters involved.

A GIS-based flood risk analysis provides the estimated benefits of each risk reduction strategy. The benefits of a flood risk reduction project are equal to the damages avoided compared to doing nothing. The procedure, outlined in Figure 1-1, is initiated for each strategy. The probability of storm surge within the bay and at the open coast is obtained by analyzing the suite of simulated surge events. The consequence of flooding relies on the assets and inundation depth within the area of interest. The damage assessment deals with quantitative, direct tangible damage. Intangible and indirect damages are partially included in the analysis.

The relation between expected cost and the expected benefits of each risk reduction strategy provides the preferred solution given a desired level of risk reduction, or available funding.

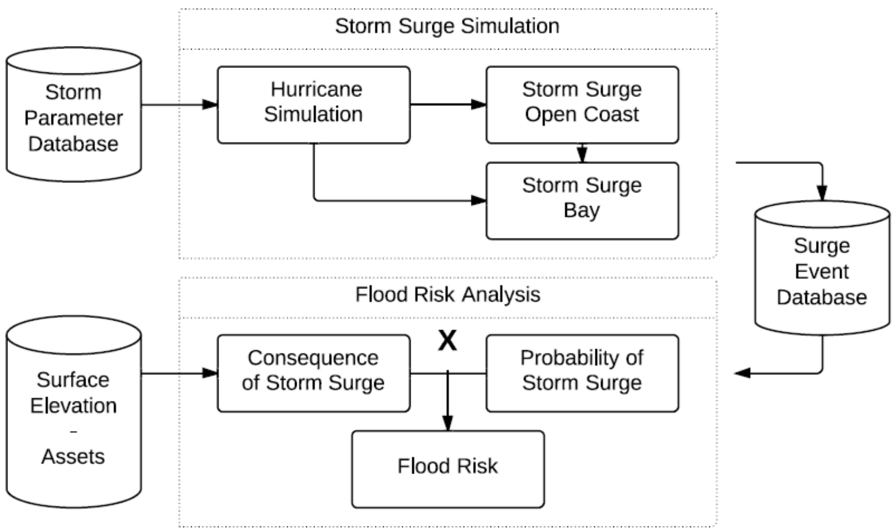

Figure 1-1 – Methodology.

1.4 Structure of the Report

Chapter 2 presents an introduction to Galveston Bay. A literature review and summary of historical observations provide insight in observed bay behavior during extreme events. Chapter 3 covers the development and validation of a one-dimensional storm surge model. Chapter 4 presents a deterministic application of the storm surge model. A sensitivity analysis provides insight into errors caused by parametric assumptions. A probabilistic application of the storm surge model is treated in Chapter 5. Chapter 6 encompasses a cost benefit analysis of selected risk reduction strategies and Chapter 7 offers a brief reflection on the methodological choices summarizes the main conclusions and gives a few recommendations.

Unless noted otherwise vertical reference with respect to North American Vertical Datum 1988 (NAVD88). Mean Sea Level (MSL) is equal to NAVD88 + 0.5 feet. The conversion rate from Euro to US Dollar equals 1.35. Prices in $US 2010 values.

Chapter 2. System Description of Galveston Bay

In this chapter, the Galveston Bay Area is described briefly. Section 2.1 introduces Galveston Bay. Section 2.2 presents an introduction to bay behavior under ordinary conditions. Section 2.3 gives a short analysis of hurricane climatology. In Section 2.4 we analyze bay behavior during three historic hurricanes. A quick introduction into bay behavior under hurricane forcing is available in Section 2.5. The wave climate is treated in Section 2.6. Section 2.7 concludes Chapter 2.

2.1 Location and Topography

Galveston Bay is a large natural semi-enclosed estuary system located along the Upper Texas Coast (Figure 2-1). The Bay is a classic example of a drowned river valley that gradually flooded when sea levels rose near the end of the last ice age. The Bay's large and irregular shaped basin has a surface area of about 1399 square kilometers (Moretzsohn, et al., 2002). The estimated length of the bay-shoreline is 374 kilometers and the average depth is only 3 meter (Phillips, 2004; Figure 2-3). The relatively flat deltaic alluvial plain surrounding Galveston Bay does not offer much protection against strong winds.

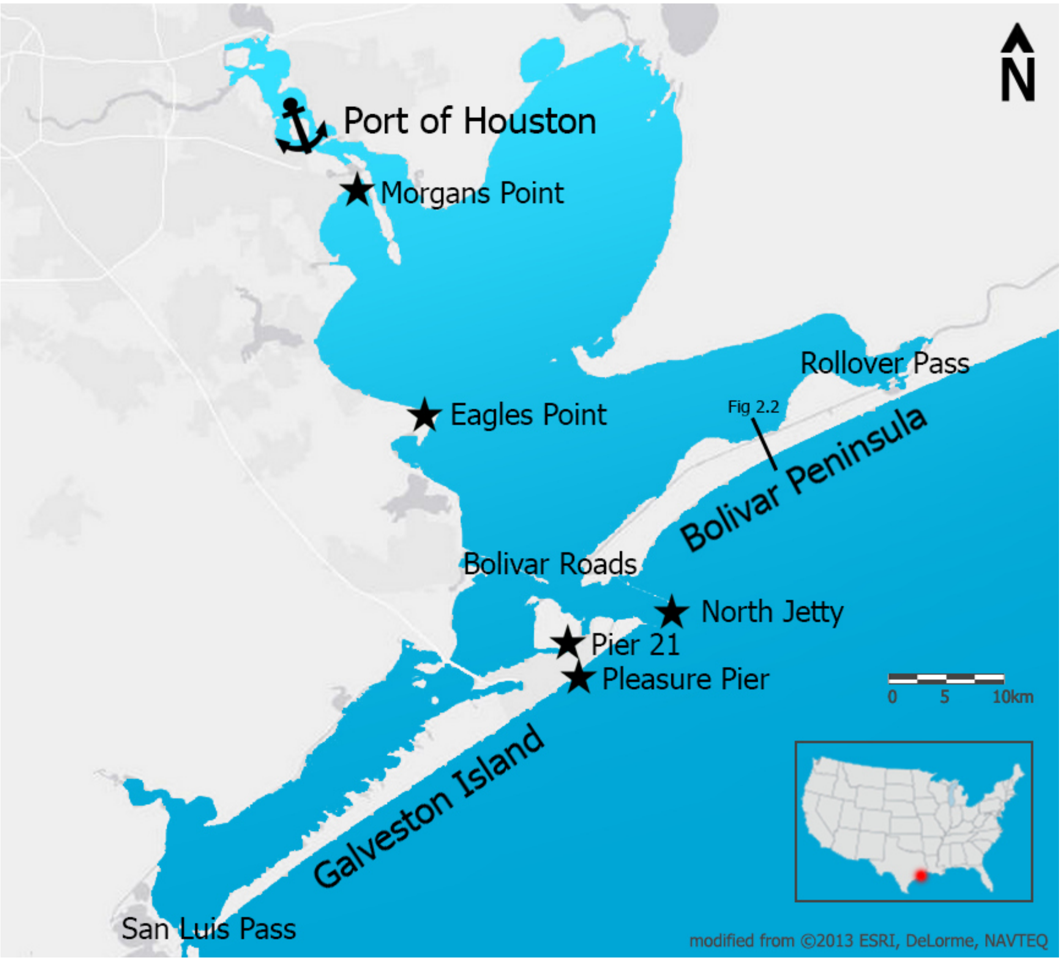

Figure 2-1 - Map of Galveston Bay. Modified from ESRI, DeLorme, NAVTEQ (2013).

Galveston Bay is separated from the Gulf of Mexico by Galveston Island and Bolivar Peninsula. Both barrier islands are relatively low (1 to 3 meter above MSL, Figure 2-2), narrow (1 to 2 km) and straight (Figure 2-1, Figure 2-3). The Gulf near Galveston is very shallow with a relatively uniform continental shelf extending approximately 150 kilometers (50 meter depth contour) into the Gulf of Mexico. The average slope of the coastal profile is about 1/2000.

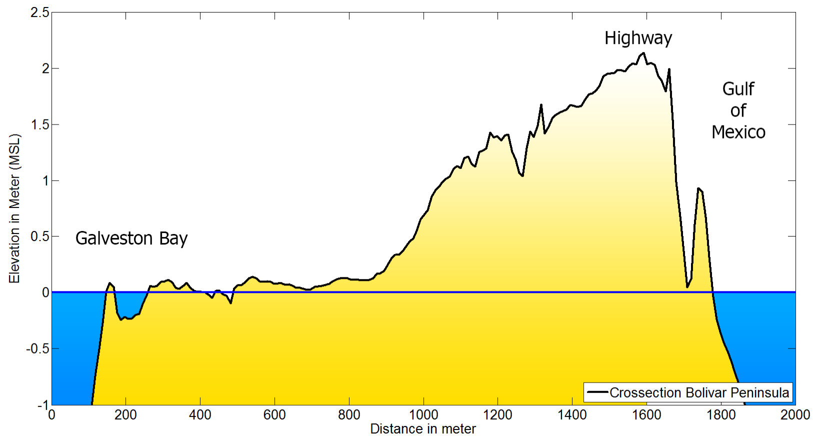

Figure 2-2 - Cross-section of Bolivar Peninsula (location denoted in Figure 2-1).

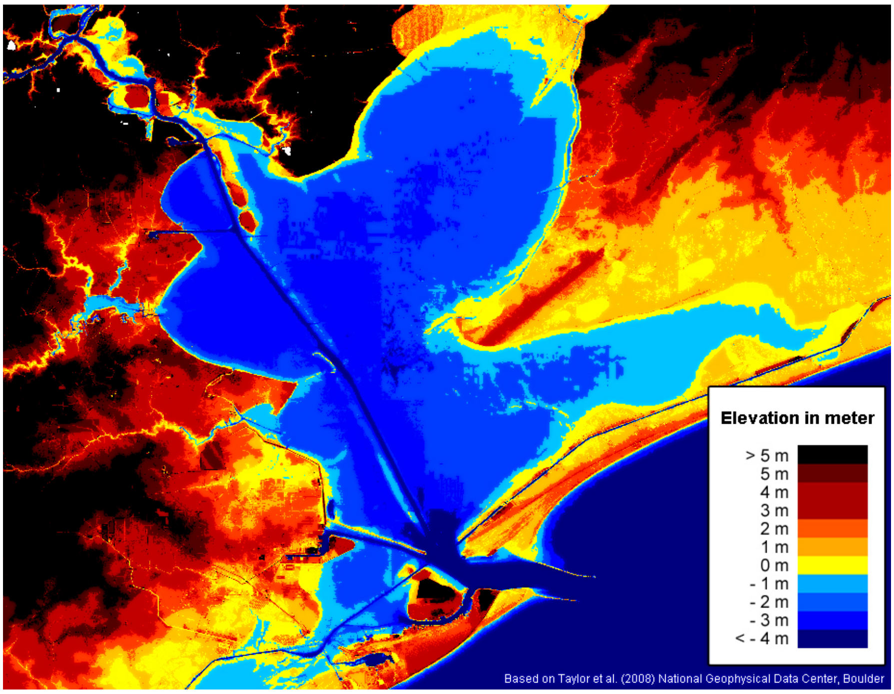

Figure 2-3 – Digital Elevation Model (NAVD88) of Galveston Bay based on Taylor et.al. (2008).

2.2 System Behavior

Galveston Bay is a micro-tidal wind dominated estuary system with an average depth of 3 meter (NGDC, 2007). Tidal exchange with the Gulf of Mexico occurs through three tidal inlets (Table 2-1); Bolivar Roads, San Luis Pass and Rollover Pass. Bolivar Roads and San Luis Pass are responsible for respectively 80% and 20% of the tidal exchange (Lester & Gonzales, 2002). The total tidal prism of Galveston Bay is about 3.5×10^8 cubic meters. Flow velocities within the channels remain below 2 ms^{-1} under ordinary conditions (NOAA, 2013a).

Table 2-1 – Galveston Bay Inlets (NGDC, 2007).

Inlet	**Width**	**Average Depth**	**Tidal Prism %**
Bolivar Roads	2800 meter	9 meter	80%
San Luis Pass	900 meter	2 meter	20%
Rollover Pass	60 meter	1.5 meter	negligible

Freshwater inflow into Galveston Bay exhibits episodic behavior and varies strongly with time. The yearly-averaged inflow is 430 m^3s^{-1} (TWDB, 2010) while individual events may be up to 20 times as large (Ruijs, 2011). The relative influence of inflow is small when compared to the astronomical tide.

Tides at the open coast are predominantly semi-diurnal and the mean tidal range measures approximately 0.6 meter. Observed phase lag between the bay and Gulf of Mexico ranges between 4 and 6 hours. The largest lag is observed near the northern end of the bay. Table 2-2 presents a list of tidal datum for the Galveston North Jetty. Permanent tide-gauges are available near the North Jetty, Morgan's point, Pier 21, Pleasure Pier and Eagle Point (Figure 2-1). Harmonic constituents are listed in Appendix C-3. The tidal ratio between the bay and the Gulf of Mexico is approximately 0.6 (Figure 2-4). The average residence time of water is 40 days (Nichols, 1989).

Table 2-2 – Datum at the Galveston North Jetty, epoch 1983 - 2001 (NOAA, 2013a).

Datum	**Value**	**Description**
MSL	NAVD88 + 0.15 meter	Mean Sea Level
MN	0.353 meter	Mean Range of tide
GT	0.51 meter	Great Diurnal range of Tide
HAT	MSL + 0.242 meter	Highest Astronomical Tide
LAT	MSL – 0.9 meter	Lowest Astronomical Tide

The seasonal range on the Texas Coast is about 0.2 – 0.3 meter (Kraus, 2007), which is similar to the tidal range. Seasonal lows occur around August and December, while seasonal highs occur around May and October.

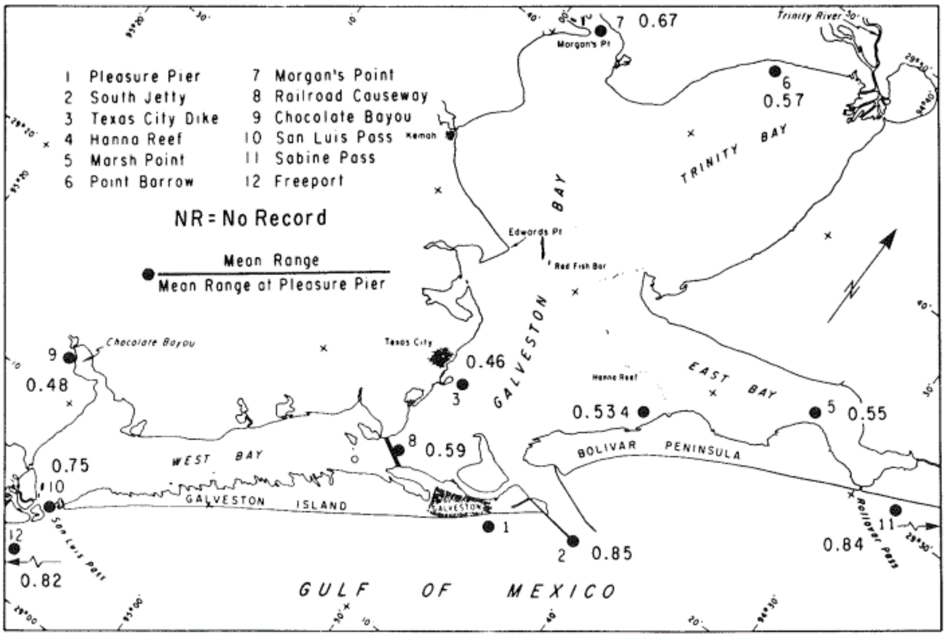

Figure 2-4 - Galveston Bay tidal range ratio distribution. Annual average 1974. (USACE, 1981).

2.3 Hurricane Climatology

Hurricanes are tropical storm systems with a low-pressure core surrounded by a spiraling arrangement of thunderstorms. Hurricanes formation requires a warm ocean, a moist atmosphere and favorable wind patterns. In the Atlantic region, these conditions frequently occur between June 1st and November 30th. One hurricane season can produce as many as 15 storms, although few make landfall on the US continent. A spatio-temporal analysis of storm return periods by Keim and Muller (2007), Figure 2-5, indicates that the Galveston area (point 4) is subject to a hurricane landfall on average every 8 years.

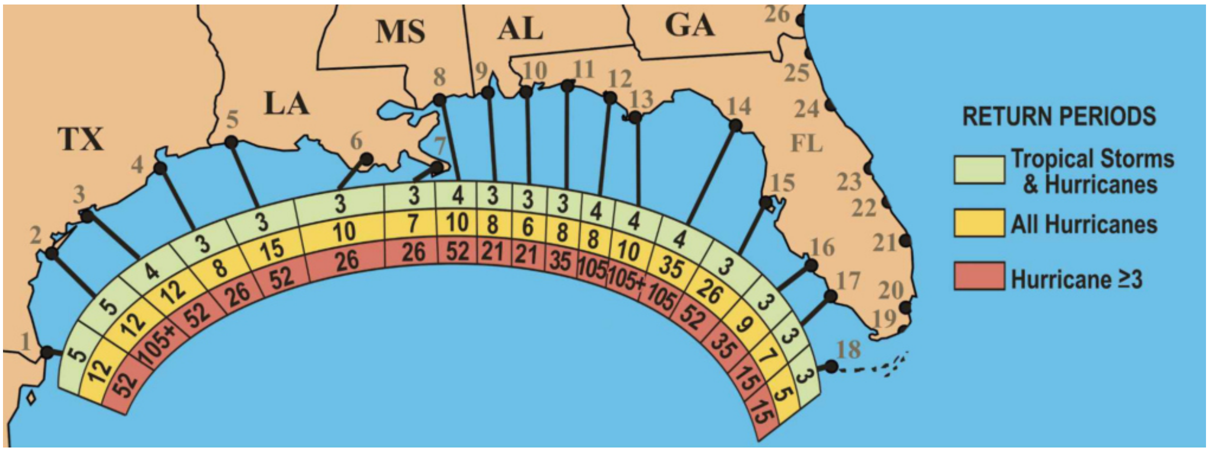

Figure 2-5 – Average return period for tropical storms, hurricanes and severe hurricanes along the US Gulf Coast source: (Keim & Muller, 2007).

On the Northern Hemisphere, hurricanes turn counter-clockwise (NOAA, 2013b). On south-facing coasts, like the Upper Texas Coast, the strongest on-land winds are found east of the eye, while locations on the opposite side experience offshore directed winds. Wind velocities in tropical cyclones can exceed velocities of over 240kmh (Smith, 1998). The theoretical upper limit of hurricane intensity, the Maximum Potential Intensity (MPI), is thought to be as low as 880 hPa (Emanuel, 1987).

Hurricanes may inflict significant damage to property, nature and may even result in loss of life. Between 1900 and 2012, 28 hurricanes made landfall within 200km from Galveston (Appendix B). The most significant hurricanes that made landfall near Galveston were the "Great Galveston Hurricane (1900), the "Galveston Hurricane" (1915) and "Ike" (2008). A recent study by Pielke et al. (2008) indicates that the present-day normalized damage of the "Great Galveston Hurricane" (1900, ~935 hPa) would amount to $US 70 billion dollar. A present-day "Galveston Hurricane" (1915, ~940 hPa) would result in $US 60 billion dollar worth of damage. The estimated 1/100 yr^{-1} landfall intensity, within a 400 km stretch of coast, is 940 hPa (Figure 2-6b).

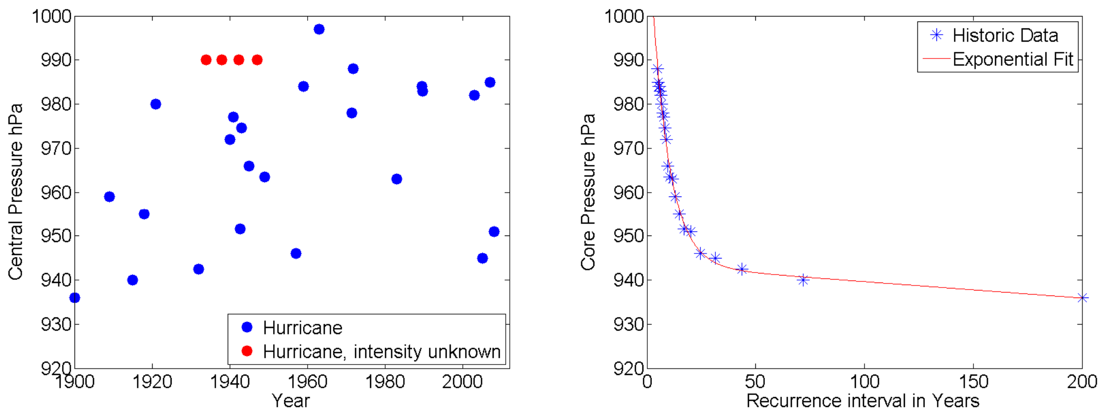

Figure 2-6 – Historic hurricanes (left) and recurrence interval of hurricane intensity (right) between 1900 and 2012 within a 200 km radius from Galveston. Data: Appendix B.

Historical hurricane records date back as far as 1527 although records prior to 1900 lack the accuracy required in storm surge modelling. Appendix B presents a statistical analysis of hurricane parameters for Galveston Bay. A comprehensive list of hurricanes that made landfall on the Upper Texas Coast is available in "Texas Hurricane History" (Roth, 2010).

2.4 Historic Observations of Hurricane Surge

In order to understand bay behavior during hurricane conditions we examine observed bay behavior during hurricanes. Water levels during Hurricane Ike (2008), hurricane Rita (2005) and hurricane Alicia (1983) are discussed in detail. Figure 2-7 presents the annual exceedence probability at the Galveston Pleasure Pier with 95% confidence intervals as estimated by NOAA (2013a). The rightmost dot indicates the number of years used (50) in the analysis.

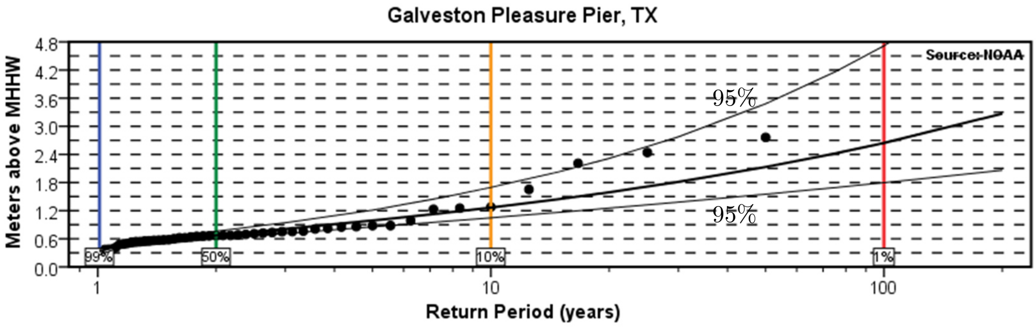

Figure 2-7 – Annual exceedence probability Galveston Pleasure Pier. Source: (NOAA, 2013a).

Table 2-3 presents an overview of observed peak surges during selected historic events. Depending on the combination of inlet length, inlet flow area, bay surface area, bay depth, barrier islands height, storm landfall location and storm intensity the surge within the semi-enclosed system may or may not exceed the surge at the open coast. Local authorities state that a northerly Six Beaufort blowing for two hours can drop water levels by as much as two feet (Gilmore & Englebretson, 1997).

Table 2-3 – Observations of storm surge within Galveston Bay.

Hurricane	**Cat**	**Landfall Location**	**Peak surge open coast**	**Peak Surge North Bay**	**Peak Surge South Bay**
Carla (1961)	5	180 km West	3 meter	4 meter	3 meter
Alicia (1983)	3	50 km West	2.5 meter	4 meter	3 meter
Ike (2008)	2	0 km	4.5 meter	4.5 meter	3.5 meter
“Surprise” (1943)	2	30 km East	unknown	-1.5 meter	-1.5 meter
Cindy (1963)	2	50 km East	0.8 meter	-1 meter	1 meter
Rita (2005)	5	120 km East	1.5 meter	1 meter	1.3 meter
Andrew (1992)	3	200 km East	-	- 1.5 meter	1.5 meter

2.4.1 Hurricane Ike (2008)

Hurricane Ike, a strong category 2 hurricane, made landfall near the city of Galveston on September 13, 2008. Observed water levels at the Galveston Pleasure Pier were about 3.0 meter MSL while 25 kilometers to the East a surge of over 4.0 meter MSL was observed. Ike's most distinct feature was its large forerunner surge resulting in significantly elevated water levels during the two prior to landfall (Kennedy, et al., 2011a). The estimated wave height during Ike was 2.0 meter. Gauges at Pier 21 and Morgan's point failed during the storm. Mean wind direction; East – South – West.

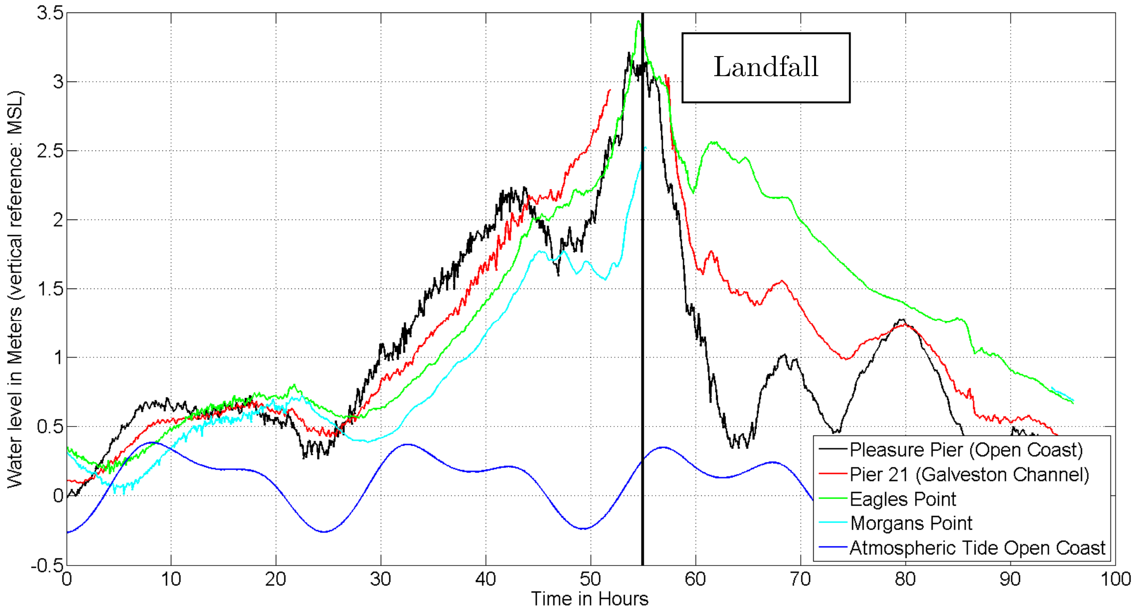

Figure 2-8 – Observed water levels during Hurricane Ike (2008). Data: (NOAA, 2013a).

2.4.2 Hurricane Rita (2005)

Hurricane Rita, a category 5 hurricane, made landfall as a category 3 hurricane about 120 kilometers east of Galveston. Hurricane Rita produced a storm surge of well over 4 meter east of its landfall location. The Galveston Pleasure Pier tide gauge reported a storm surge of approximately 1.0 meter MSL (Figure 2-9). Measurements at Eagle Point and Morgan's Point show similar excitations. Reports indicate that strong northerly winds resulted in flooding on the Bay side of Galveston Island and Bolivar Peninsula (Gilmore & Englebretson, 1997). Mean wind direction; East – North – West

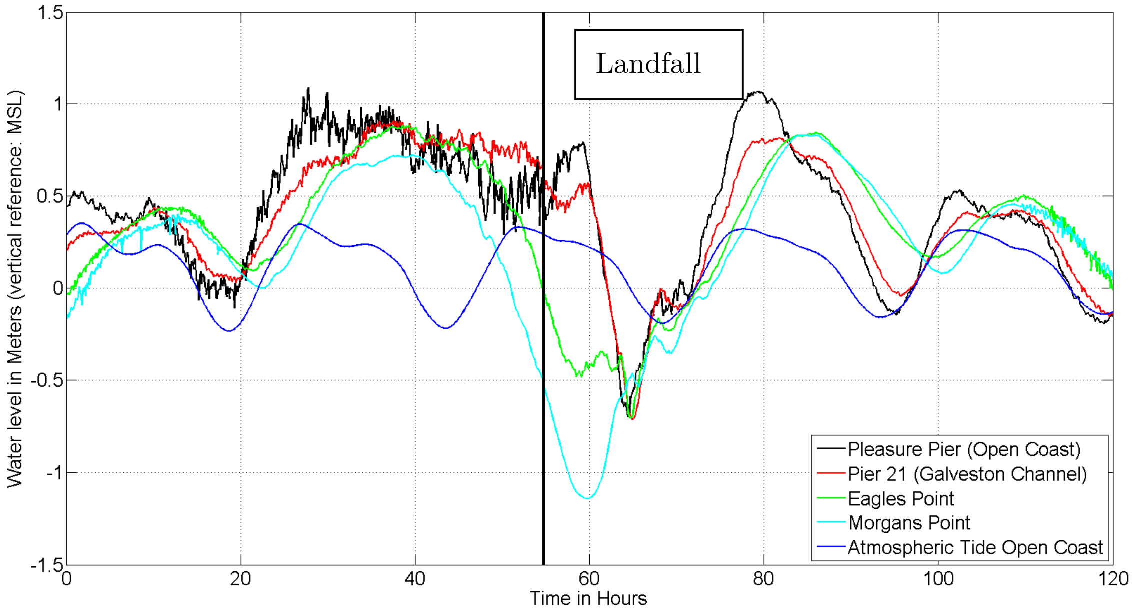

Figure 2-9 – Observed water levels during Hurricane Rita (2005). Data: (NOAA, 2013a).

2.4.3 Hurricane Alicia (1983)

Hurricane Alicia, a weak category 3 hurricane, made landfall about 50 kilometers west of Galveston. Alicia's sustained wind velocity measured about 45 ms^{-1}. Storm surge varied between 2 and 3 meter MSL at the open coast. (Figure 2-10). The Galveston Pleasure Pier recorded a surge of almost 2.5 meter above MSL. Observations along the back of Galveston Island indicate that surge levels within the Bay rose to approximately 2.0 to 2.5 meter MSL (CND, 1984). On the West coast of the Bay, near the city of Baytown, a surge of over 3 meter was recorded (CND, 1984). Mean wind direction; East – South – West

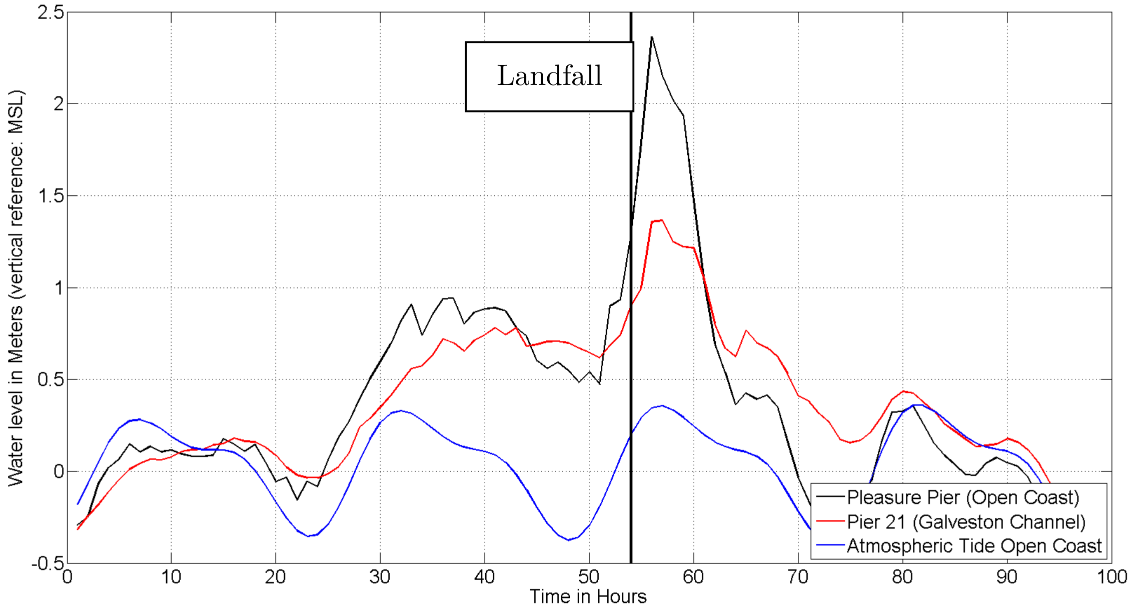

Figure 2-10 – Observed water levels during Hurricane Alicia (1983). Data: (NOAA, 2013a).

2.5 Hurricane Surge within Galveston Bay

Historical observations indicate that the Galveston Bay Area is susceptible to storm surge. Storm surge is an abnormal rise of water in a coastal or inland water body resulting from atmospheric weather systems. Storm surge at the open coast (Figure 2-11) is a combination of wind set-up, wave set-up, barometric set-up, coriolis set-up and astronomic tide (Dean & Dalrymple, 2001).

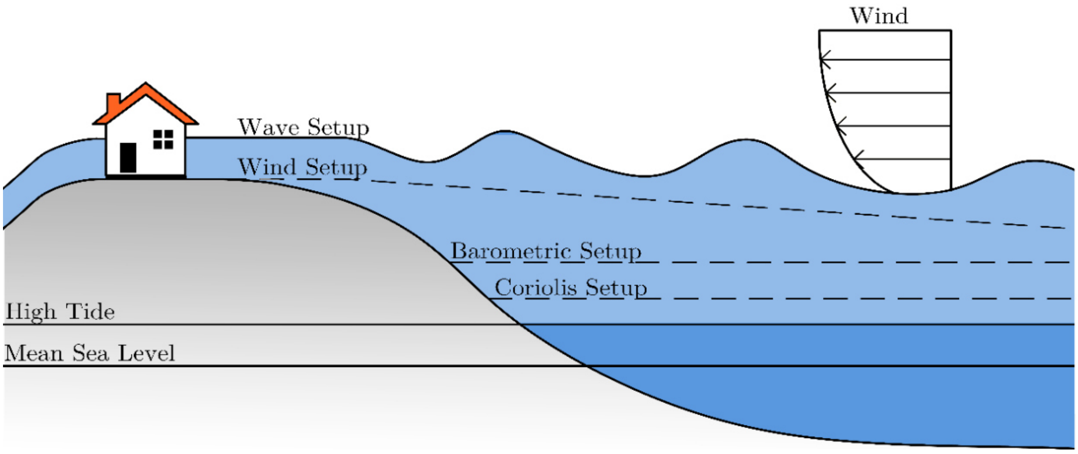

Figure 2-11 – Storm surge at the open coast.

Storm surge within a semi-enclosed bay (Figure 2-12) is a combination of local wind set-up, wave set-up, inflow through the estuary inlet and overflow of barrier islands.

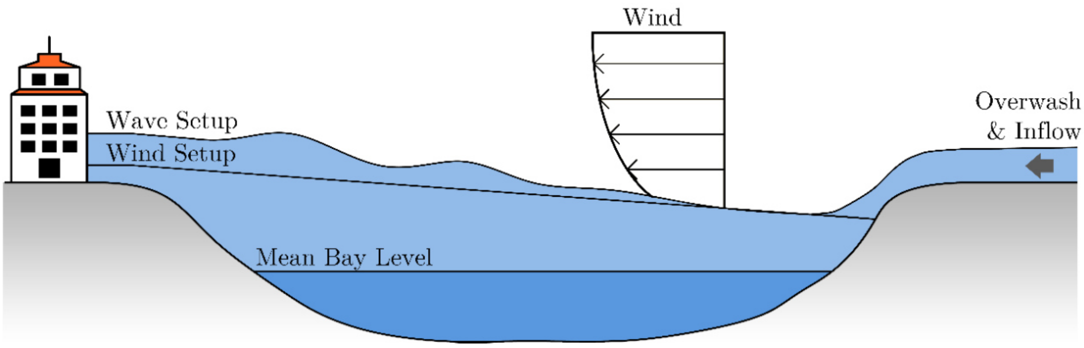

Figure 2-12 – Storm surge within a semi-enclosed bay.

During extreme storm events the barrier islands partially deflect the surge (Rego & Li, 2010). Most recently, Hurricane Ike (2008) produced significant overwash on both Galveston Island and Bolivar Peninsula. Such events are known to have occurred at least three times during the past century. Simulations show that Ike's storm surge would have been much worse with lower barrier islands (Arcadis US, 2011; Rego & Li, 2010).

Local wind set-up within shallow semi-enclosed bays is sensitive to the relative landfall location of the hurricane. Hurricanes making landfall west of a bay will force water into the system, increasing the surge (Figure 2-13; left). As the hurricane moves onshore, the wind direction shifts from East (stage 1) to South (stage 2) to West (stage 3). Hurricanes making landfall east of a bay will force water out of the bay, depressing the surge (Figure 2-13; right). As the hurricane moves onshore, the wind direction shifts from East (stage 1) to North (stage 2) to West (stage 3).

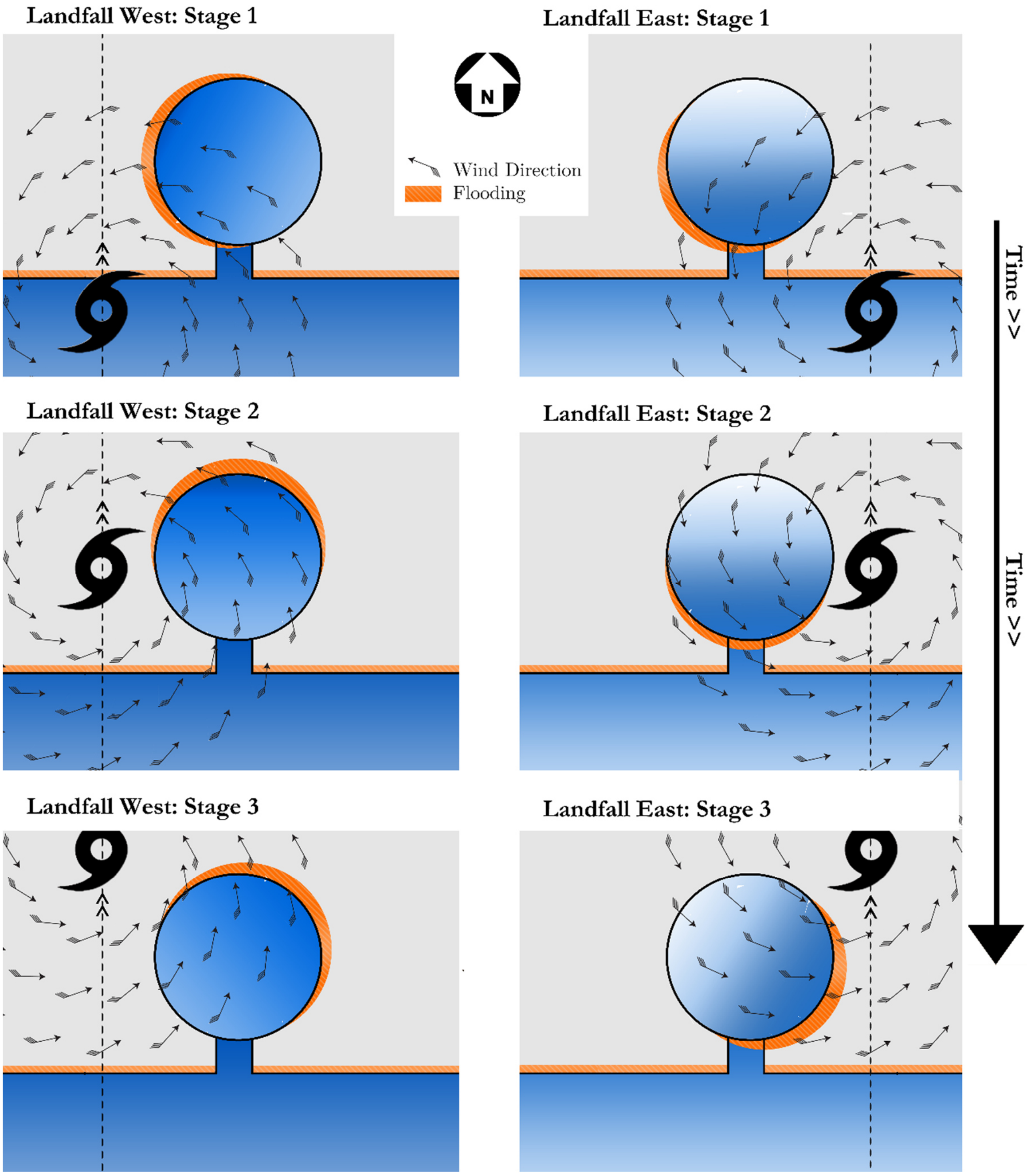

Figure 2-13 – The influence of landfall location on local wind set-up within semi-enclosed bays. Dark blue indicates areas with a higher surge.

2.6 Wave Climate

The relatively shallow and low inclination of the continental shelf hints at a dissipative wave environment. Jin et.al. (2012) simulated wave parameters for various combinations of storm surge and hurricane category, at several locations along the Upper Texas Coast. Figure 2-14 and Table 2-4 present near shore wave conditions at the San Luis Pass Bridge. Jin et.al. (2012) find that the wave height relates linearly to storm surge and is less dependent on wind velocity. The findings indicate that waves at the open coast are predominantly depth limited.

Waves within Galveston Bay are fetch or depth limited, depending on storm track, storm intensity and inflow. The maximum fetch within Galveston Bay is about 30 kilometers. The Texas City Hurricane Protection Structure was designed for a significant wave height of up to 1.5 meter (Davis, 1966).

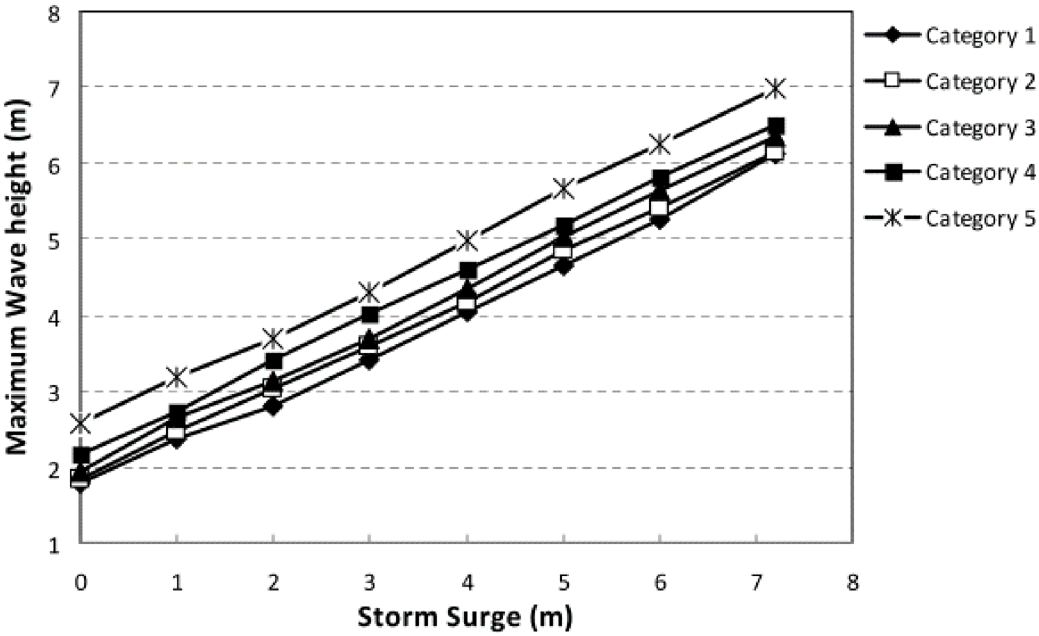

Figure 2-14 – Hmax at San Luis Pass Bridge source: (Jin, et al., 2012).

Table 2-4 – Tmax at San Luis Pass Bridge source: (Jin, et al., 2012).

Hurricane Scale	Storm Surge (m)							
	0	1	2	3	4	5	6	7.2
Category 1	2.75	3.67	8.70	9.58	9.58	9.58	9.58	9.58
Category 2	2.75	4.45	5.93	6.53	8.70	7.91	9.58	9.58
Category 3	2.75	2.75	5.93	7.18	6.53	7.18	7.91	8.70
Category 4	2.75	4.89	5.39	5.93	7.18	7.91	7.91	8.70
Category 5	2.75	3.03	5.39	5.93	5.93	5.93	6.53	7.18

2.7 Conclusion

The area of interest covers a shallow wind-dominated semi-enclosed bay within a tropical cyclone environment. Micro-tidal oscillations within the bay lag oscillations at the open coast by four to six hours and are about 0.6 times as small. Seasonal water level oscillations are of the same magnitude as the astronomical tide.

Galveston Bay is frequently exposed to hurricanes and storm surge. The relatively uniform and wide continental shelf allows large storm surges at the open coast. Storm surge within Galveston Bay is a complex interaction between the surge at the open coast, wind set-up and wave set-up. Waves at the open coast are depth limited and the wave height relates linearly to storm surge.

Hurricane storm surge in coastal bays is sensitive to storm path and landfall location. Landfall West of Galveston Bay tends to result in the highest surges as Galveston Bay encounters the strongest winds in on-shore direction. During such events, wind directions shift from East through South to West. Landfall East of Galveston Bay results in smaller storm surge because Northerly winds depress surge within Galveston Bay. During such events, wind directions shift from East through North to West.

Documentation of bay behavior under ordinary conditions is outstanding. Much research has examined the ecologic and hydraulic characteristics of the system during normal conditions. Several tide-gauges provide continuous information on water levels. The propagation of the astronomical tide is well understood. Elevation data is recent and available at high resolution.

Bay behavior under hurricane conditions is less well understood. Measurement equipment often fails during hurricanes and post-storm damage surveys solely provide estimates of storm surge and wind velocity. Measurements during Hurricane Ike, Rita and Alicia provides some insight into bay behavior during hurricane conditions.

Well-documented historic observations are rare and often provide little input for a statistical analysis of return period estimates. The limited amount of historical records proves to be a major shortcoming in storm surge statistics. Historic observations do indicate that storm surge within the bay may exceed storm surge at the open coast, depending on the track and other storm characteristics. Simulations have shown that, for storms making landfall west of Galveston Bay, the Houston Shipping Channel is subject to higher surges than the open coast.

Landfall location and inlet configuration are important in determining the ratio between open-coast and bay flooding. Further research is required to assess the impact of landfall location and storm characteristics on storm surge probabilities within the bay.

Chapter 3. Storm Surge Model

This chapter describes the development of three analytical models (hurricane wind field, storm surge at the coast and storm surge within bay) and subsequent validation of these models. The applied methodology is discussed in Section 3.1. Section 3.2 elaborates on the first component of the storm surge model; a parametric hurricane model. Section 3.3 discusses the approach followed to estimate storm surge at the open coast. Section 3.4 presents the development of a semi-analytical model used to estimate surge within semi-enclosed bays. In Section 3.5 we validate the model using a deterministic approach. Section 3.6 concludes the findings.

3.1 Modelling Concept

To assess the influence of risk reduction strategies on flood vulnerability within semi-enclosed bays a simple one-dimensional storm surge model was developed. Storm surge estimated by the model is a composite of wind set-up, barometric set-up, wave set-up and astronomical tide. The model allows rapid simulation of a large number of synthetic hurricanes. The following components are included (Figure 3-1);

1. a hurricane model describing atmospheric pressure, wind velocity and wind direction,
2. a storm surge model describing storm surge at the open coast,
3. a storm surge model describing storm surge within a semi-enclosed bay.

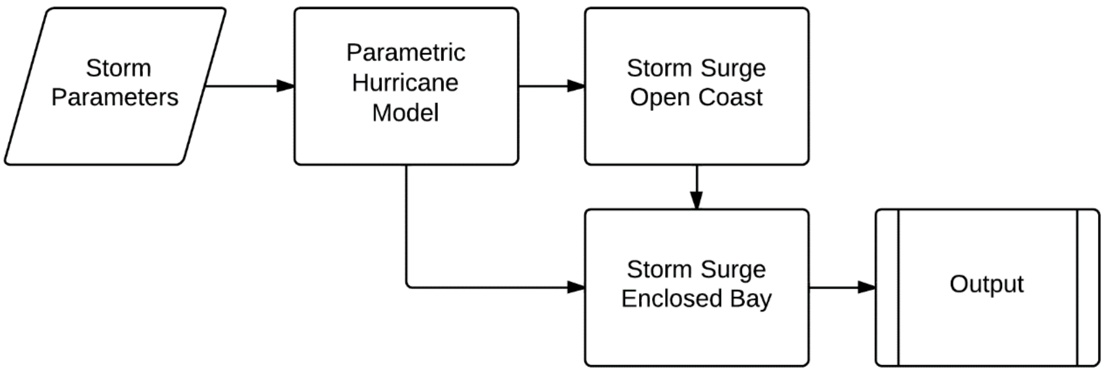

Figure 3-2 – Components of one-dimensional model.

The simplified one-dimensional model can be described as follows. The coastline is assumed straight, infinitely long and the depth contours are assumed parallel to the shoreline. A stationary parametric hurricane with the characteristics of a moving hurricane is moved along a shore-normal track towards the coast. Storm surge is computed along a single straight transect between the 50 and 3 meter depth contour lines, one Radius to Maximum Wind east of the landfall location. The model solely considers motion along this transect (x-direction) and does not include the alongshore (y-direction) direction. The transect runs orthogonal to the bottom contours.

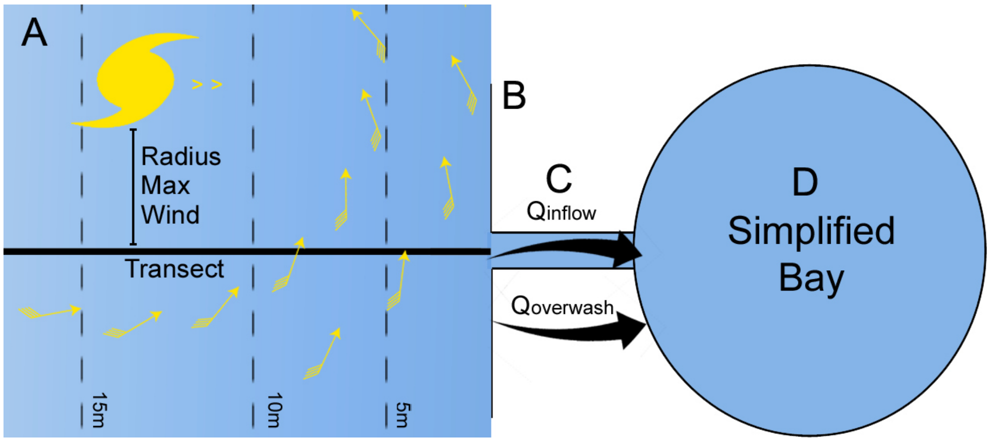

Figure 3-3 – Schematic overview of model.

Solving the 1-dimensional shallow water equations along the transect yields the time-dependent motion of storm surge at the open coast. The surge at the open-coast is subsequently transformed into surge at the bay inlet following Bodine (1969). The surge at the open coast (B) propagates through the tidal inlet and over the barrier islands (C) into a circular shaped Bay with uniform depth (D). Hurricane wind fields are assumed constant in time prior to landfall. After landfall, hurricane intensity decreases following Vickery et al. (2005).

We can summarize the assumptions as follows;

- A.1. Infinitely long coast with parallel depth contour lines.
- A.2. No alongshore (y-axis) gradients.
- A.3. Constant wind field prior to landfall.
- A.4. After landfall slow time dependent decrease of pressure deficit.
- A.5. Storms have an orthogonal angle of approach.
- A.6. Bay with uniform depth.
- A.7. Storm surge decreases linearly in along shore direction.

The Upper Texas Coast is relatively uniform and straight (Section 2.1). The assumption of constant wind fields prior to landfall will affect deterministic results because storm intensity does vary with time. Since the storm parameters are based on statistics at landfall, the model is expected to underestimate results for storms that weaken prior to landfall. Statistical analysis (Appendix B) shows that the average angle of approach is indeed almost 90 degrees. Sensitivity studies have shown that the influence of track angle on storm surge is small (Irish, et al., 2008).

The simplifications introduced in this chapter allow rapid insight into the problem while maintaining the utmost important processes. The proposed model provides a first-order estimate of surge height and surge probability within semi-enclosed bays.

Accurate simulation of alongshore flow and associated set-up requires a 2D model with alongshore boundary conditions. The aim of this thesis is to develop a simplified 1-Dimensional method to deduce the optimal risk reduction strategy for semi-enclosed bays. 2D storm surge simulations are beyond the scope of this thesis.

3.2 Wind Field and Pressure Field Modelling

Modelling the generation of storm surge and wave set-up requires representative wind and pressure fields. The wind velocity in hurricane wind fields can be simulated using a dynamic or a parametric model. Dynamical models include spatial variations in atmospheric behavior, rely on physical laws and often require significant computational power. A parametric model approximates hurricane wind fields based on a best parametric fit.

Probabilistic coastal storm surge models driven by a parametric best-fit hurricane model do not have significant larger systematic errors than those driven by a dynamic model (Resio & Westerink, 2008). Hind-casts of individual events may show errors of up to 20%. Since computational power is limited, a parametric model is utilized to simulate the atmospheric pressure and wind velocity. Wind velocity depends on the pressure gradient requiring pressure to be solved first (Figure 3-4).

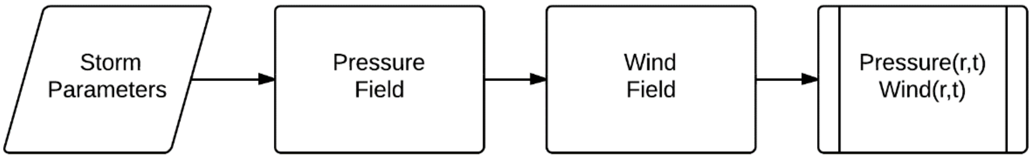

Figure 3-4 – Schematic overview of the hurricane model.

3.2.1 Parametric Hurricane

An often used hurricane wind model is the analytical cyclone model by Holland (1980), (Vickery et al. (2009b); Willoughby & Rahn (2004)). Holland expressed the radial profile of sea level pressure and winds in hurricanes with a limited set of parameters, often taken at landfall. The Holland or H80 model describes the pressure and wind velocity in the gradient and cyclostrophic regions of the hurricane wind field. Within the gradient and cyclostrophic region the influence of the Coriolis force is of the same magnitude, or smaller, as the pressure gradient and centrifugal forces.

The radial distribution of pressure p(r), relative to the storm center and ambient pressure is given by,

$$p(r) = p_c + \Delta p \cdot e^{-(R_m/r)^B} \qquad \text{Eq. 3.1}$$

where p_c [Pa] is the core pressure, Δp [Pa] is the core-pressure deficit with respect to the ambient pressure, R_m [km] is the radius to maximum winds, r [km] is the distance to the core and B [-] is the storm peakedness parameter.

The radial distribution of wind velocity V(r), relative to the storm center and radius to maximum wind (R_m) is;

$$V(r) = \sqrt{\frac{(\alpha + r \cdot f)^2}{4} + \frac{B \cdot \Delta p}{\rho} \cdot \left(\frac{R_m}{r}\right)^B \cdot e^{-(R_m/r)^B}} + \frac{\alpha + r \cdot f}{2} \qquad \text{Eq. 3.2}$$

where V(r) [ms^{-1}] is the wind velocity at gradient height, R_m [km] is the radius to max wind, B [-] is the storm peakedness parameter, r [km] is the distance to the core, ρ [kgm^{-3}] is the density of air, f [$rads^{-1}$] is the coriolis frequency and α is Blaton's correction factor represented by $Vf \cdot \sin\theta$ (Zdunkowski & Bott, 2003). Figure 3-5 presents an example of a parametric hurricane.

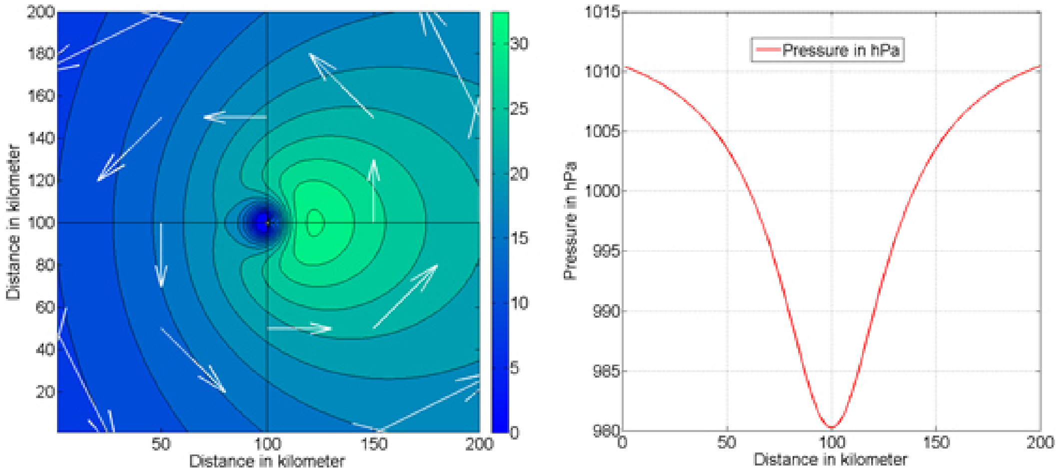

Figure 3-5 – Arbitrary parametric hurricane. p = 980 hPa, R_m = 30km, Vf = 5ms^{-1}, B = 1.27.

The B parameter is a shape parameter with typical values between 1.0 and 2.5 (Holland, 1980). Larger values of B result in a steeper pressure gradient and higher wind velocities near the radius of maximum winds. Hurricanes within the Gulf of Mexico are well represented by a constant Holland B value of 1.27 (Resio, et al., 2009). A constant value for Holland B introduces errors in the far field wind velocity and neglects variability associated with eye-wall replacement cycles (Vickery, et al., 2009b). Resio et al. (2009a) found a sensitivity of 15% in peak surge values as a function of the Holland B parameter. Following Irish et al. (2009) the interaction with land is included by decreasing B value linearly from 1.27 to 1.0 during the final 50km prior to landfall.

The H80 hurricane model estimates wind velocities at gradient height. The wind velocity at the sea surface is considerably lower because of the influence of surface drag. The relation between gradient wind velocity and surface wind velocity can be expressed by a linear conversion parameter (Table 3-1). Selection of the conversion parameter requires careful attention. Storm surge responds to increasing wind velocity in a nonlinear fashion, increasing errors in parameter selection. The model utilizes the "80% rule" (Powell et al., 2005) which assumes the surface wind velocity is 80% of the average wind velocity within the boundary layer.

Table 3-1 – Gradient to surface wind speed conversion parameters in literature.

Vsurface/Vgradient	Sea-Land reduction (coast)	Source
0.73 (80% rule)	15 % - 20 %	Powell et al. (2005)
0.85	-	Vickery et al. (2009a) (empirical model)
0.67 – 0.74	-	Vickery et al. (2009b) (dropsonde data)
0.865	15 %	Batts et al. (1980)
0.65	30 %	Sparks and Huang (2001)

Parametric hurricane models offer a fair representation of the sustained wind velocity and do not simulate rapid dynamic behavior. The temporal timescale of wind driven oceanic response is significantly larger than the temporal scale of gusts (Powell, 2012). Validations by Vickery et al. (2009) and Willoughby and Rahn (2004) show that the H80 model slightly overestimates wind velocity exceeding 50 ms^{-1} (Cat 3+), and underestimates the wind velocity closer to the geostrophic (far-field) region of the storm.

3.3 Storm surge at the open coast

Storm surge belongs to the class of long gravity waves and can last several hours to days (Platzman, 1971). The wavelength of storm surge is much larger than the depth of the water it traverses. Storm Surge shares many aspects with other well-known long gravity waves like astronomical tide or tsunamis.

The analytical methodology outlined in this section estimates storm surge at the open coast by taking into account barometric set-up, wind stress and bottom friction. Ancillary effects are superimposed on the result obtained through numeric modelling. The procedure is outlined below (Figure 3-6).

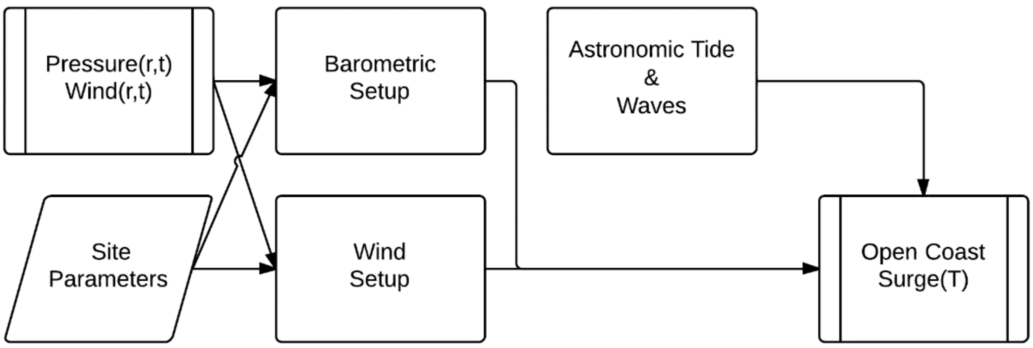

Figure 3-6 – Schematic overview of the numerical storm surge model.

The following assumptions have been made in model development;

A.8. Hydrostatic pressure.
A.9. No advection.
A.10. Wavelength $\gg$ shelf depth.
A.11. Uniform flow on the continental shelf.
A.12. Incompressible fluid.
A.13. Linear relation between atmospheric pressure and barometric set-up.
A.14. Tide and waves can be imposed linearly on storm surge.

3.3.1 Shallow water equation

The numerical scheme used to simulate storm surge relies on the depth integrated shallow water equations (SWEs). The SWEs, or depth integrated Navier-Stokes equations for fluid motion, describe the conservation of mass and momentum. Dean & Dalrymple (1991) provide a derivation of the linearized depth integrated equation of motion in shore normal (x-axis) direction;

$$\frac{\partial q_x}{\partial t} = -\frac{D}{\rho}\frac{\partial p_\eta}{\partial x} - D \cdot g \cdot \frac{\partial \eta}{\partial x} + \frac{1}{\rho}(\tau_{v:x} - \tau_{b:x}) \qquad \text{Momentum} \qquad \text{Eq. 3.3}$$

where q_x [m^2s^{-1}] is the depth integrated flow, D [m] is the total water depth, ρ [kgm^3] is the mass density of water, p_η [hPa] is the barometric pressure, g [ms^{-2}] is the gravitational constant, η [m] is the surge at location n, $\tau_{v:x}$ [Pa] is the wind shear stress and $\tau_{b:x}$ [Pa] is the bottom shear stress.

For constant wind velocity, a negligible pressure gradient and sufficiently long duration, the flow velocity towards the coast approaches zero. Rewriting Eq. 3.3 into the steady state equation Eq. 3.4 shows that storm surge is inversely proportional to the depth.

$$\frac{\partial \eta}{\partial x} = \frac{1}{g \cdot (d + \eta) \cdot \rho} \cdot (\tau_{v:x} - \tau_{b:x}) \qquad \text{Eq. 3.4}$$

where η is the surge at location n, ρ is the mass density of water, g is the gravitational constant, d is the initial depth, $\tau_{v:x}$ [Pa] is the wind shear stress and $\tau_{b:x}$ [Pa] is the bottom shear stress.

Conservation of mass for incompressible fluids is described by Eq. 3.5 which states that net inflow is balanced by a linear increase in volume.

$$\frac{\partial q_x}{\partial x} + \frac{\partial \eta}{\partial t} = 0 \qquad \text{Continuity} \qquad \text{Eq. 3.5}$$

where q_x is the depth integrated flow and η is the surge at grid cell n.

3.3.2 Wind shear stress

Wind shear stress is represented by τ_v (Eq. 3.6) and is a function of the momentary wind velocity and a dimensionless empirical derived friction factor K

$$\begin{Bmatrix}\tau_{v:x} \\ \tau_{v:y}\end{Bmatrix} = \begin{Bmatrix}\cos(\theta) \\ \sin(\theta)\end{Bmatrix} \cdot \rho \cdot K \cdot |V|V \qquad \text{Eq. 3.6}$$

Where $\tau_{v:x}$ and $\tau_{v:y}$ are the x and y components of the wind stress, θ is the angle of the wind with respect to the coast and V is the wind velocity.

Commonly used expressions for the wind stress coefficient include the empirical relations by Wu (1969) and Van Dorn (1953) (Dean & Dalrymple, 1991). Van Dorn (1953) derived the empirical values for K (equal to $\rho \cdot C_d$) during tests on an artificial pond. The wind stress coefficient dimensionless K is a function of the wind velocity and given by;

$$K = 1.2 \cdot 10^{-6} \qquad \text{for} \quad V \leq V_c \qquad \text{Eq. 3.7}$$

$$K = 1.2 \cdot 10^{-6} + 1.8 \cdot 10^{-6} \cdot \left(1 - \frac{V_c}{V}\right)^2 \qquad \text{for} \quad V \geq V_c \qquad \text{Eq. 3.8}$$

where V_c is the critical wind velocity; $V_c = 5.6$ [ms^{-1}] and V [ms^{-1}] is the wind velocity at the free surface.

The Van Dorn wind stress coefficients are independent of waves and were derived under ideal conditions and uniform wind velocities. The temporal timescale of wind driven oceanic response is significantly larger than the temporal scale of variations in wind velocity (Powell, 2012). The assumption of uniform wind velocity is not expected to impact results. Combining the steady state equation Eq. 3.4 and Eq. 3.6 shows that storm surge scales with the square of the wind speed. An increase in wind speed results in a quadratic increase in surge height.

3.3.3 Bottom shear stress

The bottom shear stress in shore normal direction, ($\tau_{b:x}$), depends on both flow velocity and bottom roughness. A common method to describe bottom friction is Manning's equation (Eq. 3.9). Manning's empirical equation does not vary with flow conditions and assumes uniform flow. The bottom shear stress in shore normal direction is expressed by;

$$\tau_{b:x} = \frac{\rho_w \cdot M^2 \cdot |q_x| q_x}{(d + \eta)^{7/3}} \qquad \text{Eq. 3.9}$$

where ρ_w [kgm^{-3}] is the density of water, M [$m^{1/3}s^{-1}$] is the Manning roughness coefficient, q_x [m^3s^{-1}] is the flow in shore normal direction, d [m] is the initial water depth and η [m] is the surge at location.

It is assumed that the Manning equation is valid for long waves. This implies that it is assumed that for slowly varying flows the velocity variation over the depth is similar to the steady state solution.

3.3.4 Barometric set-up

Barometric set-up, or pressure set-up, is a rise in water level resulting from a reduction in atmospheric pressure. The pressure gradient $\frac{\partial p_\eta}{\partial x}$ represents barometric set-up in the SWEs (Eq. 3.3). Schloemer (1954) assumed a linear relation between barometric set-up and atmospheric pressure gradients (Eq. 3.10). This assumption is reasonable because the timescale of storm surge significantly exceeds the timescale of local deviations in atmospheric pressure.

$$p_\eta(r) = c \cdot (p_a - p(r)) \qquad \text{Eq. 3.10}$$

where η_{bar} [m] is the barometric set-up in meters, p_a [hPa] is the ambient atmospheric pressure, $p_\eta(r)$ [hPa] is the atmospheric pressure at the location of interest and c is a dimensionless coefficient between 1.0 and 1.05, often assumed equal to 1.04 (Dean & Dalrymple, 2001).

3.3.5 Numerical Solution

The momentum equation (Eq. 3.3) and continuity equation (Eq. 3.5) are solved along a single transect (Figure 3-7), for discrete increments of time $(\Delta t)_i$ and space $(\Delta x)_n$. The numerical method relies on an explicit Leap-Frog scheme similar to the numerical schemes by Bodine & Reid (1968), Pearce (1972) and Dean et al. (1994). Figure 3-7 presents an overview of the numerical grid with n cells.

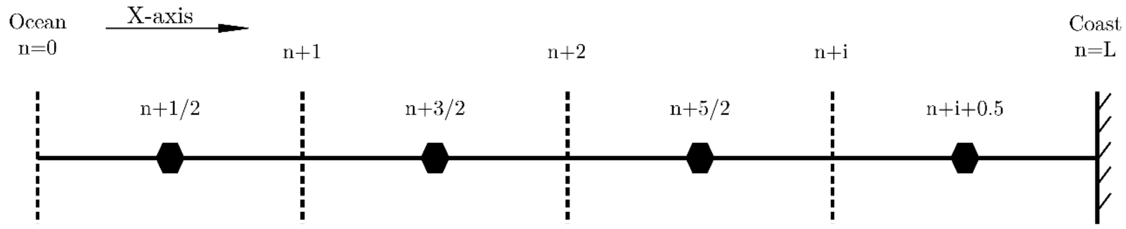

Figure 3-7 – Numerical grid including discretized stepped depth profile.

The surge η at cell n is a function of inflow $q_x(n)$ minus outflow $q_x(n+1)$. The flow $q_x(n)$ is a function of the hydrostatic pressure, barometric pressure gradient, wind stress, bottom friction and local depth and represents the seaward boundary of each cell. The surge η, pressure p and shear stress τ are assumed uniform over once cell and are located at the midpoint of each cell.

The accuracy of the numerical scheme is $\sigma = (\Delta t^2, \Delta x^2)$. Numerical stability requires the wave not to travel beyond the distance of one cell, during one time step. The time-step ought to adhere to the following CFL condition;

$$\frac{\Delta t}{\Delta x} \leq \frac{1}{\sqrt{g \cdot d_{max}}} \qquad \text{CFL condition} \qquad \text{Eq. 3.11}$$

where Δt [s] is the time-step, Δx [m] is the cell size, g [ms^{-2}] is the gravitational constant and d_{max} [m] is the maximum depth in the system.

3.3.6 Boundary Conditions and Initial Conditions

The 1-dimensional model requires two boundary conditions. The following boundary conditions apply;

1. At the landward boundary ($x = L$) the flow q_x is equal to zero (impermeable vertical wall without reflection).
2. At the seaward boundary A, ($x = 0$), the depth is assumed infinite. This means there is no wind set-up, and the surge at ($x = 0$) is solely a function of the barometric set-up. This is the barometric boundary condition.

Initial conditions assume a flat surface ($\eta = 0$) and zero flow ($q_x = 0$). It must be noted that the system is relative insensitive to initial conditions as the numerical scheme contains friction terms. The system requires sufficient time to "spin-up" in order to let the initial conditions dissipate. This can be achieved by initiating the model before the hurricane significantly influences water levels on the continental shelf.

3.3.7 Discretization in space and time

Numerical application of continues parameters requires discretization in space and time. Discretization of the computational domain may affect computational results significantly.

The spatial resolution of the numeric grid is often related to the available resources. Pearce (1972) uses a uniform cell size of 10 kilometers while Reid & Bodine (1968) use a uniform cell size of about 4 kilometers. To prevent significant overestimation of the near-shore surge height we perform a few runs for different cell sizes. Figure 3-8a presents results for an arbitrary hurricane and cell size between 500 and 2000 meter. Cell sizes larger than 1000-meter result in a larger error. A cell size below 1000 meter does not reduce discretization errors.

Cell size requirements in deep water depend on the discretization of the atmospheric pressure gradient (Blain, et al., 1998). The spatial resolution of the numeric grid in deep water ought to be smaller than the radius to maximum winds (20-100km) in order capture the barometric surge within approximately 12% (Blain, et al., 1998).

Discretization averages continuous values over small increments of time or space. The CFL condition restricts the maximum time step to about 50 seconds for a 1000-meters cell. The governing time scale of pressure and wind fields in surge computations are significantly larger than 100 seconds. Figure 3-8b presents the surge at the open coast for 4 different time-steps. error introduced by utilizing a 1000 meters grid as opposed to 500 meters grid size is negligible. The model uses a cellsize of 1000 meters and a time step of 50 seconds.

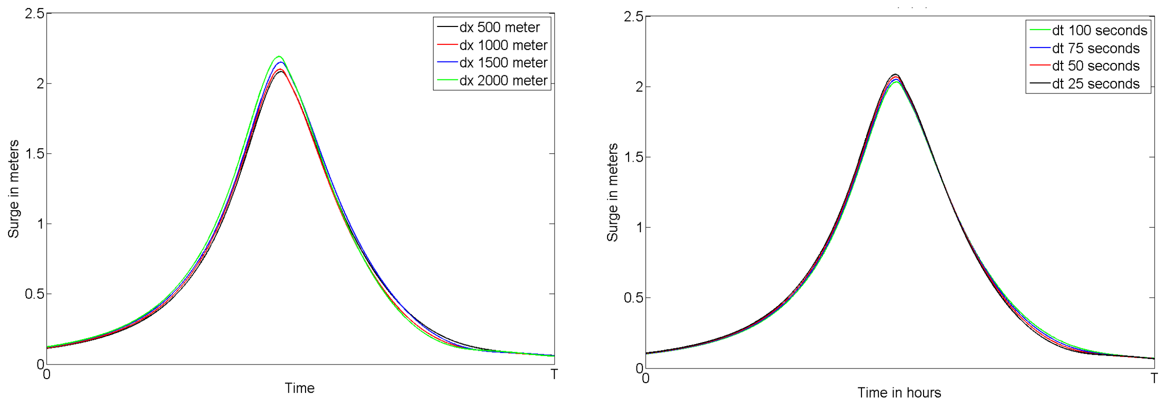

Figure 3-8 – Influence discretization of space (left) and discretization of time (right).

3.3.8 Astronomical Tide and Waves

Astronomical tides may increase or decrease the magnitude of storm surge. Storm surge increases the depth and thereby the propagation velocity of the tidal wave. The model superimposes astronomical tide on storm surge, a reasonable assumption in micro-tidal regions. The influence of astronomical tide is included in the probabilistic application (Chapter 5) by randomly selecting a starting point between June 1st and October 30th (hurricane season) and subsequently superimposing astronomical tide on simulated storm surge.

Breaking waves contribute to the near-shore surge by transporting wave momentum towards the coast. The relative influence of wave set-up is smaller on shallow (dissipative) coastal profile than on steep (reflective) coastal profiles (Figure 3-9). Neglecting wave set-up results in a significant error because wave set-up contributes 15 to 35% to the total flow through tidal inlets (Irish & Canizares, 2009).

In Section 2.6 we concluded that wave set-up on the Upper Texas Coast relates almost linearly to storm surge. A first estimate of wave set-up follows from the ratio of the transfer rate of wave momentum to the transfer rate of wind momentum (R) (Resio & Westerink, 2008);

$$\eta_{\mathrm{wave}} = \frac{\mathrm{R}}{1-\mathrm{R}} \cdot \eta_{\mathrm{simulated}} \qquad \text{Eq. 3.12}$$

where η_{wave} [m] is the wave set-up, R [-] is the wave set-up ratio and $\eta_{\mathrm{simulated}}$ [m] is the simulated surge in meter.

Figure 3-9 presents the envelope of R as a function of the bottom slope, for non-sheltered coasts within the Gulf of Mexico. The envelope of R results from considering different theoretical approaches, breaker forms and wave-momentum loss rates (Resio & Westerink, 2008). On the Upper Texas Coast R equals 0.10 to 0.15. Deterministic simulations use a value of R = 0.125 while the probabilistic simulations assume a uniform distribution of R between 0.10 and 0.15. The applied methodology provides a reasonable yet somewhat conservative estimate of wave set-up at the open coast (USNRC, 2012).

Wave set-up within Galveston Bay is neglected because the relative influence of wave set-up within the Bay is assumed small.

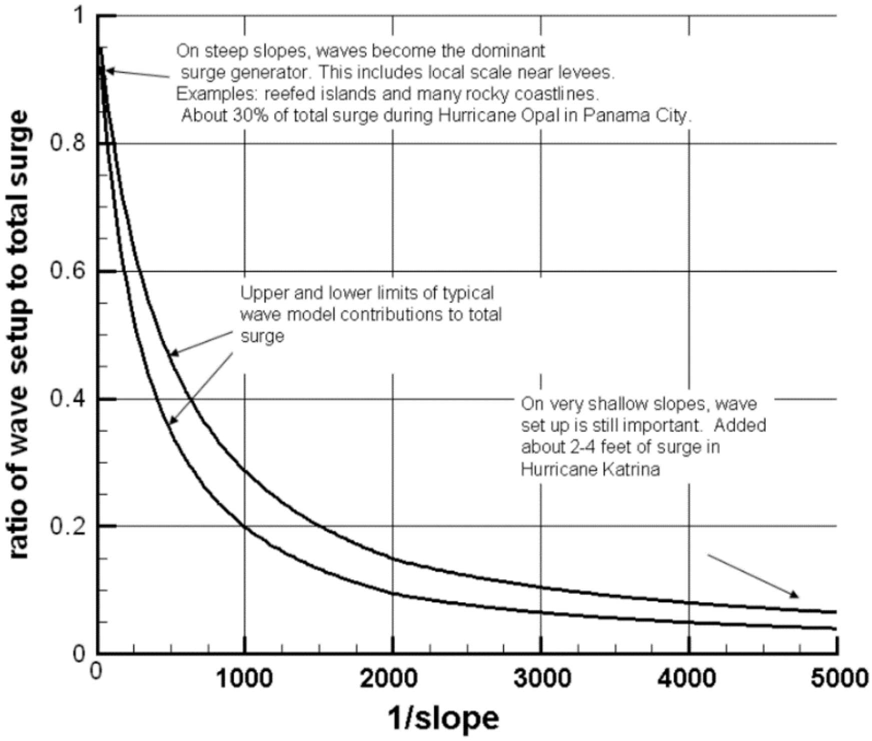

Figure 3-9 – Estimated upper and lower limit of R. Source: (USNRC, 2012).

3.4 Storm Surge within Semi-Enclosed Basins

Storm surge within a semi-enclosed bay is a function of inflow, local wind set-up and local wave set-up (Figure 2-12). The required input includes a time dependent hurricane wind field (Section 3.2) and storm surge at the open coast. The surge within the simplified bay is computed along two transects (L1, L2) and solved at four locations (Figure 3-10).

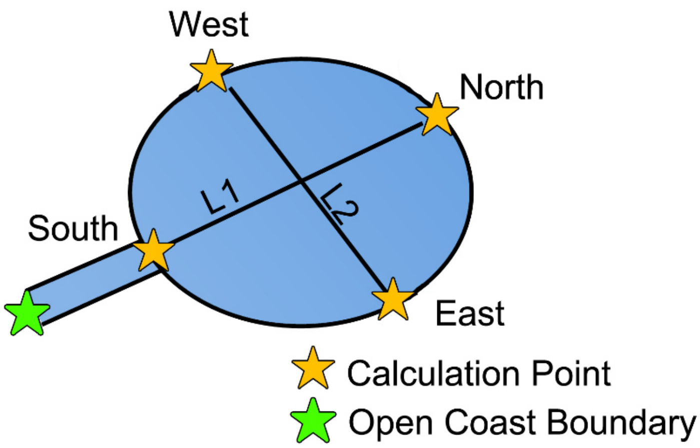

Figure 3-10 – Calculation points within the simplified bay.

The response of a bay to external tide or surge is a complex non-linear process. Numerous analytical inlet-bay models exist (Dronkers, 1964; Keulegan, 1967) and provide a realistic way to simulate the relation between bay excitation and astronomical tides at the open coast. Wind set-up within a bay or lake does not differ much from wind set-up on the open ocean and depends on wind velocity and local depth.

Instantaneous water levels within a bay are affected by both wind stress and inflow, requiring a simultaneous coupled solution to both problems. Figure 3-11 presents a schematic overview of the model.

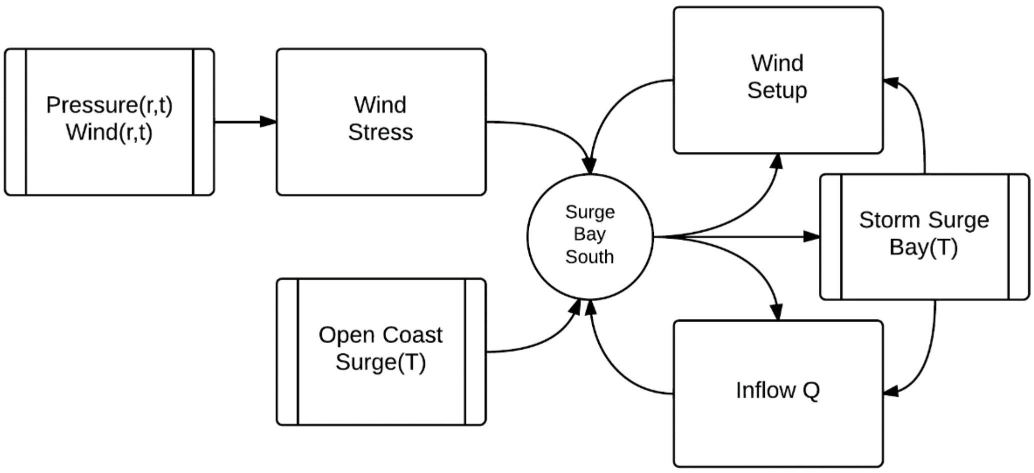

Figure 3-11 – Storm surge within simplified semi-enclosed bay.

The model consists of four components that, when combined, describe the surge within the bay as a function of wind stress and water level at the open coast. These four equations (Eq. 3.13, Eq. 3.14, 2x Eq. 3.15) respectively describe inflow and local wind set-up. To solve this set of four equations the following assumptions apply;

A.15. No inflow other than inlet or barrier overflow.
A.16. The walls of bay are vertical.
A.17. Bay water level responds instantaneously.
A.18. Constant flow area inlet.
A.19. Friction dominated inlet.
A.20. Uniform flow in inlet.
A.21. Inflow quasi-steady with respect to wind set-up.

3.4.1 Inlet - Bay relation

For a straight and short channel ($l_{inlet} \ll l_{wave}$) with negligible storage ($A_{inlet} \ll A_{bay}$), negligible inertia (friction $\gg$ inertia) and steady, uniform flow we can express the flow through an inlet by rewriting the Chezy equation into;

$$h_{Coast} - h_{South} = L_c \cdot \frac{|Q_c|Q_c}{C^2 \cdot W_c^2 \cdot D_c^3} \qquad \text{Eq. 3.13}$$

where h_{Coast} [m] is the surge on the open ocean, h_{South} [m] is the surge in the bay, at the inlet, L_c [m] is the length of the inlet, Q_c [m^3s^{-1}] is the flow through the inlet, C [$m^{1/2}s^{-1}$] is the Chezy coefficient, W_c [m] is the width of the channel and D_c [m] is the depth of the channel.

Inertia and resistance within a bay are negligible when a bay is sufficiently deep ($T_{forcing}>20T_{Bay}$, (TUD, 2009)) that the tide propagates across the bay instantaneously (Keulegan, 1967). Although this may not always be completely true, often the tide propagates sufficiently fast to make the “pumping mode” assumption reasonable. If this conditions holds the flow Q_c through the inlet channel equals;

$$Q_c = \frac{d(h_{bay})}{dt} \cdot A_{bay} \qquad \text{Eq. 3.14}$$

where Q_c [m^3s^{-1}] is the flow through the inlet, h_{bay} [m] is the surge in the bay and A_{bay} [m^2] is the surface area of the bay.

3.4.2 Wind Set-up

Wind set-up is computed along two single transects. At each time step, the model assumes stationary conditions along each transect, while the influence of inflow on the average bay elevation is assumed quasi-steady with respect to the wind set-up. For such conditions, the hydrostatic pressure balances both wind and bottom stress.

$$\frac{h_{South} - h_{North}}{L1} = \frac{\tau_{w:x}}{\rho \cdot g \cdot (d + h_{bay})} \quad \text{Eq. 3.15}$$

$$\frac{h_{West} - h_{East}}{L2} = \frac{\tau_{w:y}}{\rho \cdot g \cdot (d + h_{bay})} \quad \text{Eq. 3.16}$$

where τ_w [Pa] is the wind shear stress, U [ms^{-1}] the wind speed at the free surface, ρ [kgm^3] is the density of water, g [ms^{-2}] is the gravitational constant, d [m] is the mean water depth, h_{bay} [m] is the surge in the bay and L1 [m] and L2 [m] are the computational transects within the bay.

Combining Eq. 3.13 with Eq. 3.14 and subsequently combining the result with Eq. 3.15 following van Ledden (2013) yields an expression for the water level on the bay side of the inlet as a function of the wind shear stress and water level at the open coast.

Above methodology yields an estimate of storm surge within a semi-enclosed bay. The steady state assumption requires constant wind velocity over a long time. An assumption that holds during the initial approach. Closer to landfall wind directions may shift up to 180 degrees within a few hours, which defies the limits of the steady state assumption. The time to steady-state set-up in the simplified bay under hurricane forcing is about 2 hours (Dean & Dalrymple, 1991).

Wind set-up and set-down are solely equal under idealized conditions. Such conditions require a constant unidirectional wind blowing over a symmetric basin with uniform roughness and constant depth (USACE, 1984). Eq. 3.15 and Eq. 3.16 provide a first approximation of wind set-up in an enclosed basin with non-exposed bottom (USACE, 1984). Eq. 3.15 and Eq. 3.16 are valid when set-up does not exceed local depth. Wind set-up during hurricanes may prove significant because of the high wind velocities. During hurricanes, additional inflow will increase the surface elevation in the bay. The assumption of small wind set-up compared to bay depth should be verified on application of the model.

3.4.3 Barrier Island

Propagation of long waves over reefs or sandbanks can be represented by a submerged or broad crested weir (Sobey, et al., 1980). Barrier islands share many characteristics with sandbars allowing a similar approach (Reid & Bodine, 1968). In addition, the elevated coastal highway does represent a weir like structure. By assuming the barrier islands can be schematized as a broad-crested weir, we ignore the bottom roughness induced friction loss term. This assumption holds if the relative influence of the friction loss term is small.

The Hydraulic Engineering Center approach (HEC, 2010) provides analytic solutions to weir overflow under uniform flow conditions. The methodology assumes a linear relation between weir coefficient C'_w and flow;

$$q = \pm C_{df} \cdot C'_w \cdot \sqrt{g} \cdot {h_1}^{1.5} \qquad \text{Eq. 3.17}$$

where q [m^2s^{-1}] is the flow per unit length, C_{df} [-] is the submergence correction factor, C'_w [-] is the dimensionless weir discharge coefficient, g [ms^{-2}] the gravitational constant and h_1 [m] is the upstream surface elevation.

For broad-crested weirs the weir submergence correction factor, C_{df}, relies on the CMS-FLOW (Reed & Sanches, 2010) implementation of the USACE EM 1110-2-1603.

$$C_{df} = 1 - \exp\left(-8.5 \cdot \frac{h_2}{h_1}\right) \qquad \text{Eq. 3.18}$$

where C_{df} is the weir coefficient, h_2 [m] is the downstream surface elevation and h_1 [m] is the upstream surface elevation.

The applied methodology is applicable to sheet-wash overflow. Breaching of barrier islands is not taken into account.

3.4.4 Seiching

A first approximation (Dean & Dalrymple, 1991) of the seiching period of Galveston Bay hints at a seiching period of 2 to 4 hours. Fluctuations in wind velocity have magnitude of minutes and should not pose any problem. When a hurricane traverses the Bay the wind shifts from East to West. Combinations of track and translation speed that cause wind shifts with temporal scales of 2 to 4 hours do exist. A historic hurricane induced seiching event on Lake Okeechobee, Florida in 1928 (seiching period: 4 to 6 hours) resulted in major flooding (NRC, 2005). Additional research is required to assess Galveston Bays sensitivity to seiching. Seiching is not accounted for in this thesis.

3.5 Deterministic Model Validation

Validating a location specific storm surge model is a precarious task given the limited historical records. In this section, we compare hind-casted events to historic observations of the same event.

3.5.1 Validation Parametric Hurricane Model

Historic datasets of hurricanes are obtained through the NOAA H*wind 1-minute sustained surface wind analyses (NOAA HRD, 2013c). The 1-minute averaged velocities are corrected to 30-minute mean wind velocities following Powell et al. (2010).

Table 3-2 list the measured and simulated surface wind velocity at landfall for eight historic hurricanes. The correlation R^2 between the observed and simulated surface wind velocity is $R^2 = 0.88$. The simulated wind velocity is on average slightly lower than the observed wind velocity.

Table 3-2 – Observed and simulated peak surface velocity prior to landfall.

Hurricane	**Year**	**Date**	**Core Pressure**	**$V_{10:max}$ Measured**	**$V_{10:max}$ Simulated**
Ike	2008	13/09	951 hPa	40 ms^{-1}	42 ms^{-1}
Humberto	2007	13/09	985 hPa	34 ms^{-1}	29 ms^{-1}
Rita	2005	23/09	945 hPa	46 ms^{-1}	44 ms^{-1}
Claudette	2003	17/08	982 hPa	34 ms^{-1}	30 ms^{-1}
Jerry	1989	16/10	983 hPa	32 ms^{-1}	29 ms^{-1}
Chantal	1989	03/08	984 hPa	36 ms^{-1}	42 ms^{-1}
Bonnie	1986	28/07	992 hPa	39 ms^{-1}	36 ms^{-1}
Alicia	1983	20/08	963 hPa	50 ms^{-1}	56 ms^{-1}

Figure 3-12, Figure 3-13 and Figure 3-14 present reconstructed NOAA H*wind surface wind fields (400kmx400km) and simulated wind fields during Hurricane Ike (2008), Hurricane Rita (2005) and Hurricane Humberto (2007). The reconstructed surface wind fields are "snapshots" and do not represent the average hurricane shape. As expected, the parametric model does not capture the spatial detail present in real hurricanes. In addition, the influence of land is not included in the parametric hurricane model. The parametric model does depict the average shape of the hurricane reasonably well. In addition, the simulated hurricanes have similar wind field structure. Hurricane Rita's simulation confirms the model overestimates far field wind velocities, and clearly shows the interference with coastal boundaries.

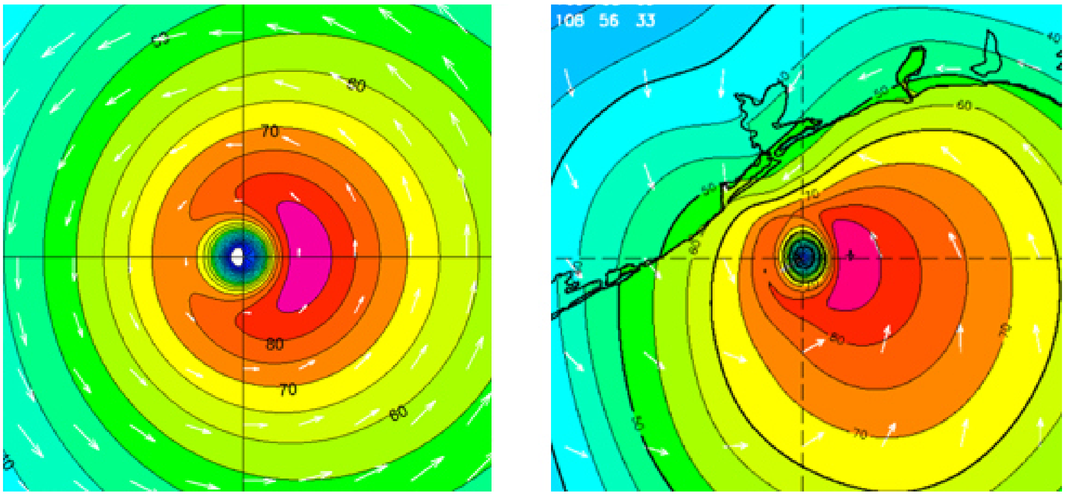

Figure 3-12 – Ike 0430 UTC 13 SEP 2008 Sustained surface winds. Simulated and observed (NOAA, 2013c).

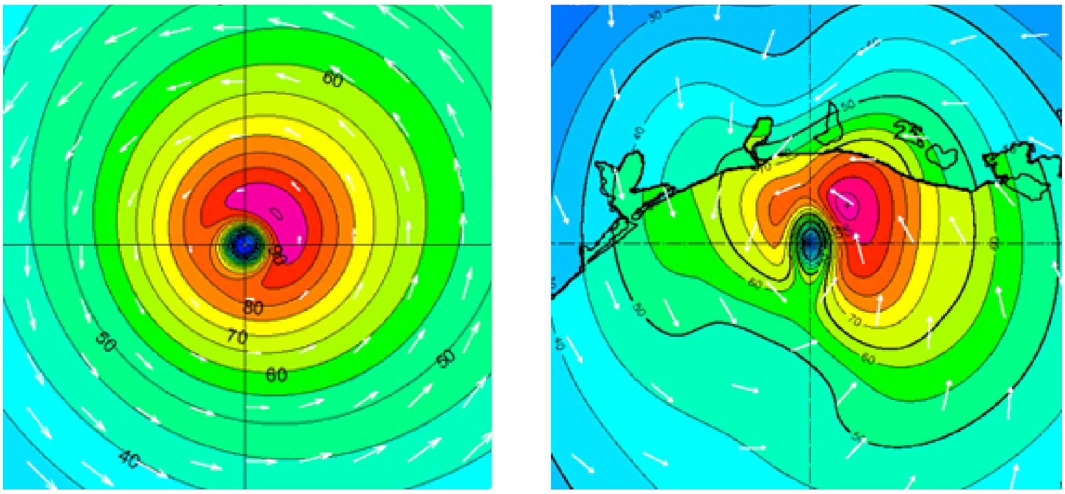

Figure 3-13 – Rita 0430 UTC SEP 25 2005 Sustained surface winds. Simulated and observed (NOAA, 2013c).

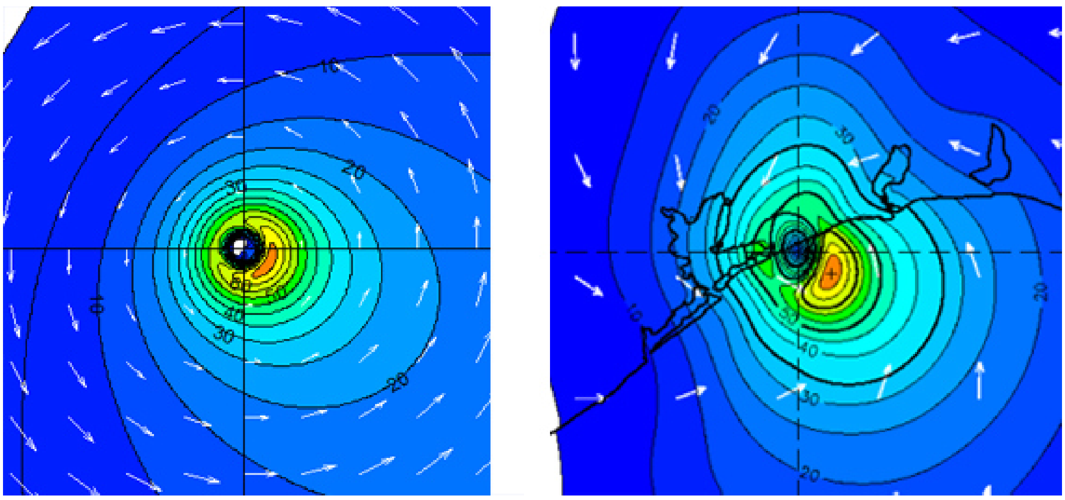

Figure 3-14 – Humberto 0652 UTC SEP 13 2007 Sustained surface winds. Simulated and observed (NOAA, 2013c).

To assess the influence of the Holland B parameter we simulate Hurricane Rita with a Holland B value of both 1.27 and 1.1. Figure 3-15 presents a cross-section of Hurricane Rita's simulated and observed wind and pressure field. A Holland B value of 1.1 provides the best fit, especially in the areas further away from the core. The error in peak wind estimates is negligible.

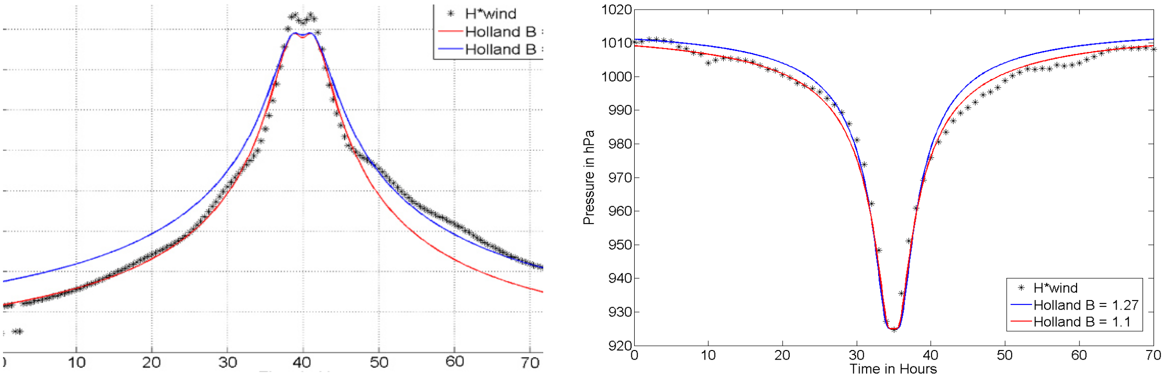

Figure 3-15 – Simulated and measured surface wind speed and pressure during Rita (2005).

3.5.2 Storm Surge Model Validation

In order to assess the validity of the storm surge at the open coast we compare simulated results to five historic storm surge records. Table 3-3 lists the five historic hurricanes, the simulated peak surge, measured peak surge and corresponding error in peak surge.

Table 3-3 – Measured and simulated storm surge for three historic hurricanes.

Hurricane	**Landfall Location**	**Peak Surge Measured**	**Source**	**Peak Surge Simulated**	**Error**
Ike	Bolivar Island, TX	4.0 meter MSL	(Kennedy, et al., 2011a)	3.4 meter MSL	- 0.6 meter
Humberto	High Island, TX	1.48 meter MSL-	(Needham & Keim, 2012)	1.4 meter MSL	- 0.1 meter
Jerry	Galveston, TX	0.96 meter MSL	(NOAA, 2013a)	1.2 meter MSL	+ 0.2 meter
Chantal	High Island, TX	2.13 meter MSL	(Needham & Keim, 2012)	1.75 meter	- 0.4 meter
Alicia	San Luis Pass, TX	3.1 meter MSL	(CND, 1984)	2.9 meter MSL	- 0.2 meter

Figure 3-16 and Figure 3-17 presents tide corrected (linear) time series of measured and simulated surge elevations during Hurricane Ike (2008) and Hurricane Jerry (1989). Time series of Hurricane Chantal, Hurricane Humberto and Hurricane Alicia are not available.

Hourly observations at the Galveston Pleasure Pier, a few kilometers East of the Radius to Maximum Winds, provide the best observed storm surge during Hurricane Jerry (NOAA, 2013a). Measured and simulated water levels during Jerry show good correlation. The model slightly underestimates the initial rise and slightly overestimates the peak surge.

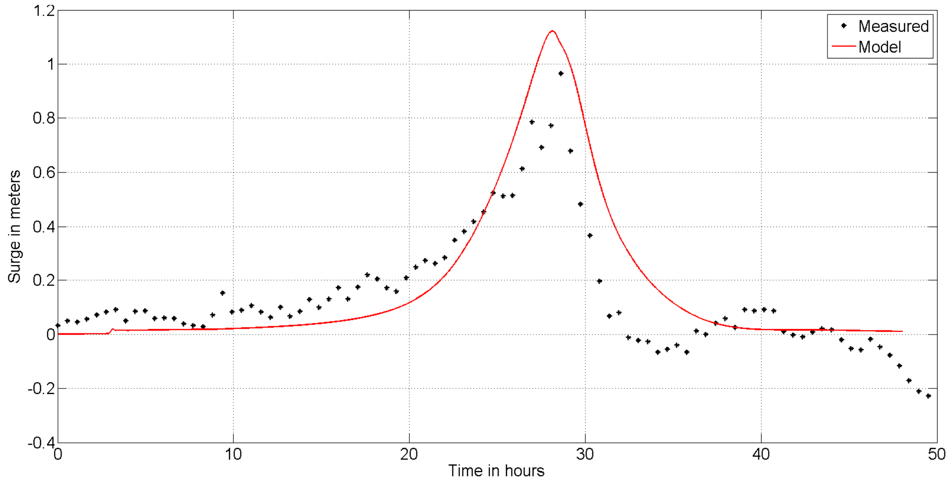

Figure 3-16 – Simulated and observed storm surge (MSL) Hurricane Jerry (1989).

During Hurricane Ike water levels were recorded at both the Pleasure Pier (NOAA, 2013a) and Bolivar Peninsula (East, et al., 2008). Hurricane Ike's storm surge was preceded by a large, unpredicted water level increase that arrived 12-24 hours prior to landfall. The early initial rise, also known as forerunner surge (Bunpapong, et al., 1985), is induced by alongshore currents propagating over a wide continental shelf. Forerunner surge is relatively infrequent and occurs when a strong, large storm moves with moderate speed over a very wide and uniform continental shelf (Kennedy, et al., 2011b). Simulations of Hurricane Ike's storm surge show poor correlation, especially during the initial rise. This can be explained by the inability of the one-dimensional model to include the forerunner surge because it does not simulate the alongshore flow component.

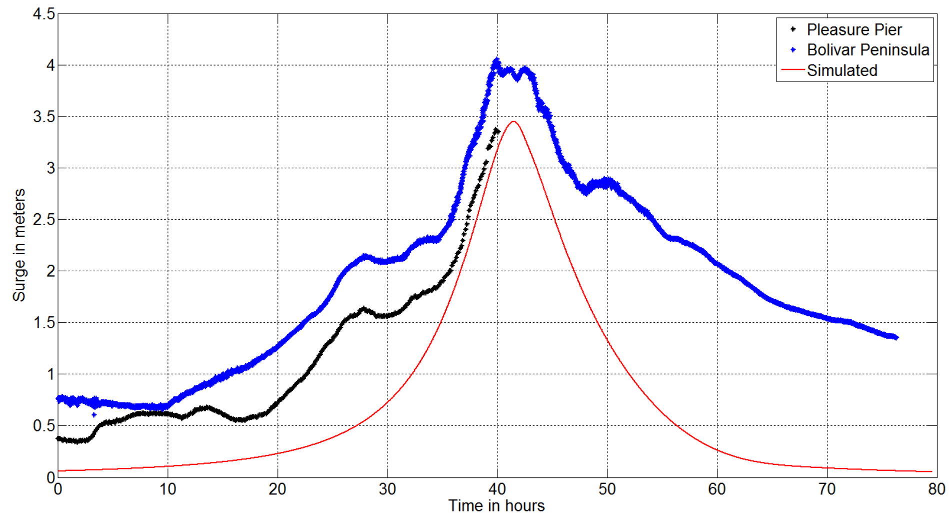

Figure 3-17 – Simulated and observed storm surge (MSL) Hurricane Ike (2008).

3.5.3 Validation of Semi-Enclosed Bay

The average depth of Galveston Bay is about 3 meter (Phillips, 2004). A long wave, propagating with forward velocity $c = \sqrt{gd}$, requires about two hours to traverse Galveston Bay. Neglecting inertia and resistance requires a sufficiently deep bay that the tide propagates across the bay instantaneously (Keulegan, 1967) (see: Figure 2-4). Historic observations during Ike (2008), Rita (2005) and Alicia (1983) (Section 2.2) confirm that the average duration of the main storm surge envelope exceeds 40 hours satisfying the time requirement.

The estimated duration of a peak surge event is about 12 hours. During peak surge water levels are already elevated resulting in a higher propagation speed within the bay. In addition, the constant depth assumption neglects the influence of the Houston Ship Channel resulting in an over-estimate of the long wave propagation time. The propagation of inflow does adhere, from an engineering standpoint, sufficiently enough to the "pumping mode" requirement.

The Bolivar Roads inlet is a few magnitudes smaller than the wavelength of both astronomical tide and storm surge. Within the channel, friction dominates inertia and storage potential is negligible compared to storage potential within Galveston Bay.

The broad-crested weir approach neglects the influence friction or bottom roughness on wide barrier islands. Figure 2-2 (Chapter 2) presented a cross section of Bolivar Peninsula. Route 87, located on the Gulf of Mexico side of the Island, is slightly elevated and thereby does represent a weir like structure. Simulations indicate that the average flow velocity remains below 1 ms^{-1}. The resistance loss on associated with a 1,000 meter wide barrier island and flow velocities near 1 ms^{-1} is estimated at 0.6 meter. The used methodology greatly overestimates barrier island overflow. The influence on model results is limited because of the relatively small total influx.

Historic surge data is limited, and often of poor quality. Surveyed surge estimates are often less accurate because in surveys the surge height is estimated based on observed high water marks. A clear example is Alicia's high water mark on the north end; a newspaper article stated that "several oil storage tanks floated away" (CND, 1984). Height surveys indicate that the oil storage tanks were located at an elevation of approximately 3.5 to 4.0 meter above MSL. Table 3-4 presents observations and hind-casts of five historic events.

Table 3-4 – Peak surge (inflow + wind set-up) in meters above MSL within Galveston Bay.

Hurricane	**North**			**South**			**West**			**East**		
	O	S	E	O	S	E	O	S	E	O	S	E
Ike	3.5	3.5	0	3.7	3.3	-0.4	3.5	3.6	+0.1	4.5	3.7	-0.8
Humberto	-	-0.3	-	-	0.4	-	0.3	0.2	-0.1	-	0.2	-
Jerry	2.0*	2.2	+0.2	0.8	1.1	+0.3	2.1*	1.8	-0.3	1.5*	1.8	+0.3
Chantal	-	-0.2	-	0.8	0.9	+0.1	1.3*	0.7	-0.4	-	0.7	-
Alicia	3.5+*	4.0	+0.5	2.2	2.5	+0.3	3.5	3.2	-0.3	-	3.2	-

O = Observed, S = Simulated, E = error in meter. *estimated post-surveyed value. Sources: (CND, 1984), (NOAA, 2013a), (NOAA, 2013d), (Hurricane Central, 2013)

Presented hind-casts of historic storms suggest that the model is typically within +/- 0.5 meter of the observed peak surge. Although an error of +/- 0.5 meter might be regarded large, it would require significantly more sophisticated models to improve accuracy.

Rego and Li (2010) simulated the "sloshing" behavior of Galveston Bay during hurricane Ike and identified a gradient of about 0.08m/km. Post processing of Ike surge-gauge datasets by East et.al. (2008) returns a maximum gradient of 0.09m/km along the East – West transect (Figure 3-18 top).

The simplified bay model slightly lags the observed values and somewhat underestimates the elevation difference between West and East. The error, albeit small, results from both parametric errors and model errors. The simulated gradient is about 0.085m/km (Figure 3-18 bottom).

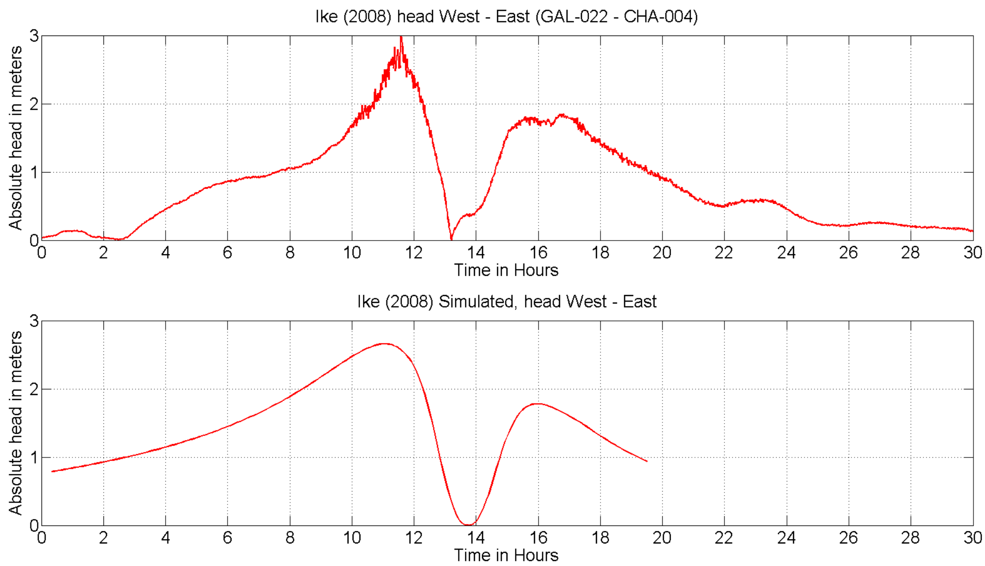

Figure 3-18 – Observed (East, et al., 2008) and simulated elevation difference along East – West transect.

3.6 Conclusion

Chapter 3 presents a one-dimensional storm surge model consisting of four components. The first component, a parametric stationary hurricane model, simulates the sustained wind velocity at gradient height. A strong correlation between simulated and observed peak wind velocity was found. The model slightly overestimates (5% - 10%) far field wind velocities. Conversion of gradient wind speed to surface wind speed requires special attention as storm surge responds in a nonlinear fashion.

The second component simulates storm surge at the open coast. The applied methodology relies on the depth integrated shallow water equations. The one-dimensional nature of the model imposes some restrictions on its applicability. Ignoring the non-linear terms, including convection, results in an underestimation of approximately 2 to 5% (Bodine, 1971). Ignoring variability in alongshore bathymetry may result in local under- or overestimates. Careful selection of the cell size $(\Delta x)_n$ and time step $(\Delta t)_i$ keeps discretization errors small (ε<5%) (Blain, et al., 1998). Computational efficiency may be improved by using multiple (unstructured) grids with varying cell-size.

The weakest aspect of the 1-dimensional model is its inability to simulate the forerunner surge. Neglecting forerunner surge will result in an underestimation of the initial rise for large, strong storms moving with moderate speed over wide continental shelves (Bunpapong, et al., 1985).

The third component simulates storm surge within a simplified semi-enclosed bay. The applied methodology requires a sufficiently deep bay and zero storage in the channel. Hindcasts of five historic events suggest that the model is typically within +/- 0.5 meter of the observed peak surge. Although an error of +/- 0.5 meter might be regarded large, it would require significantly more sophisticated models to improve accuracy.

The storm surge model is expected to return a somewhat conservative estimate of storm surge within semi-enclosed bays. It is expected to over-estimate wind set-up because the model assumes stationary wind set-up, which is not completely true. Selection of several parametric values requires careful attention. It is important to emphasize the assumptions, initial conditions and neglected processes.

Chapter 4. Deterministic Application to Galveston Bay

This chapter describes a deterministic application of the storm surge model. A series of sensitivity experiments is conducted to assess the influence of parameter and model uncertainty. Section 4.1 treats the deterministic methodology. We assess the influence of landfall location on storm surge in Section 4.2. Section 4.3 discusses the relation between bay depth, wind set-up and additional inflow of water. Sections 4.4 and 4.5 treat the sensitivity of storm surge to a selection of constant model parameters. Section 4.6 concludes our findings.

4.1 Deterministic Methodology

In the previous Chapter, we briefly introduced the error term ε that includes, among others, errors because of model uncertainty and parameter uncertainty. Parameter uncertainty comes from model parameters whose exact value and distribution are unknown. Examples include bottom roughness and the gradient/surface wind parameter. Model uncertainty results from schematizations and simplifications introduced during model development.

In this Chapter, we assess both types of uncertainty by means of a partial sensitivity analysis. To assess the sensitivity of storm surge to errors in data and parameter selection we construct a synthetic parametric hurricane (Table 4-1). The estimated return interval of the surge at the open coast generated by the hurricane is estimated at 1/100 yr^{-1} along a 200-kilometers stretch of coast (See: Appendix B). The parametric hurricane is synthesized following the methodology outlined in Section 3.2. At most one parameter varies in each sensitivity analysis.

Table 4-1 – Hurricane and Model Parameters used in deterministic analysis.

Hurricane Parameter	**Value**
Core Pressure	950 hPa
Radius to Maximum Winds	30 km
Forward Velocity	5 ms^{-1}
Vsurface / Vgradient	0.73 [-]
Landfall Location	50 km West
Angle of Approach	90 degrees

Model Parameter	**Value**
Bay Depth	3 .0 meter
Bay Area	1400 km^2
Inlet width	2800 meter
Inlet depth	9.0 meter
Chezy	40 (Manning 0.035)
Barrier Island Elevation	1.5 meter

4.2 Sensitivity to Landfall Location

To determine the relation between landfall location and storm surge within the Bay we synthesize a single storm with the parameters listed in Table 4-1.

After generating the parametric wind and pressure fields, the hurricane is moved onshore along one of four tracks (A, B, C and D) presented in Figure 4-1. The lateral distance of track A, B, C and D is respectively 100km West, 50km West, 50km East and 100km East relative to the central bay axis. Locations denoted with North, West, East or South referenced in Figure 4-1.

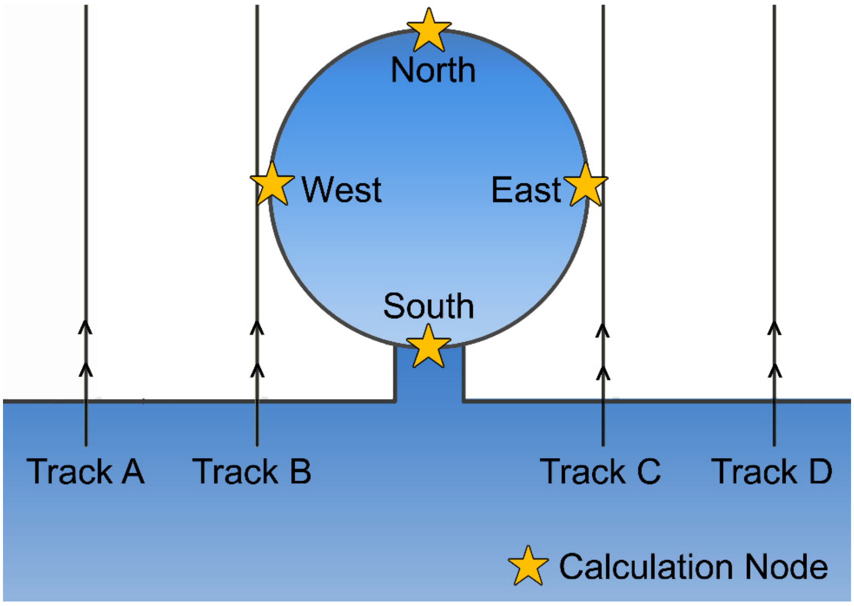

Figure 4-1 – Synthetic hurricane tracks A, B C and D.

Figure 4-2 presents storm surge levels within the bay for track A and track C. Track A represents the most severe condition, where the strongest winds blow onshore while the surge at the inlet is at its peak.

The combination of inflow and wind set-up within the bay exceeds the surge at the open coast for track A. Inflow contributes approximately 75% to the peak surge while local wind set-up contributes about 25% to the surge. Prior to landfall, the easterly winds cause a set-up on the west bay end and a set-down on the east end. At landfall winds are predominantly directed North resulting at a set-up within the upper bay region. After landfall the dominant wind direction becomes westerly resulting in a set-up on the eastern bay end.

Strong Northerly winds associated with storms traversing track C depress surge within the bay but do cause significant elevated water levels near the downwind edge of the bay. Inflow contributes approximately 50% to the surge.

Track A: 50 kilometers West | Track C: 50 kilometers East

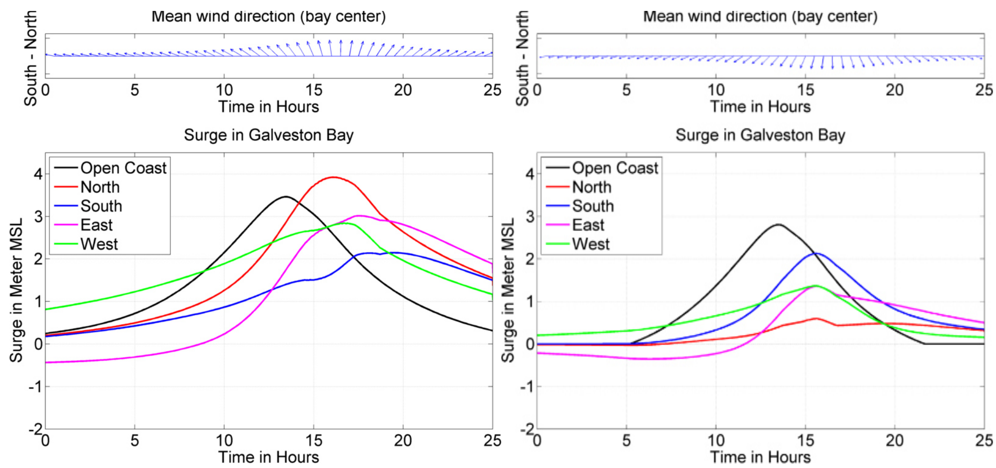

Figure 4-2 – Surge within the Bay; 50 kilometers West (left) and 50 kilometers East (right).

Figure 4-2a clearly shows the impact of the assumed quasi-steady relation between inflow and wind set-up. The simulated hydraulic head between the open coast and the bay is larger than observed during historic events (see Section 2.2). As a result the model somewhat over-estimates inflow, and somewhat underestimates wind set-up.

Figure 4-3 presents storm surge levels with in the bay for track B and D. The overall pattern is similar to track A and C. The surge at the open coast is slightly lower when compared to track A and C. The surge within the bay is significantly lower as the bay is not exposed to the strongest winds.

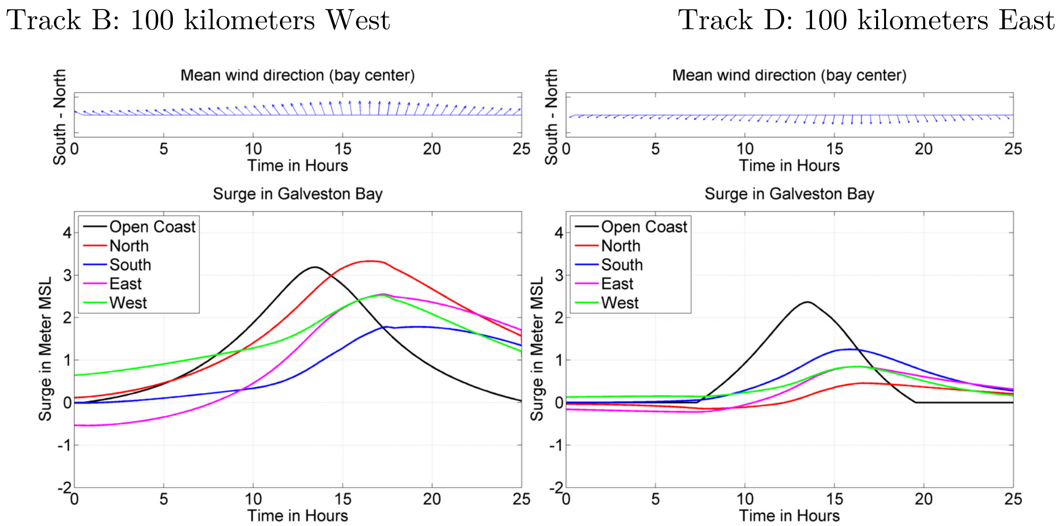

Figure 4-3 – Surge within the Bay; 100 kilometers West (left) and 100 kilometers East (right).

Obtained results confirm the presumptions mentioned in Section 2.2. Landfall location profoundly influences the behavior surge within the bay. Uncertainty that originates from landfall location is included in the probabilistic application presented in Chapter 5.

4.3 Sensitivity of Wind Set-up to Inflow

Wind set-up within lakes or semi-enclosed bays is a function of the wind velocity, fetch and water depth (See: Paragraph 3.3.2). The magnitude of wind set-up is inversely proportional to depth; the largest set-up may be expected in shallow lakes. To assess the influence of elevated bay levels on wind set-up we perform surge simulations for a closed basin under hurricane forcing (Table 4-1), with elevated bay levels of respectively 0, 1, 2 and 3 meter. The "inflow", schematized by an elevated bay level, is assumed to behave quasi-steady with respect to the wind set-up (see: 3.4). Wind set-up within the bay is simulated with a local depth dependent solution.

Previous assessment of landfall location showed that the most severe surge may be expected at the northern and western bay end. Figure 4-4 illustrates the relation between inflow, wind velocity and peak surge at the north and west end within the Bay.

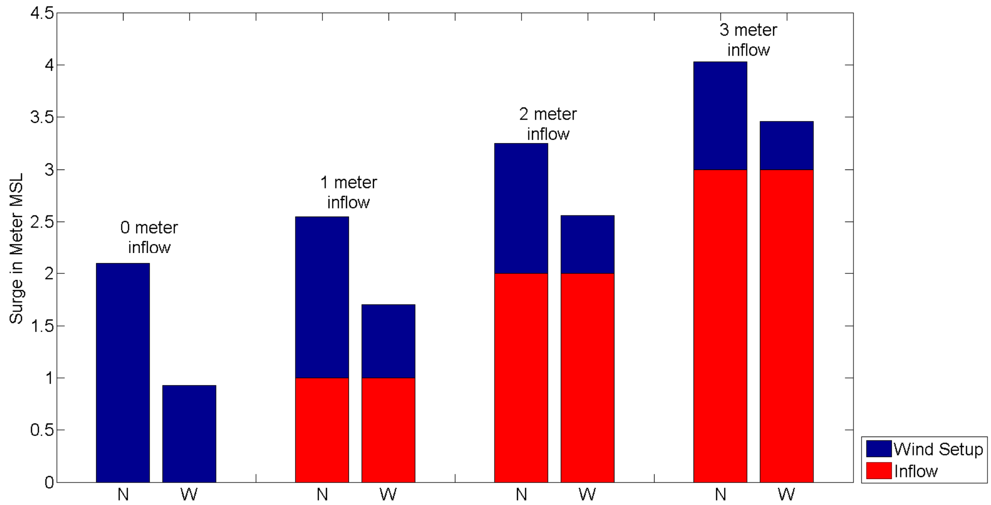

Figure 4-4 – Wind set-up at the north end and west end of a semi-enclosed bay (depth 3 meter) for different levels of bay elevation.

Figure 4-4 does confirm that the magnitude of wind set-up decreases with increasing depth. In addition, Figure 4-4 indicates that additional inflow results in an increased surge within the bay. The relative increase in peak surge for each additional meter of inflow increases exponentially. For a shallow bay a small increase in mean water level does not result in significant higher peak surge.

4.4 Hurricane Model Sensitivity

Most parameters used to construct synthetic storms follow from a statistical analysis of historic storms. The variation of these parameters is included in the probability density functions used in the probabilistic simulations (Chapter 5). Exceptions are the Holland B parameter, which is assumed equal to 1.27 offshore and 1.0 onshore, and the surface wind velocity, which is assumed equal to 0.8 times the average boundary layer wind velocity.

4.4.1 Gradient Wind to Surface Wind

The sensitivity to variations in the gradient to surface wind conversion parameter, V_s/V_g, is evaluated by simulating five identical storms with a different surface/gradient conversion parameter. The deterministic value used in the model is $V_s/V_g = 0.73$ [-], while the estimated range is 0.65 – 0.85.

Figure 4-5 presents the influence of a -10%, -5%, 0, +5% and +10% variation in V_s/V_g. A larger wind conversion parameter, and thereby surface wind velocity, increases the surge significantly. A 10% increase in the conversion parameter yields a 16% increase in surge at the open coast. Previously mentioned behavior was expected due to the nonlinear relation between wind velocity and storm surge.

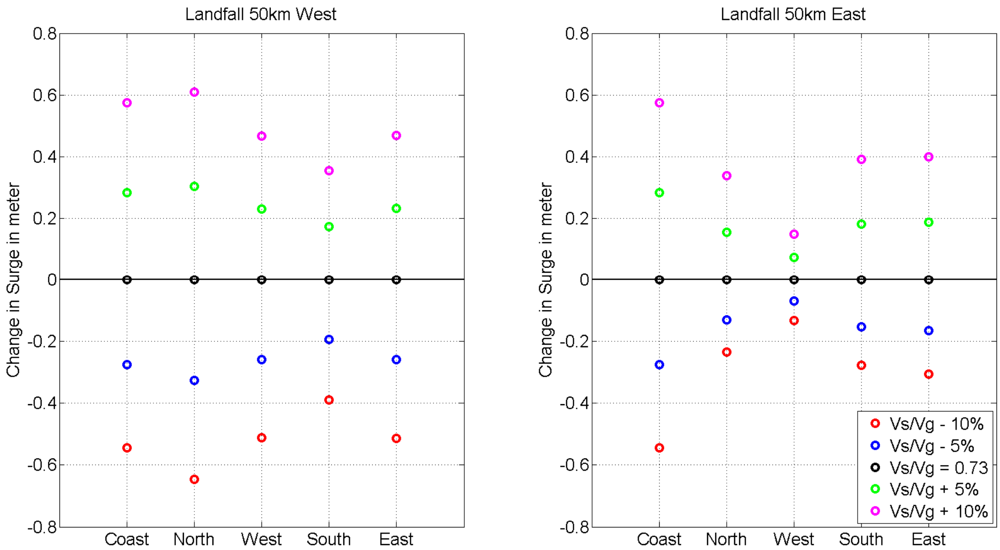

Figure 4-5 – Relation between storm surge and the wind conversion parameter.

Storm surge generated by hurricanes that follow a westerly track is susceptible to variations in V_s/V_g. For such storms, the strong onshore winds amplify the surge within the bay. Storms traversing along an Easterly track are less susceptible to variations because the associated off-land wind velocities are significantly lower while wind set-up tends to limit inflow.

The actual ratio of V_s/V_g varies with each storm, location and time. It must be noted that varying the wind velocity as opposed to the conversion parameter yields similar results.

4.4.2 Holland B parameter

Sensitivity to variation in B, also known as Holland B or storm peakedness, is evaluated by simulating five almost identical storms that solely differ because of variations in storm peakedness. The default offshore value is B = 1.27. Resio et al. (2007) find that the B parameter for storms within the Gulf of Mexico varies between 0.9 and 1.6. Runs are made with deviations of -20%, -10%, +10% and + 20% which corresponds to the observed range.

Figure 4-6 presents an almost linear negative relationship between variations in the B parameter and storm surge. This finding is in agreement with findings by Irish et al. (2009) who obtained a similar result. An increase in B results in a lower peak wind velocity and a decrease in surge at the open coast. Inflow is inversely related to the B parameter.

For a Westerly track, the delicate balance between inflow and wind set-up amplifies the influence of variations in the B parameter. The strongest effects are observed near the southern end. At the Northern boundary the influence of local wind set-up reduces the impact of variations.

For an Easterly track variations in surge show a similar pattern albeit winds are not as strong. Because of timing the surge near the west end of the bay is not as sensitive to variations in B. Locations that are dominated by wind set-up are more sensitive to variations in the B parameter. Surge arising from storms traversing along a Westerly track is slightly more sensitive to variations in B. Varying a normal distributed B parameter would introduce a slight bias towards increasing the surge in a probabilistic application.

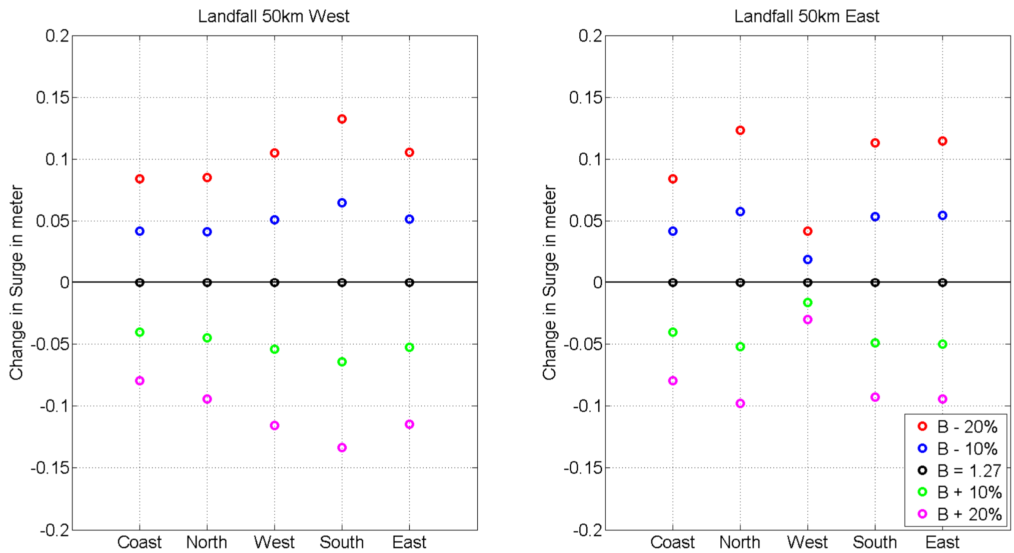

Figure 4-6 – Relation between storm surge and variations in Holland B.

4.5 Storm Surge Model Sensitivity

Storm surge within a semi-enclosed bay is a function of local wind set-up and surge at the open coast. Simplifications introduced in model development required a few deterministic parametric assumptions. These parameters include fetch, inlet roughness and barrier island height.

4.5.1 Fetch

Fetch is the distance across the water that a given wind travels. The simplified model employs a fetch of 30 kilometers, which is the average of the maximum fetch in Galveston Bay. To assess the sensitivity to variations in fetch we synthetize one synthetic storm (Section 4.1) and subsequently perform a series of ten simulations.

Figure 4-7 presents the relation between storm surge and fetch. As expected, a longer fetch results in a larger surge. Variations in fetch have limited influence on storm surge generated by storms making landfall east of the bay. The predominantly off-land directed winds cause a set-down in the upper bay area and a set-up in the lower bay area. A larger fetch increases the wind set-up at bay side of the inlet, which reduces the inflow. Although a larger fetch results in more set-up, it also decreases inflow and thereby reduces the average bay elevation. Peak surge follows from this delicate balance between surge at the open coast and wind set-up.

Surge arising from storms traversing along a westerly track is slightly more sensitive to variations in fetch. Variations in fetch do not influence surge near the southern boundary as much because the surge is primarily a function of the surge at the open coast. For such storms, a 10% decrease in fetch results in a 5 to 6% decrease in surge. The surge response exhibits slight nonlinear behavior that originates from the non-linear relation between wind set-up and inflow.

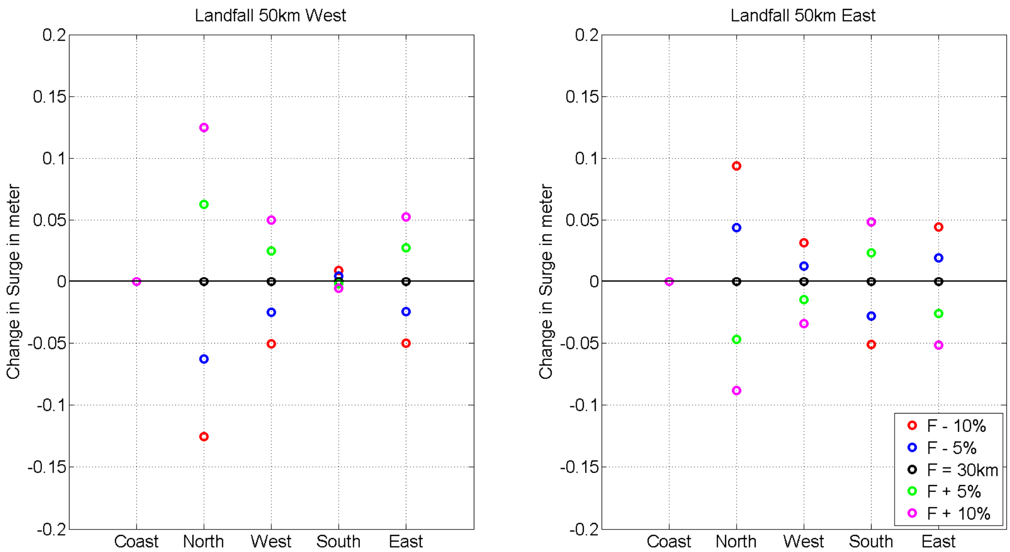

Figure 4-7 – Relation between storm surge and fetch.

4.5.2 Friction Factor Inlet

Channel roughness, or friction, contributes to turbulence in channels, which reduces the flow capacity. Friction is often expressed by a single friction parameter. The model assumes constant friction, represented by the Chezy coefficient. The selected representative value is 40 $m^{1/2}s^{-1}$, which is equal to a Manning factor of about 0.035 $sm^{-1/3}$. To assess the sensitivity of storm surge within the Bay to variations in inlet roughness we perform three simulations for C = 32 (rough channel), C = 40 (normal channel) and C = 48 (smooth channel).

Figure 4-8 presents the relation between variations in the Chezy coefficient and storm surge within the bay. A larger Chezy coefficient (lower friction) results in a larger influx and thereby a higher still-water surge within the bay. For a westerly track, the largest impact is observed near the west end. Peak surge at the west end is profoundly affected by variations in initial rise. The impact is positively related albeit lower for other locations within the bay. An increase in inflow and subsequent increase in depth results in a reduction of wind set-up within the bay.

For an easterly track, variations in Chezy have limited influence on surge within the bay. The relation between wind set-down, inflow and timing of peak surge at a specific location is important. The largest impact is observed near the north end. Additional inflow increases the still-water surge, which in turn decreases wind set-up. The reverse is true for the southern boundary. Surge arising from storms traversing along a westerly track is significantly more sensitive to variations in inlet friction. In a probabilistic analysis, the error is expected to decrease the surge.

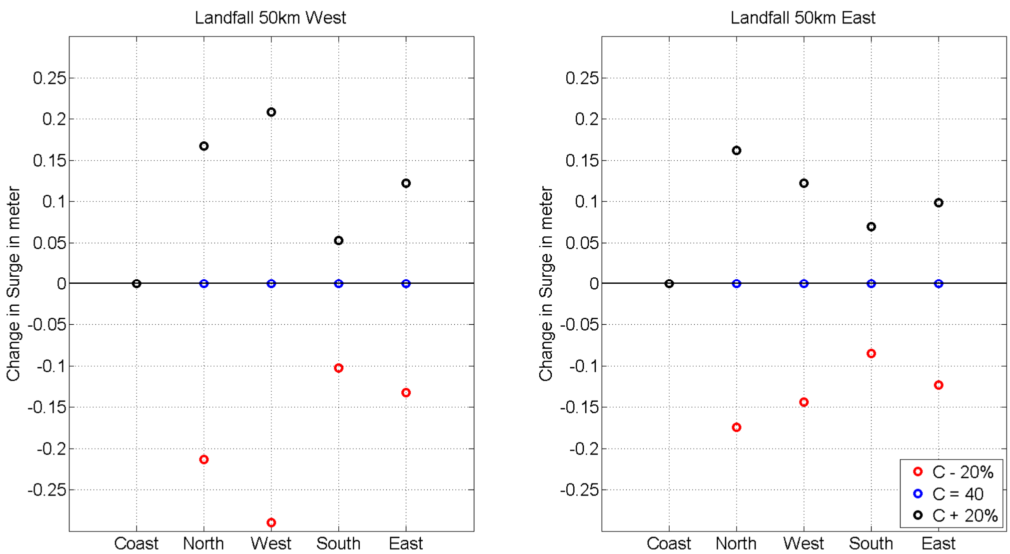

Figure 4-8 – Relation between storm surge and inlet friction.

4.5.3 Barrier Island Elevation

Overflow and overwash of the barrier islands contributes to the inflow of surge into the bay. Simulations show that Ike's storm surge would have been much worse with lower barrier islands (Arcadis US, 2011; Rego & Li, 2010). The model assumes a fixed barrier height of 1.5 meter, based on the average elevation of the barrier islands. The average elevation is derived from a Digital Elevation Model (DEM, Appendix C) with a vertical accuracy of 0.2 to 0.3 meter. To assess the sensitivity of storm surge within the bay to barrier island elevation we perform three simulations with barrier island elevations of 1.0 meter, 1.5 meter and 2.0 meter.

Figure 4-9 presents the relation between surge and barrier height. Barrier height and inflow are negatively related, an increase in height results in a decrease in inflow. The behavior for western landfalls looks suspicious; one would expect a more significant response for a lower barrier. A closer analysis of the surge time series indicates that a by increased depth induced reduction in wind set-down reduces the hydraulic head over the barrier islands. Although the still-water elevation rises significantly, the balance between wind set-up and depth reduces the overall impact. An increase in barrier island elevation yields a significantly lower inflow because both the duration and the magnitude of the inflow decreases.

Results obtained for landfalls east of the bay show slightly different behavior. Wind set-up near the south end limits the hydraulic head. Lower barrier islands do result in a higher still-water elevation within the bay. The still water elevation within the bay increases for decreasing barrier island elevation, while wind set-up decreases with increasing depth. Depending on peak-surge timing, the relationship between inflow and set-up limits the impact of variations in barrier island elevation. The overall impact of barrier island overflow is limited.

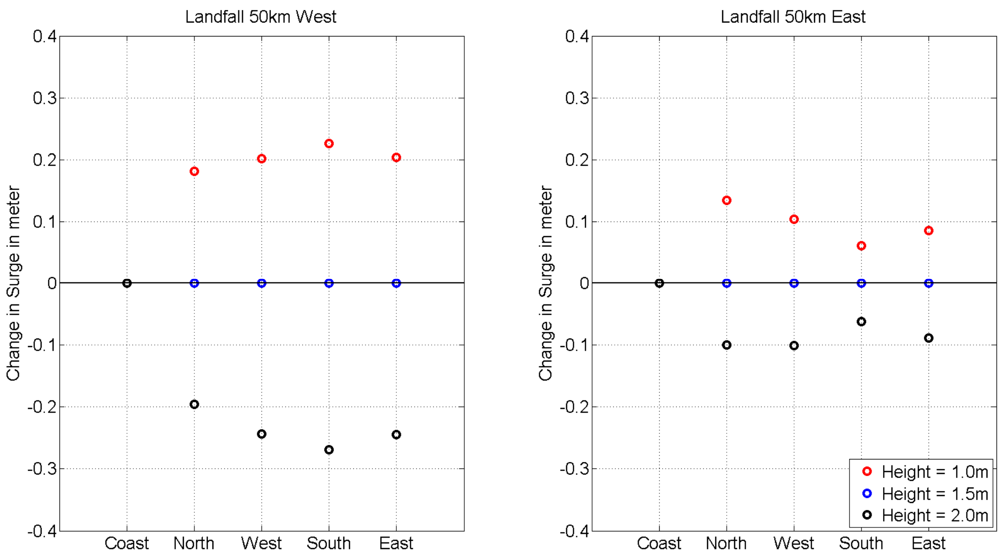

Figure 4-9 – Relation between storm surge and barrier island height.

4.6 Conclusion

Hurricane surge heights in coastal bays are highly sensitive to storm path and landfall location. Landfall west of Galveston Bay tends to result in the highest surges as Galveston Bay encounters the strongest winds in on-shore direction. A landfall location one Radius to Maximum Winds (RMW) west of Bolivar Roads marks the most severe scenario with the highest storm surge at the bay entrance and maximum wind set-up within Galveston Bay.

The mean water level within the bay depends on a delicate balance between inflow and wind set-up within the bay. The beneficial inverse proportionality between bay depth and wind set-up results in a relatively low impact of inflow. During severe storm events, an increase in mean water level from 3 to 4 meter results in a 0.3 to 0.5 meter higher peak surge along the bay shoreline. The beneficial influence diminishes rapidly with increasing depth.

The quasi-steady relation between inflow and wind set-up implies an instantaneous distribution of influx over the bay. In reality, water does not spread instantaneously. The model is expected to under-estimate the impact of inflow near the inlet, and over-estimate the impact of inflow near the northern boundary. As a result the model will over-estimate inflow, and under-estimate wind set-up within the bay. The magnitude of this model error depends on the configuration of both track and storm.

The sensitivity analysis indicates that surge generated by storms making landfall west of the bay is more prone to errors. For such storms, wind set-up amplifies the surge in the bay and thereby the parametric error. The relative sensitivity of specific locations depends on both timing, points that attain peak-surge after landfall show a profoundly different behavior than points that attain peak-surge prior to landfall. Variations in the gradient/surface wind conversion parameter V_s/V_g have a major impact on storm surge. A 10% increase in surface wind velocity results in a 16% higher surge at the open coast and a 10% to 18% higher surge within the bay. Storms that make landfall to the East of the bay are somewhat less susceptible to variations in V_s/V_g because the associated off-land wind velocities are significantly lower.

The parametric error increases with increasing storm intensity. The largest parametric error may be expected for the low probability high intensity events. The parametric uncertainty increases with decreasing storm probability. Although dependent on the exact representation of the parameters involved, we may expect a parametric error induced increase of surge in a probabilistic application.

Chapter 5. Probabilistic Application to Galveston Bay

The previous chapters presented the development, validation and deterministic application of a one-dimensional storm surge model. In this chapter, we utilize a probabilistic method to apply the storm surge model to various scenarios. Section 5.1 outlines the used methodology. Section 5.2 treats the probabilistic validation of the model developed in previous chapters. In Section 5.3 we perform probabilistic simulations for various scenarios. Section 5.4 presents a set of inundation maps and Section 5.5 concludes our findings.

5.1 Probabilistic Methodology

The probabilistic methodology outlined in this chapter addresses the uncertainty associated with long-term flood risk. Assessing the long-term risk of hurricanes is problematic because of the limited availability of historical records (Emanuel & Jagger, 2010). A probabilistic simulation provides a quantified statement on the probability of flooding within a timeframe. The most significant source of uncertainty is uncertainty about the events that will occur within the timeframe of interest. This type of uncertainty is captured by the probabilistic method, which re-samples or bootstraps the original sample distributions.

Resampling the original sample distributions requires the assumption that the suite of historic observations represents true climatology. To keep the error originating from both sample size limitations and spatial variability to a minimum the optimal spatial sample size was determined following Chouinard et al. (1997). The influence of climatologic uncertainty is significant and increases with a decreasing probability of occurrence (Resio, et al., 2009). Quantified statements about the magnitude of the error are not available since this would require data on the future storm population. The sample of historic storms is assumed to represent the long-term climatology.

The probabilistic approach utilizes a Monte Carlo bootstrap methodology to construct a realistic suite of synthetic events. Following Resio et al. (2009) and IPET (2009) storm surge at the open coast is parameterized as a function of the pressure deficit Δp, Radius to Maximum Winds RMW, storm translation velocity V_f, angle of approach θ_i, Holland parameter β, distance from landfall location x and an error term ε_c (Eq. 5.1). Other model parameters are assumed constant. The surge at the open coast, η_{coast}, is a function of;

$$\eta_{coast} = \varphi(\Delta p, RMW, V_f, \theta_i, \beta, x) + \varepsilon_c \qquad \text{Eq. 5.1}$$

where the error term ε includes errors because of sampling uncertainty, model uncertainty, parametric uncertainty, non-linear tide interaction and non-linear bottom friction.

Synthetic storms are constructed by random selection of storm parameters from empirical joint probability density functions. Storm intensity, forward speed and landfall location are generated by selecting a random value between 0 and 1, and subsequent entering the parameter distribution function at the random generated location. The Radius to Mean Winds is selected randomly from a, depending on storm intensity, truncated probability distribution function. The angle of approach is assumed constant.

Upper and lower limits of the parameters that describe the Joint Probability Density Function (JPDF) are listed in Table 5-1. Probability Density Functions are presented in Appendix B. The astronomical tide is included by simulating a full hurricane season of tidal harmonics and subsequent entering the tidal harmonics at a random time. A list of tidal constituents is appended in Appendix C.3. Figure 5-1 summarizes the applied methodology.

Table 5-1 – Upper and Lower limit of parameter distributions.

Parameter	**Distribution**	**Lower Limit**	**Upper Limit**
Central Pressure	Gumbel	990 hPa	880 hPa
RMW	Lognormal	25 km	25 + 0.3(110 - Δp) km
Forward speed	Gumbel	2 ms^{-1}	15 ms^{-1}
Landfall Location	Uniform	- 200 km - RMW	200 km - RMW
Astronomical Tide	Uniform	0 days	120 days
Wave Set-up (R)	Uniform	0.10	0.15

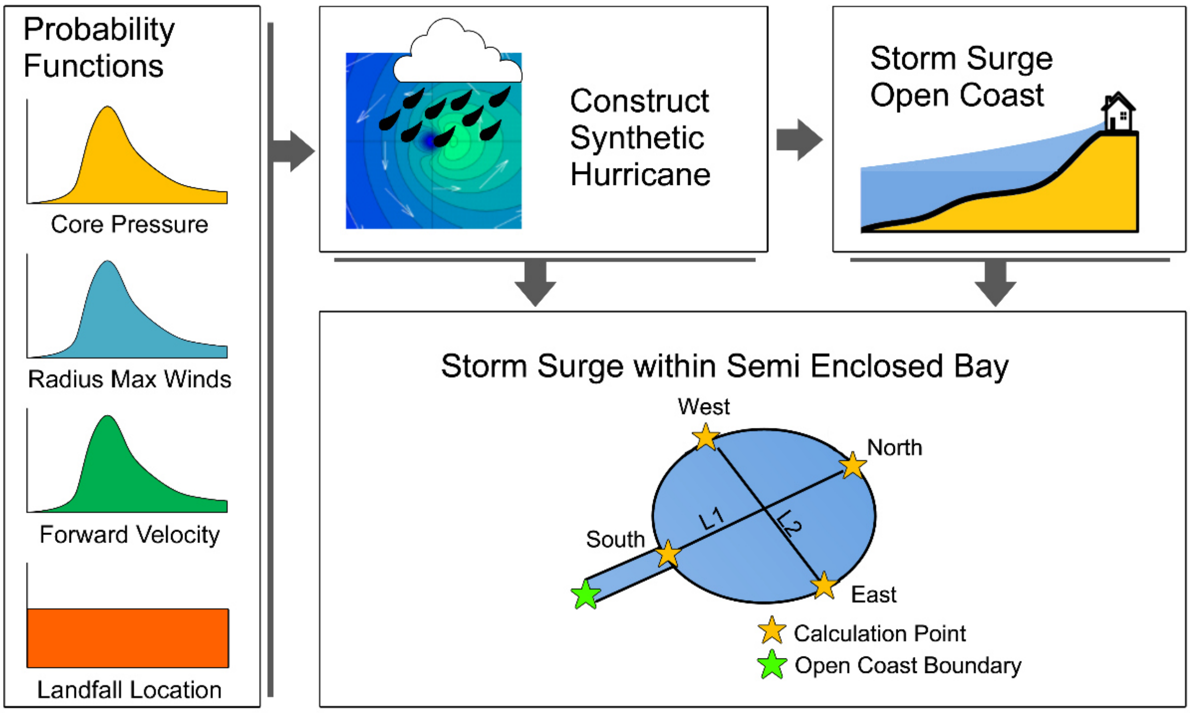

Figure 5-1 – Probabilistic Methodology.

The Monte Carlo method yields a large number of plausible independent surge events. To determine the exceedence probability of storm surge the obtained results are arranged in decreasing order with a second column showing the ranked position. Subsequent application of the probability paper methodology due to Gringorten (1963) as treated by Shaw (1983) provides the probability of exceedence $P(\eta)$ per event;

$$P(\eta) = \frac{i - 0.44}{n + 0.12} \qquad \text{Eq. 5.2}$$

where $P(\eta)$ [-] is the probability of a surge equal to or exceeding η, i [-] is the sorted position of the extreme and n [-] is the total number of events.

The return period $RP(\eta)$ of an event with a surge equal to or exceeding η is obtained by;

$$RP(\eta) = T_s \cdot \frac{1}{P(\eta)} \qquad \text{Eq. 5.3}$$

where $RP(\eta)$ [yr^{-1}] is the return period of an event with a surge equal to or exceeding η, T_s is the average time between events and $P(\eta)$ [-]is the probability of a surge equal to or exceeding η.

5.2 Probabilistic Model Validation

In order to assess the overall accuracy of the model we perform a probabilistic validation of storm surge at the open coast. The probabilistic results are subsequently compared to return periods found in literature. A probabilistic validation of storm surge within the Bay is not feasible because of the lack of accurate observations. Often, recurrence intervals of storm surge are expressed as a function of the Saffir-Simpson scale, although the correlation between surge magnitude and hurricane categories is rather weak (NHC, 2012; Resio & Westerink, 2008).

Table 5-2 lists estimates of the one percent per year surge event found in literature. The large variation in estimated surge elevation results from spatial domains, temporal domains and statistical methods. A larger domain significantly increases the probability of encountering higher extremes. The method and domain used by Bodine (1969) and Davis (1966) are similar to the methods used in this report.

Table 5-2 – Recurrence interval of $1/100$ year^{-1} storm surge at the open coast near Galveston.

1 per 100 year event	**Statistical Methodology**	**Spatial Domain**	**Temporal Domain**	**Source**
3.6 meter	Statistical analysis (POT) of tide records near Galveston.	Local	1900-1963	(Bodine, 1969)
4.5 meter	Statistical analysis (POT) of tide records at Bolivar Roads inlet.	Local	1900-1960	(Davis, 1966)
6 meter	Statistical analysis (POT) of historical observations on the Upper Texas Coast.	Upper Texas Coast	1880-2010	(Needham & Keim, 2012)
2.7 meter	GEV fit of annual max at Galveston Pleasure Pier.	Local	1960-2012	(NOAA, 2013)

Figure 5-2 presents the simulated probabilistic results. The simulated probabilistic return periods lie well within the range of the estimates found in literature.

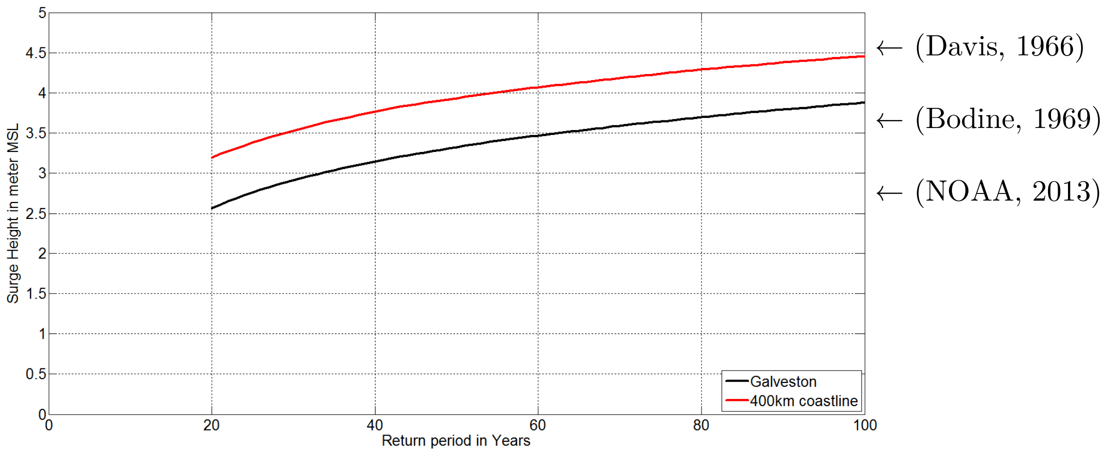

Figure 5-2 – Return period of storm surge at Galveston and along a 400km stretch of coast.

5.3 Probabilistic Simulations

Following above methodology the model is initiated for a suite of 10^6 synthetic storms. The simulation yields approximately 100 independent 10^4 yr^{-1} events that together form the average 10^4 yr^{-1} event. A total of two simulations are performed;

Simulation 1: Baseline;
Present or current situation. Used as reference scenario. Can be validated with historic observations.

Simulation 2: Coastal spine;
Baseline simulation without exchange of water between the Gulf of Mexico and the simplified bay. Used to investigate bay behavior in the hypothetical case of a structure (coastal spine) that prevents interaction between the bay and the Gulf of Mexico.

Obtained results are subsequently processed with Eq. 5.1 and Eq. 5.2. A statistical extreme-value analysis of the synthetic baseline simulation is provided in Figure 5-3. The surge at the northern end exceeds the estimated surge at the open coast for each recurrence interval. Surge at the west, south and east end tends to be lower than the surge on the open-coast.

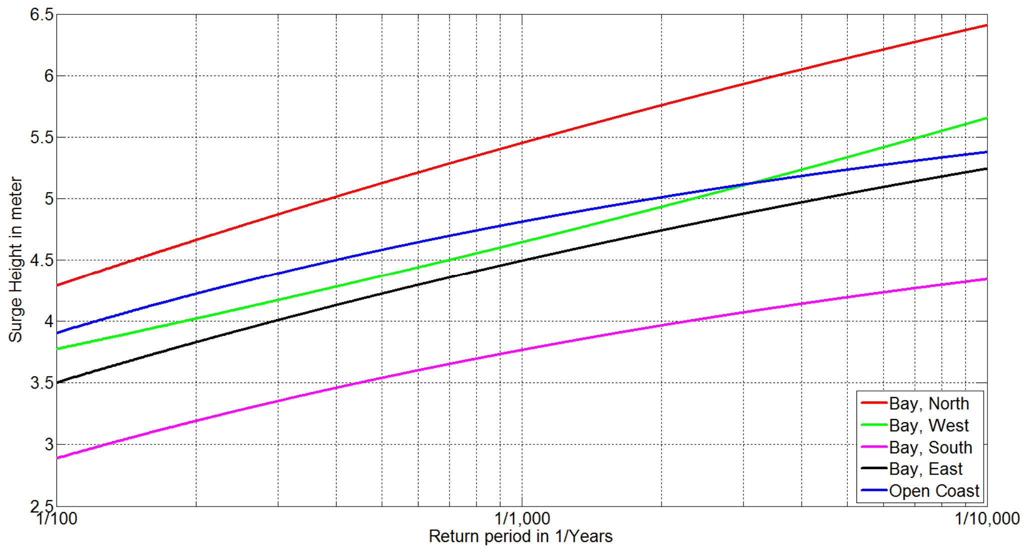

Figure 5-3 – Return interval of surge at the open coast and within the bay.

Table 5-3 to Table 5-5 present the estimated surge heights for the 1/100 yr^{-1}, 1/1,000 yr^{-1} and 1/10,000 yr^{-1} events. Simulations indicate that the typical 1/100 yr^{-1} water level elevation at the open coast equals 4 meter. The typical 1/100 yr^{-1} storm surge at the north end of the bay equals about 4 meter without and 2 meter with a coastal spine. The 1/10,000 yr^{-1} surge at the north end equals about 6.5 meter without and 3.5 meter with a coastal spine. It is important to note that the 1/10,000 yr^{-1} event at the open coast does not have to be the same event as the 1/10,000 yr^{-1} event at one of the locations within the bay.

Table 5-3 – 1/100 yr^{-1} water level elevation.

ID	Simulation	Open Coast	North	South	West	East
S1	1. Baseline	3.9 m	4.2 m	2.9 m	3.6 m	3.4 m
S2	2. Coastal Spine	3.9 m	1.8 m	1.1 m	1.4 m	1.0 m

Table 5-4 – 1/1,000 yr^{-1} water level elevation.

ID	Simulation	Open Coast	North	South	West	East
S1	1. Baseline	4.9 m	5.5 m	3.8 m	4.7 m	4.5 m
S2	2. Coastal Spine	4.9 m	2.8 m	1.8 m	2.2 m	1.8 m

Table 5-5 – 1/10,000 yr^{-1} water level elevation.

ID	Simulation	Open Coast	North	South	West	East
S1	1. Baseline	5.4 m	6.4 m	4.4 m	5.7 m	5.3 m
S3	2. Coastal Spine	5.4 m	3.5 m	2.3 m	3.0 m	2.5 m

Table 5-5 indicates that even without inflow significant surge may be expected. The model employs a method with fixed vertical boundaries and an average depth. In reality, many basins have time-dependent moving boundaries while depth varies locally. Under ordinary conditions, without barrier, the influence of the vertical boundary assumption remains small. Wind set-up contributes only 25% to 50% to the surge. The absolute value of wind set-up during hurricane conditions is about 1 to 1.5 meter.

A closed system without exchange between the Gulf of Mexico and the bay is more prone to the vertical boundary assumption. Obtained results indicate wind set-up may approach local depth, which defies the range of applicability of the methodology. An analytical analysis indicates the model will somewhat over-estimate wind set-up within a closed bay. Obtained results for the 1/10,000 yr^{-1} surge within a closed basin should be interpreted with the greatest care.

5.4 Max Envelope Of Water

Previous section presented the recurrence interval of storm surge within Galveston Bay. The cost benefit analysis conducted in Chapter Six requires the depth and extent of flooding on the coastal floodplain. A first-estimate indicative inundation map can be obtained with the "bathtub" or still-water surge method by Eastman (1993). The still-water surge method assumes that surge on the floodplain can be modelled as a flat plain with a surface elevation equal to the surge at the shoreline.

Derivation of the inundation layers relies on ArcGIS ® by ESRI. Gridded elevation data is obtained by converting the DEM (Appendix C-2) to a 100x100 meter grid using a bilinear sampling method. The simulated surge elevation points are mapped to the bay (Figure 5-4). The surge elevation in the area between two points is interpolated using a nearest neighbor interpolation method. The inundation depth at a specific location is obtained by intersecting the elevation grid and the surge grid.

Figure 5-4 presents the 1/100, 1/1,000 1/10,000 yr^{-1} Max Envelope Of Water (MEOW). A MEOW does not depict the surge extent for a specific hurricane, it illustrates the area that is under threat of all hurricane scenarios within a timeframe. The obtained inundation pattern for a 1/100 yr^{-1} event shows pattern similar to the existing FEMA Q3 floodmaps (FEMA, 2013a).

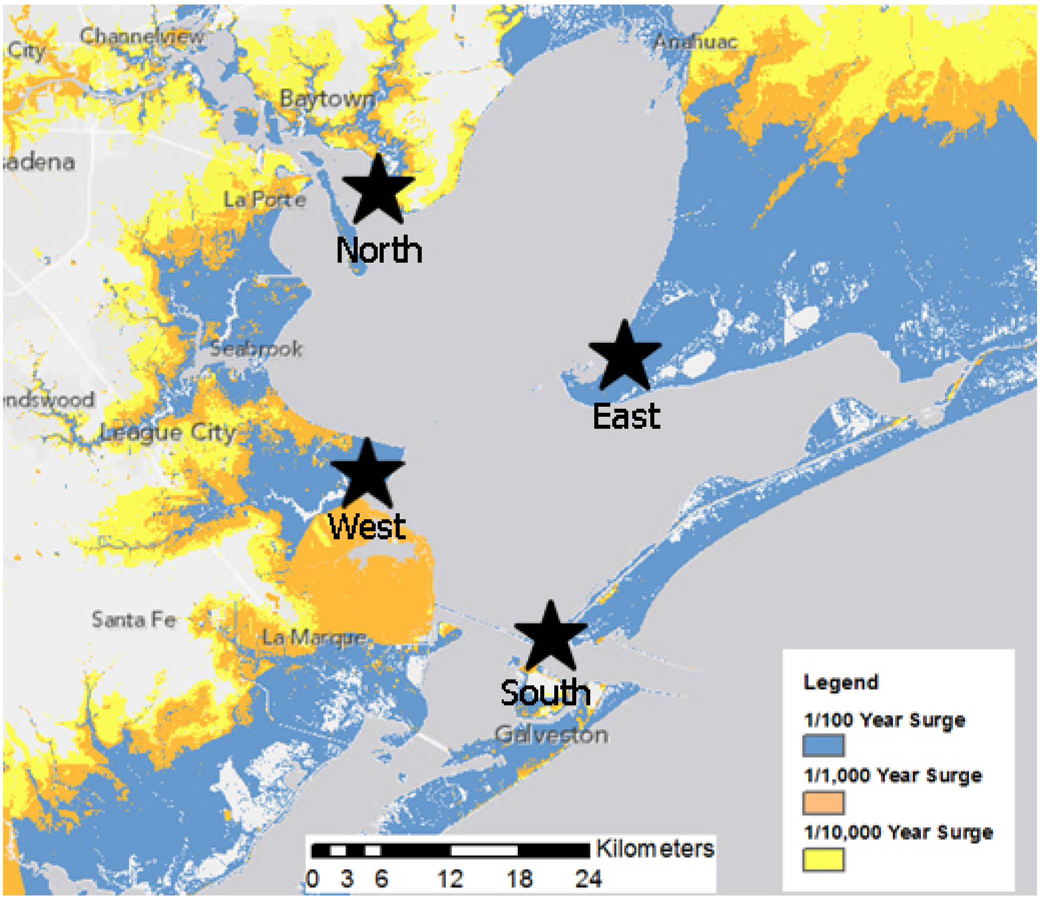

Figure 5-4 – Present day simulated 1/100, 1/1,000 and 1/10,000 yr^{-1} MEOW for Galveston Bay.

5.5 Conclusion

In this chapter, we conducted a series of probabilistic simulations to assess the probability of flooding within Galveston Bay. Probabilistic validation of storm surge at the open coast indicates that the model performs reasonably well. The estimated return periods of storm surge at the open coast lie well within the range of estimates listed in literature.

Additional simulations indicate that surge within the bay exceeds surge at the open coast at least once per 100 year. The 1/1,000 yr^{-1} and 1/10,000 yr^{-1} surge at the north end exceeds the surge at the open coast by respectively 0.5 and 1.0 meter. A coastal spine significantly reduces surge within the bay. Results do indicate that even with a coastal spine wind set-up within the bay may result in local flooding. The 1/1,000 yr^{-1} event at the open coast does not have to be related to the 1/1,000 yr^{-1} event within the bay. We can summarize the findings as follows;

- The 1/100 yr^{-1} or less probable event at the north end exceeds the 1/100 yr^{-1} or less probable event at the coast.
- The 1/10,000 yr^{-1} or less probable event at the west end exceeds the 1/10,000 yr^{-1} or less probable event at the coast.
- A 1/100 yr^{-1} event will flood most of Galveston Island, all of Bolivar Island and significant areas along the west end of the bay.
- A 1/1,000 yr^{-1} event will flood Galveston Island, Bolivar Island, Texas City and some areas along the Houston Ship Channel.
- A 1/10,000 yr^{-1} event will flood significant areas along the Houston Ship Channel.

Chapter 6. Flood Risk Assessment

This chapter presents a preliminary application of the results gained in previous chapters. Section 6.1 covers the applied methodology. Section 6.2 highlights existing flood reduction measures. Section 6.4 addresses residential and industrial exposure to flooding. Section 6.3 treats the proposed risk reduction strategies. Section 6.5 assesses the proposed risk reduction strategies and Section 6.6 concludes our findings.

6.1 Methodology

In Chapter 5, we estimated the probability of flooding within Galveston Bay. This chapter provides a sample application of the previously obtained probability and extent of flooding. The applied methodology yields indicative results and aims to derive the preferred flood risk reduction strategy given a desired magnitude of risk reduction. The surge maps and associated probability of flooding derived in Chapter 5 serve as input for the flood risk assessment performed in this chapter.

To assess the performance of the individual risk reduction strategies we utilize a Cost-Benefit Analysis (CBA) methodology. A cost-benefit analysis estimates the present day monetary value of an intervention and provides a measure of how well a project performs. The benefits of a flood risk reduction project are equal to the damages avoided. The cost of a project is equal to the required investment and yearly maintenance.

The purpose of a CBA is to assess whether a project is worthwhile. Investing in risk reduction measures is worthwhile if the present-day benefits of a system exceed the present-day cost of investment and maintenance. The present-day benefits are equal to the present-day value of all cash flows throughout the project lifetime. If benefits exceed cost, the Rate Of Return (ROR) of a project is said to be positive. Expressed mathematically;

$$\mathrm{ROR} = \frac{\$_{\mathrm{benefit}} - \$_{\mathrm{cost}}}{\$_{\mathrm{cost}}} \qquad \text{Eq. 6.1}$$

where $\$_{\mathrm{benefit}}$ [$] is the present-day benefit and $\$_{\mathrm{cost}}$ [$] is the present-day cost.

In this Chapter, we estimate the benefits of each risk reduction strategy at safety levels of 1/100, 1/1,000, 1/5,000 and 1/10,000 yr^{-1}. Assessing the benefits and cost of strategies requires (1) the exposure to flooding before and after implementation, (2) the probability off flooding before and after implementation and (3) the cost of reducing floodrisk as a function of the safety level.

Figure 6-1 presents the procedure followed to obtain the expected flood damage. The procedure outlined in Figure 6-1 is performed for each strategy, and the existing condition. The benefits of a proposed risk reduction strategy are equal to the flood damage avoided.

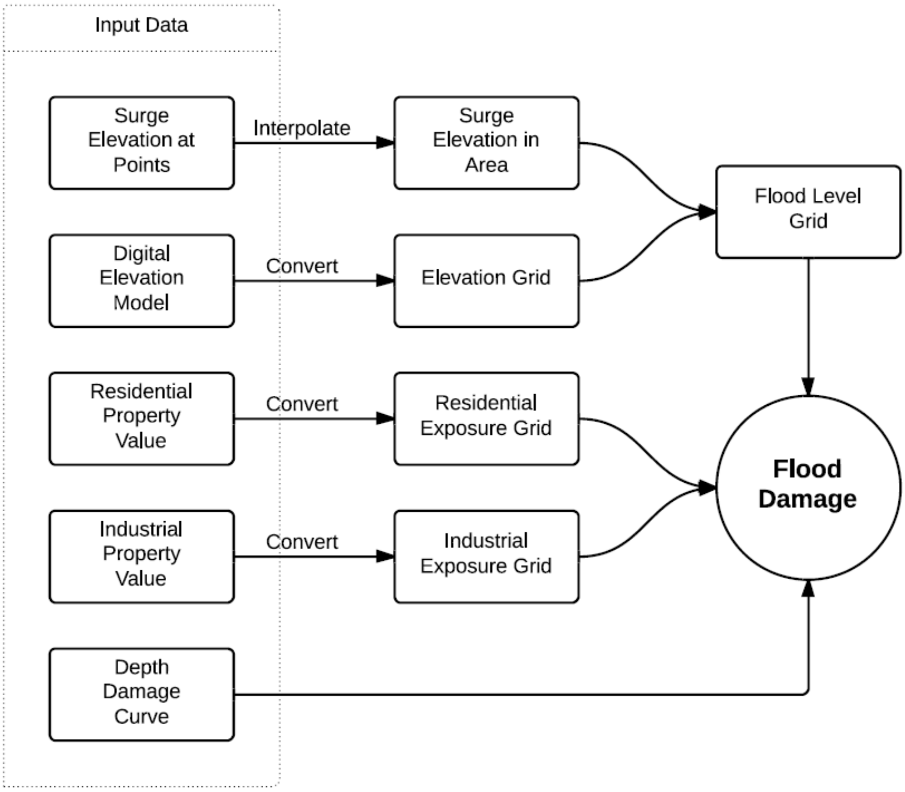

Figure 6-1 – Flood risk assessment methodology.

Because of constraints in both time and data we resort to a rapid flood risk assessment that relies on indicative damage and cost figures. The exposure to flooding before and after implementation of selected risk reduction strategies is obtained by combining risk reduction strategies with land use and property value datasets. Damage figures are estimated based on both historic data and indices. Cost figures are estimated using known investment cost of existing barriers. The flood risk assessment explicitly excludes wind damage, wave damage, flow velocity and loss of life. The flood exposure analysis covers by no means all direct and indirect tangible terms and is likely to underestimate the total exposure.

6.2 Existing Flood Protection Measures

Few flood protection structures exist within the Galveston Bay Area, presumably because most of the US flood hazard mitigation policies focused on prediction and mediating effects of storm surge (Bijker, 2007).

The Galveston seawall, built after the 1900 hurricane, is a 16-kilometers long 5.5-meter high wall that protects Galveston City against surge from the Gulf of Mexico. The seawall does not protect against surge from the bayside. After the 1900 "Great Galveston" Hurricane the city was artificially raised to an elevation of approximately 3 meter above MSL.

Building regulations on Galveston Island and Bolivar Peninsula require a minimum floor elevation above the 100-year Base Flood Elevation (BFE). The majority of utility buildings and residential property are elevated above this obligatory level.

The Texas City Hurricane Protection Structure (Figure 6-2) protects Texas City up to the $1/100\ yr^{-1}$ surge event, which corresponds to approximately 5 meter above MSL. The Texas City levee is the only FEMA accredited flood protection system within the Galveston Bay area.

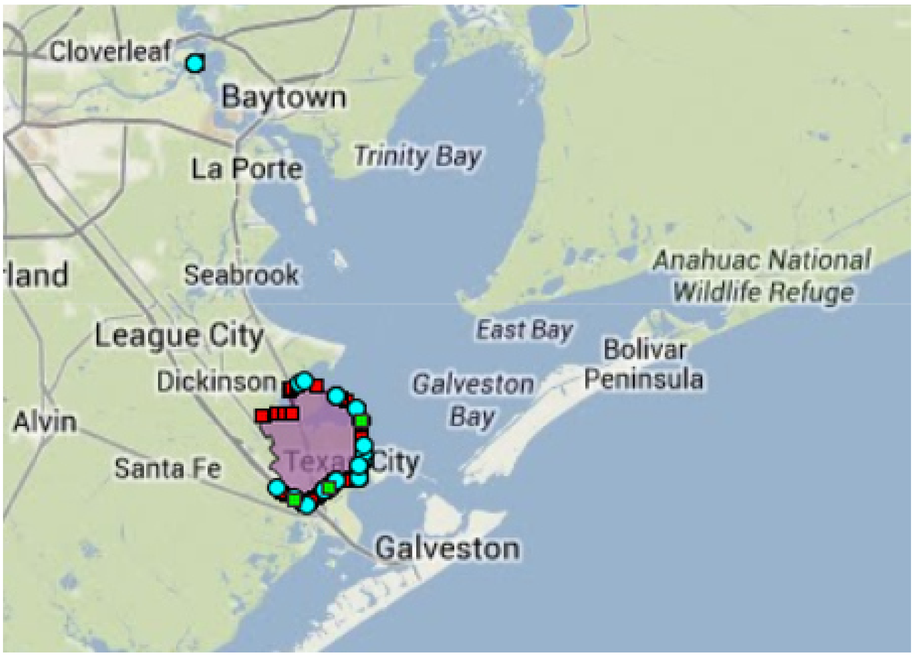

Figure 6-2 – Purple areas protect by levees that are part of the National Levee Program. (Source: USACE National Levee Database).

FEMA regulations require industrial complexes to protect up to the 1/100 yr^{-1} flood event. Refineries, chemical plants and harbors are either elevated above the 1/100 surge elevation or protected by privately maintained levees. Figure 6-3 presents the estimated inundation depth for a 1/100 and 1/1,000 yr^{-1} event at the Port Road, Seabrook, terminal. The simulations indicate that the artificially elevated terminal is indeed able to withstand a 1/100 yr^{-1} surge event while some flooding may be expected during a 1/1,000 yr^{-1} event. Table 6-1 summarizes the present-day safety levels within the Galveston Bay Area, based on the storm surge simulations in chapter 5.

Table 6-1 – Estimated present-day level of protection based on simulations.

Location	**Inundation when: (estimated)**	**Estimated Safety level**
Galveston (bay-side)	WL > 1 meter MSL	25 - 50 yr^{-1}
Galveston (ocean-side)	WL > 4.5 meter MSL	100 yr^{-1}
Texas City	WL > 5 meter MSL	100 yr^{-1}
Houston Ship Channel	WL > 4 meter MSL	100 yr^{-1} - 500 yr^{-1}
Kemah (west bay)	WL > 2 meter MSL	25 - 50 yr^{-1}

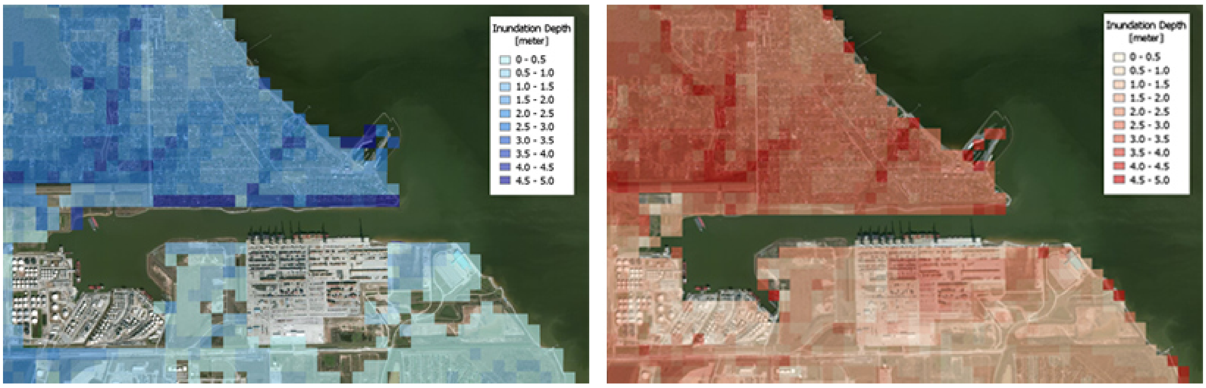

Figure 6-3 – Simulated 1/100 year (left) and 1/1,000 year (right) Max Envelope Of Water at Port Road, Seabrook, TX.

6.3 Proposed Risk Reduction Strategies

Three independent flood risk reduction strategies are assessed; a coastal spine, a ship channel gate and an upgrade of the Texas City Levee System (Figure 6-4). The purpose of each strategy is to modify the susceptibility to flood damage and disruption on community level. A system wide local solution was considered however deemed infeasible based on investment requirements. Investing in one of these risk reduction structures is worthwhile if the present-day benefits of a strategy exceeds the present-day costs of implementation and maintenance. A cost breakdown of each strategy is available in Appendix E.

Figure 6-4 – Risk reduction strategies (indicative outline).

The present-day cost of each strategy, or investment cost, is estimated using unit cost prices deduced from similar systems. Table 6-2 presents an overview of the estimated investment cost as a function of the safety level. The assumed lifetime of the risk reduction measures is 100 years.

Table 6-2 – Estimated investment cost of strategy as a function of the desired safety level.

Return Frequency [1/year]	**1/100**	**1/1,000**	**1/5,000**	**1/10,000**
Coastal Spine	$US 3.9 billion	$US 5.1 billion	$US 5.7 billion	$US 6.0 billion
Ship Channel Gate	$US 0.9 billion	$US 1.3 billion	$US 1.5 billion	$US 1.6 billion
Texas City Levee Upgrade	n/a	$US 0.5 billion	$US 0.8 billion	$US 1.0 billion

The surge within the bay exceeds the surge on the open coast by about 1 meter for a 1/10,000 yr^{-1} event (Chapter 5). The relation between surge barrier cost and retaining height is non-linear. An equal albeit one meter higher barrier is about 20% to 30% more expensive (Appendix E). Although a 20% increase in cost is significant, it is of similar magnitude as other factors including barrier width, local geography and existing safety level.

6.4 Exposure

Exposure is defined as the total value of property and assets that can be subject to losses from a specific hazard. This risk assessment addresses the exposure of residential property and industrial assets to storm surge. Exposure of small and medium sized business is not included due to the lack of data.

To estimate direct tangible losses one requires information on; (1) elevation, (2) value of structure and contents, (3) frequency of occurrence and (4) a depth-damage relation (Grigg & Helweg, 1975). A depth-damage relation expresses damage to a specific type of asset as a function of value and inundation depth.

6.4.1 Residential Exposure

An estimate of residential exposure is obtained by combining data on land-use and home value. Data on land use was obtained through TNRIS (2013) while the US Census (2010) provides estimates on median home value within Census block groups. The average value of home contents is estimated at 40% of the home value (Czajkowsky, et al., 2013).

After Hurricane Ike (2008) a total of 44,000 NFIP claims were filed with a combined value of over $US 2.6 billion dollar. Policyholders residing in Galveston County filed about $US 1.3 billion dollar in flood insurance claims (Perry, et al., 2008). The frequency of Hurricane Ike's surge at the open coast is estimated at 1/75 to 1/125 yr^{-1} (Chapter 5). A flood exposure assessment by CoreLogic (2013) indicates that the maximum residential exposure within the Galveston Bay Area is about $US 15 billion.

Combining the inundation grid (Section 5.4) with residential property values and land-use patterns yields the estimated number of property at risk as a function of the probability of occurrence. The obtained property numbers show fair correlation with the estimates by CoreLogic (2013). Relating property within the flood zone with inundation depth and a depth-damage curve provides an indicative damage estimate. Because of time and data constraints, we resort to a generic depth-damage curve for Single Family Residential 2-story structures (FEMA, 2011). The applied depth-damage curve is appended in Appendix C-4.

Table 6-3 presents the estimated number of residential property within the floodplain. Table 6-4 presents the estimated direct tangible damage to structure and contents. Estimated damage for a 1/100 yr^{-1} event on the Galveston West End and Bolivar Peninsula are assumed equal to zero because of existing FEMA BFE requirements. The estimated direct tangible flood damage for a 1/100 yr^{-1} event is lower than observed after Hurricane Ike because it is assumed that lost or severely damaged property was rebuild to contemporary building standards.

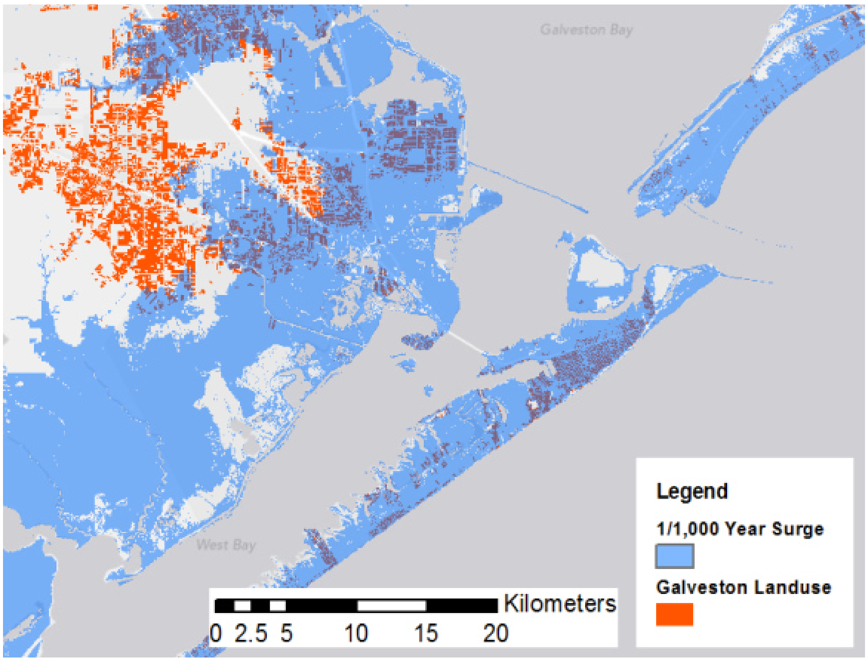

Figure 6-5 – Residential property combined with the 1/1,000 yr^{-1} MEOW.

Table 6-3 – Estimated number of residential property within floodplain.

Return Frequency [1/year]	**1/100**	**1/1,000**	**1/5,000**	**1/10,000**
Galveston Island	12,000	14,000	14,000	14,000
Bolivar Peninsula	800	800	800	800
Texas City	0	12,200	12,200	12,200
Other Areas	34,600	44,300	63,800	70,400
SUM	46,800	71,300	90,800	97,400

Table 6-4 – Estimated direct tangible flood damage in million $US.

Return Frequency [1/year]	**1/100**	**1/1,000**	**1/5,000**	**1/10,000**
Galveston Island	750	1,450	1,780	1,850
Bolivar Peninsula	20	140	140	140
Texas City	0	840	840	840
Other Areas	600	1,100	1,400	1,500
SUM:	1,370	3,530	4,160	4,330

The inundation pattern obtained in Chapter 5 suggested that even with a coastal spine local flooding may occur. The 1/10,000 yr^{-1} surge extent with coastal spine is smaller than the 1/100 yr^{-1} surge extent without barrier. The estimated tangible flood damage within the 1/10,000 yr^{-1} MEOW with a coastal spine is $US 0.5 billion dollar.

Obtained results indicate that Texas City is vulnerable to flooding despite its existing Hurricane Protection Structure. Failure of the protection system results in rapid inundation with inundation depths of up to 2 or 3 meter.

6.4.2 Industrial Exposure

The Port of Houston and Texas City are important drivers of Texas' economy and home to some of the largest oil refining facilities in the United States. The Port of Houston is the second largest port in the United States with an estimated direct economic impact of 178.5 billion dollars a year (Martin Associates, 2011). Its largest asset is the chemical and petrochemical industry with a total crude oil processing capacity of 1,120,000 bpd, almost 10% of the nationwide capacity. The Port of Houston suffered minor damage during Hurricane Ike as surge levels remained approximately 0.6 meter below the docks (Bedient, 2012).

Texas City is located about 40 kilometers South of Houston and home to three oil refineries with a combined processing capacity of 707,000 bpd (EIA, 2013). Texas City did not suffer flood damage during hurricane Ike, however the Texas City Dike was overtopped.

Recovering flooded harbor facilities, refineries or infrastructure may take months depending on the severity of the damage. The replacement cost of a petroleum refinery is approximately 30,000 dollars per bpd (Handwerk, 2001). The replacement value of docks, container terminals and other industry is estimated at \$US 650/m^2 (adopted from Admiraal, 2011). Damage values are determined using the generic depth-damage curve appended in Appendix C-4.

By relating the previously acquired land-use grid to the inundation grid, we obtain an estimate of industrial exposure. Figure 6-6 presents the 1/10,000 yr^{-1} MEOW for the Houston Ship Channel. Results indicate that the 1/10,000 yr^{-1} inundation pattern covers about 25 km^2, whereas the 1/1,000 yr^{-1} inundation pattern covers about 5 km^2. Again, Texas City proves to be highly vulnerable.

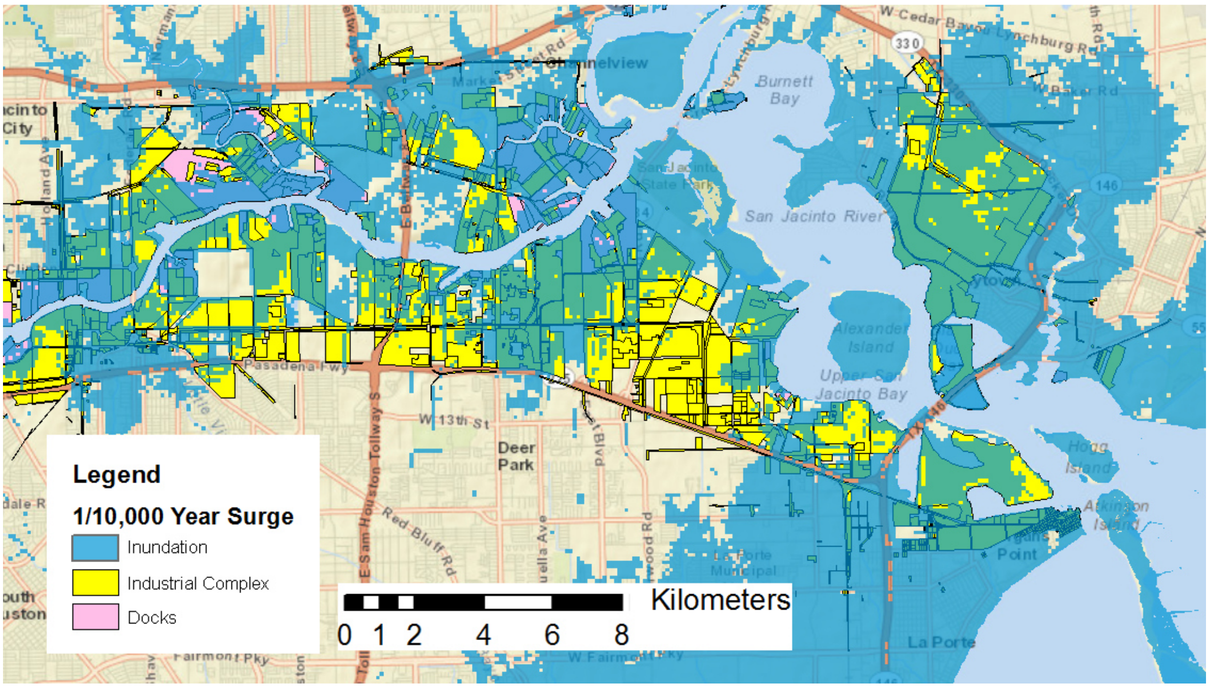

Figure 6-6 – 1/10,000 per year inundation pattern at the Port of Houston.

Table 6-5 presents the estimated direct tangible flood damage at the Port of Houston and Texas City.

Table 6-5 – Estimated direct tangible flood damage to industry in billion $US.

Return Frequency [1/year]	**1/100**	**1/1,000**	**1/5,000**	**1/10,000**
Port of Houston	0	3.5	8	16
Texas City	0	2.0	6.0	8.4

Indirect tangible damage, resulting from disruption of the economy, is harder to assess because effects may last years and may even affect nationwide economy. The U.S. Coast Guard estimates that a one month closure of the Port of Houston will cost the national economy $60 billion dollar (USCG, 2013). Studies indicate that a five week disruption at a large oil refinery adds about $US 5,000/bpd to nationwide refined product expenses (CPRA, 2007). Additional losses relating to loss of sales and earnings amount to $US 12,000/bpd per five weeks of downtime (CPRA, 2007).

Rebuilding oil refineries, docks or other industrial areas may take months. It is assumed that a 1/10,000 yr^{-1} event results in a 2-month disruption attributable to flooding. Short and thereby relatively inexpensive when compared to rebuilding efforts after Hurricane Katrina, which lasted up to one year (Admiraal, 2011). Indirect tangible damage figures of the 1/1,000 yr^{-1} and 1/5,000 yr^{-1} relate to the 1/10,000 yr^{-1} event by expressing them as a percentage of the direct damage. Table 6-6 presents the estimated indirect flood damage.

Table 6-6 – Estimated indirect tangible flood damage to industry in billion $US.

Return Frequency [1/year]	**1/100**	**1/1,000**	**1/5,000**	**1/10,000**
Port of Houston	0	26	60	120
Texas City	0	4.5	16	20

6.4.3 Other Exposure

Besides damage to residential and industrial property, many other types of assets may suffer damage in a flood. These assets include public infrastructure, waterways and agriculture. In addition, indirect damage to the economy may contribute significantly to total damage figures. The Perry Report (2008) shows that out of a $US 29.4 billion funding request for federal assistance a total of $US 14.3 billion dollar was assigned to address long-term economic impact. A significant amount when compared to the $US 2.7 billion dollar the NFIP program spend on flood insurance reimbursements. The question remains however, how much of the $US 14.3 billion figure can be attributed to flooding.

Table 6-7 presents funding requests after Ike of which a significant part can be attributed to flood damage. Although quite likely to be an underestimate, it is assumed the highest feasible direct damage to other assets within the area of interest.

Table 6-7 –Damage estimates after hurricane Ike (Perry, et al., 2008).

Asset	**billion $US dollar**	**% of NFIP expenditure**
Critical Infrastructure	1.9 billion	70 %
Transportation	0.5 billion	18 %
Navigation and Waterways	3.2 billion	118 %
Agriculture and Fisheries	0.6 billion	22 %
SUM:	6.2 billion	229 %

6.4.4 Combined Exposure

Figure 6-7 presents the estimated damage potential within the area of interest as a function of the probability of occurrence. The relationship between flood damage and flood probability is obtained through a second order polynomial interpolation. Existing risk protection structures are assumed to fail during a design event. The influence of the surge on business establishment other than ports and refineries was neglected due to lack of data. It is expected that the underestimate introduced by this uncertainty will severely affect the coastal spine estimate and somewhat impact the Texas City and ship channel gate estimates.

Figure 6-7 indicates that both the coastal spine and the Texas City upgrade already reduce damage at safety levels beyond 1/100 yr^{-1} while the ship channel gate effectively reduces damage at safety levels beyond 1/500 yr^{-1}. Because of existing regulations, the ship channel gate is less effective at safety levels below 1/500 yr^{-1}. The steep line at the 1/100 yr^{-1} marker results from failure of the existing Texas City protection structure.

The damage curve of the coastal spine and the ship channel gate look rather similar in the low probability range. A significant part of the estimated damage results from low probability high value exposure within the Houston Ship Channel.

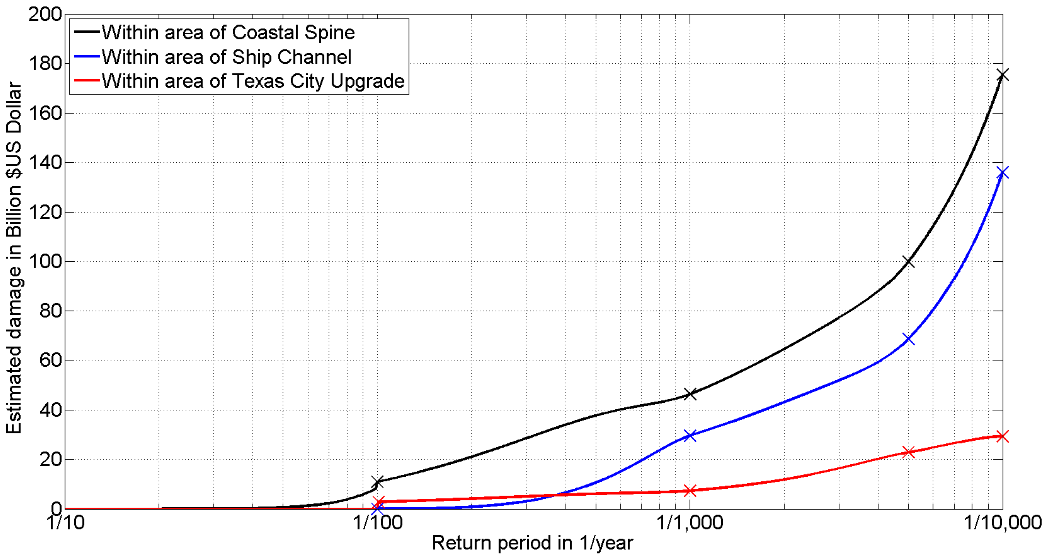

Figure 6-7 – Estimated damage within area of interest as a function of the return period.

6.5 Assessment of Individual Strategies

In the previous sections, we estimated (1) the extent of flooding, (2) the exposure to flooding, (3) the expected damages and (4) the cost of reducing floodrisk. In this section, we estimate the expected benefits in terms of risk reduction, of each strategy, at safety levels of 1/100, 1/1,000, 1/5,000 and 1/10,000 yr^{-1}.

The benefits of a risk reduction system are equal to the damages avoided. The Expected Annual Damage (EAD) of event x with annual probability P_x and expected damage D_x is equal to the probability of occurrence multiplied by the expected damage. Expressed in a mathematical form by;

$$EAD(x) = D_x \cdot P_x \qquad \text{Eq. 6.2}$$

The annual benefits of a flood protection project that solely prevents flood-damage by event x are equal to the EAD(x). The annual benefits are incurred for each year that the flood protection project performs its function.

If the value of money were constant in time, the total benefits of a project would be equal to the EAD(x) multiplied by the project lifetime. In reality, the value of money is expected to deprecate with time; the present-day value of a future benefit decreases with increasing time. When comparing the investment cost with benefits the deprecation of monetary value may significantly affect the rate of return.

The concept of present-value (PV) is a method to discount future cost or benefits to present day value, as if they existed today. The present-day value PV(t) of benefit $D_x \cdot P_x$ in year t equals;

$$PV(t) = D_x \cdot P_x \cdot \left(\frac{1}{1+\delta}\right)^t \qquad \text{Eq. 6.3}$$

where PV(t) [$] is the present-day value, P_x [yr^{-1}] is the probability of occurrence, δ [%] is the discount rate, D_x [$] is the present-day avoidable damage and t is the time in years.

When assuming that damage grows at the same rate as the economic growth the present-day value of a future accruement at time t becomes (Hallegatte, 2006);

$$PV(t) = D_x \cdot (1+g)^t \cdot P_x \cdot \left(\frac{1}{1+\delta}\right)^t \qquad \text{Eq. 6.4}$$

where PV(t) [$] is the present-day value, P_x [yr^{-1}] is the probability of occurrence, δ [%] is the discount rate, g [%] is the growth rate, D_x [$] is the present-day avoidable damage and t is the time in years.

The present-day value of the total benefit of a project that prevents damage from event x is obtained by taking the sum of Eq. 6.4 between t = 0 and the assumed project lifetime t = n. Expressed in a mathematical form by;

$$B(t) = \sum_{t=0}^{t=n} \left[D_x \cdot (1+g)^t \cdot P_x \cdot \left(\frac{1}{1+\delta} \right)^t \right] \qquad \text{Eq. 6.5}$$

where B [$] is the present-day benefit, n [-] is the lifetime of the project and PV(t) is the present-day value of each increment.

Application of Eq. 6.5 yields the present-day benefit of a project that prevents damage due to event x with annual probability P_x. Often surge barriers protect against a wide range of events, up to a predefined probability of occurrence, or safety level. When the damage as a function of probability is known (example: Figure 6-7) the expected annual damage may be approximated by integrating the damage function between p = 0 and the design safety level of the barrier p = s. Expressed in a mathematical form;

$$B(t,p) = \sum_{t=0}^{t=n} \left[(1+g)^t \cdot \left(\frac{1}{1+\delta} \right)^t \cdot \int_{p=0}^{p=s} D(p)\, dp \right] \qquad \text{Eq. 6.6}$$

where B [$] is the present-day benefit, n [yr] is the lifetime of the project, δ [%] is the discount rate, g [%] is the growth rate, t [years] is the time in years, s [yr^{-1}] is the design safety level and D is the probability-damage curve.

Both the discount rate and the growth rate affect the present day value of a future benefit. Uncertainty about future discount or growth rates implies that the present day value of future benefits is susceptible to economic developments. Small variations in the discount or growth rate result in significant variations in Net Present Value (NPV) over a 100-year period. Selection of the discount and growth rate requires careful selection.

Figure 6-8 presents the Expected Annual Benefits (EAB) as a function of the safety level, for each strategy. When flood damage behind a proposed barrier is assumed nonexistent the EAB are equal to the Expected Annual Damage (EAD), the area underneath the damage curve presented in Figure 6-7. A mathematical expression of the EAB is provided by the integral included in Eq. 6.6.

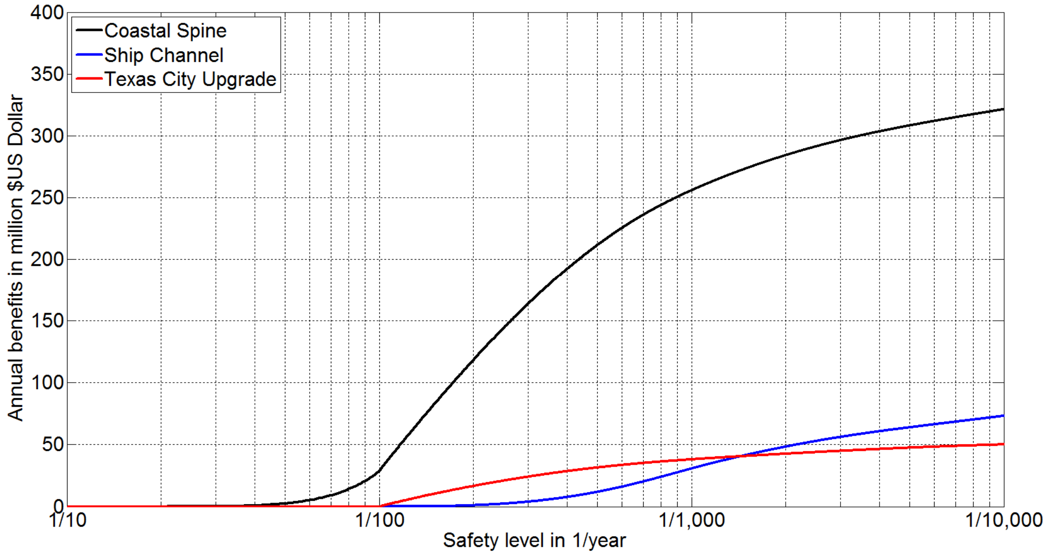

Figure 6-8 – Estimated present-day annual benefits as a function of safety level.

Figure 6-9a presents the expected present-day net benefits of each strategy, as a function of the safety level. Solving Eq. 6.6 for each safety level provides the present-day benefits as a function of the safety level. Subtracting the cost of investment from the present-day benefits returns the present-day net benefits. Future payments were converted to present day values with a reduced discount rate of 2%.

Figure 6-9b presents the Rate of Return (ROR) for each strategy, as a function of the safety level. A positive ROR indicates that the present-day benefits exceed the present-day cost.

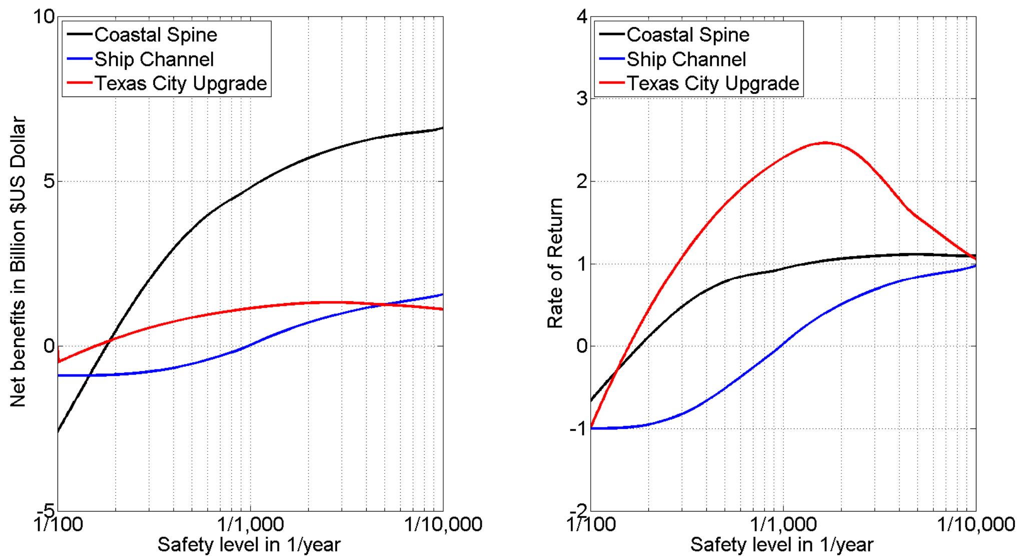

Figure 6-9 – Net Benefits (left) and Rate of Return (right) of each strategy as a function of safety level.

Figure 6-9 indicates the Texas City levee upgrade provides the highest rate of return and requires ample investment. An upgrade of the Texas City levees provides limited system-wide risk reduction and should only be considered if budget is limited. The cost/benefit analysis indicates the estimated optimal safety level is 1/2,000 per year.

The ship channel gate does not provide a high rate of return but does protect assets that are of national strategic importance. Existing safety level regulations limit the impact of a ship channel gate in the 1/100 to 1/1,000 yr^{-1} range. The cost/benefit analysis indicates the optimal safety level exceeds 1/10,000 per year

The coastal spine significantly reduces surge within the bay, provides the highest benefits in terms of risk reduction and protects all assets. Even with a coastal spine, wind set-up within the bay could result in limited local flooding. Figure 6-10 presents the strategy that maximizes benefits or achieves the highest rate of return at a specific safety level.

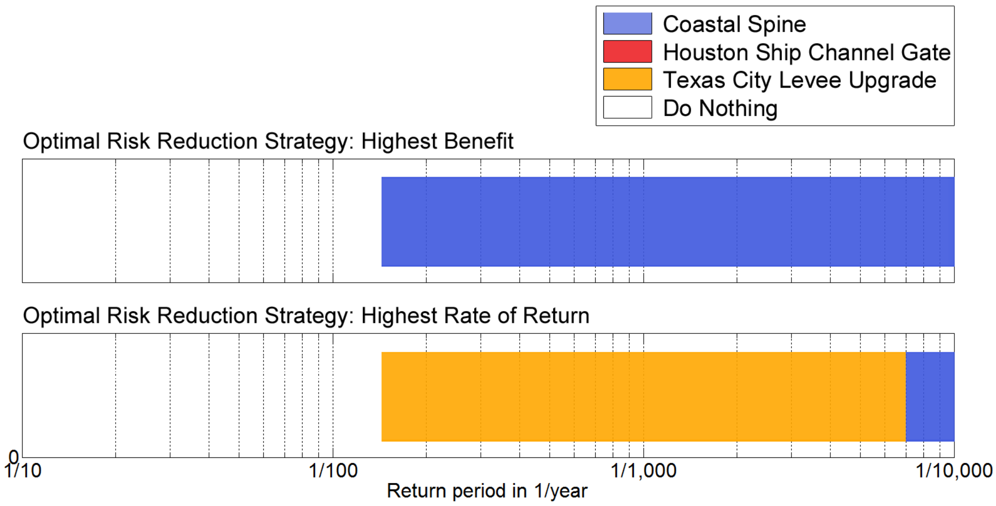

Figure 6-10 – Highest Benefit and Highest Rate of Return.

6.6 Assessment on System Level

In the previous section, we assessed the individual performance of three individual strategies. From an economic point of view, the Texas City Levee Upgrade provides the highest rate of return. It is arguable whether it is the best strategy. The Texas City Levee Upgrade solely reduces risk in a small area within the area of interest.

To assess how well each strategy performs on system level we compare the investment cost of each system with the benefits in terms of system wide risk reduction. Figure 6-11 presents the estimated investment cost, risk and total cost (risk + investment) for each strategy as a function of the safety level. It is assumed that the maximum potential damage within the system is equal to the damage associated with a system-wide 1/10,000 yr^{-1} event.

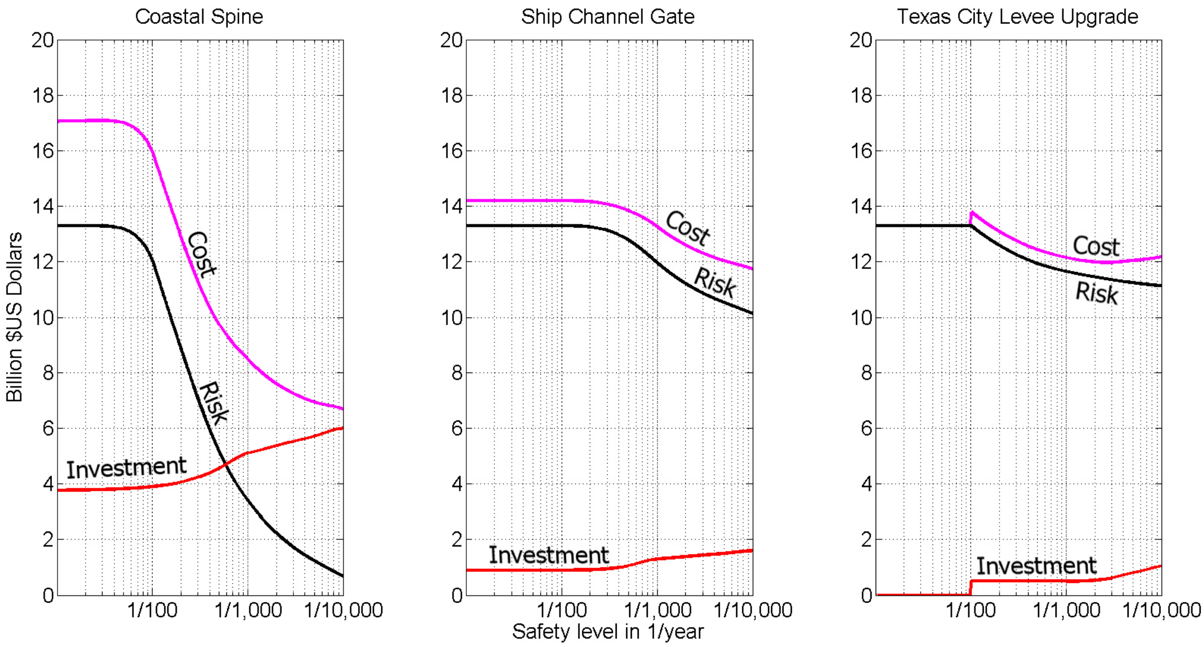

Figure 6-11 – Total present-day cost of risk reduction strategies.

Figure 6-11 indicates that a coastal spine yields the most benefits. A coastal spine does require a significant investment. If budget constraints do not allow such investment one could resort to alternative solutions.

Figure 6-12 presents the optimal solution as a function of available budget. Each solution or combination of solutions maximizes the net benefits. Preliminary results indicate that when budget is very limited ($\leq$ \$1.5 billion) an upgrade of the Texas City offers the highest benefit. If budget is slightly larger, a combination of the Texas City Levee and Ship Channel Gate might prove fruitful. However, the preliminary assessment indicates that the desired solution that minimizes risk and maximizes benefits remains the Coastal Spine.

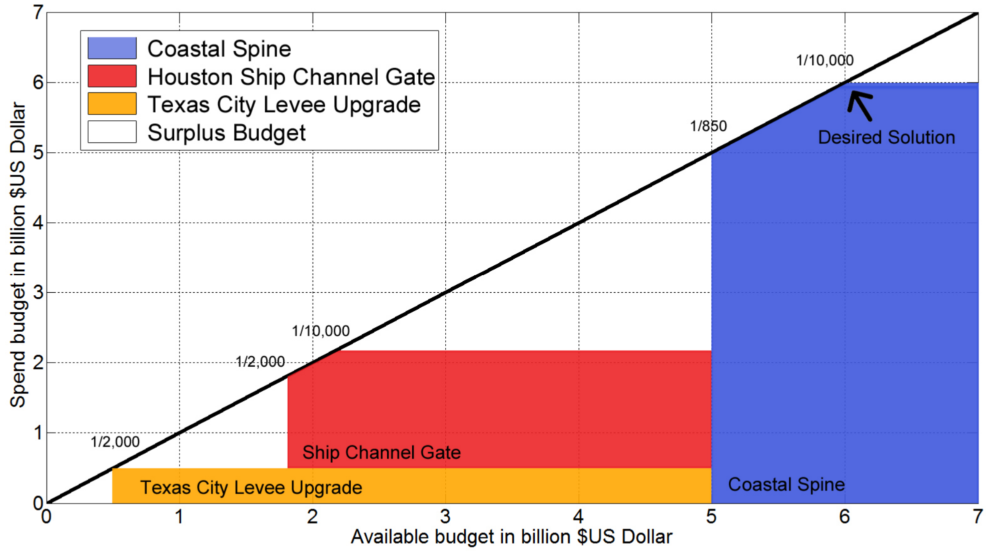

Figure 6-12 – Available versus spend budget of risk reduction strategies.

6.7 Sensitivity

This study encompassed a preliminary first-order cost-benefit analysis. To assess the sensitivity of the results to errors in damage estimates, cost estimates or the reduced discount rate we perform a sensitivity analysis.

Table 6-8 summarizes the results of the sensitivity analysis. The optimal safety level of the Coastal Spine and Ship Channel Gate is not very sensitive to variations in discount rate, flood damage or investment cost. The Texas City Levee is considerably more sensitive to variations in discount rate, damage or investment cost.

Table 6-8 – Sensitivity analysis of flood risk reduction strategies.

	Baseline	**Discount Rate**		**Flood Damage**		**Investment Cost**	
		- 50 %	+ 50%	- 50%	+ 50%	- 50%	+ 50%
Coastal Spine	$\geq$ 1/10,000	$\geq$ 1/10,000	$\geq$ 1/10,000	$\geq$ 1/10,000	$\geq$ 1/10,000	$\geq$ 1/10,000	$\geq$ 1/10,000
Ship Channel	$\geq$ 1/10,000	$\geq$ 1/10,000	$\geq$ 1/10,000	$\geq$ 1/10,000	$\geq$ 1/10,000	$\geq$ 1/10,000	$\geq$ 1/10,000
Texas City Levee	1/2,500	1/3,000	1/2,000	1/2,000	1/4,000	1/7,000	1/2,000

6.8 Discussion

In this Chapter, we solely estimated the financial returns of selected risk reduction strategies. One might argue whether financial returns are a satisfying criterion when estimating the true benefits of flood risk reduction. After all, financial returns do not include non-monetary losses such as increased vulnerability of survivors, post-traumatic stress or loss of cultural heritage.

It is the author's opinion that a coastal spine offers the best solution to the problem. Other alternatives protect significant industrial assets but often leave citizens exposed. One might argue the worth of a factory whose employees are left without shelter.

Ultimately, the desired level of risk reduction is inherently political. It is not solely a decision involving costs or benefits, it is a decision influenced by many parameters including available resources and political or public opinion.

The preliminary findings presented in this report should warrant future research and support a broader discussion on flood vulnerability within the Galveston Bay Area.

Chapter 7. Conclusions and Recommendations

The main conclusions of this thesis are listed below. Section 7.1 offers a brief reflection on chosen methodology. Section 7.2 summarizes the main conclusions. Section 7.3 summarizes the recommendations.

7.1 Reflection on Methodology

The first objective of this thesis was to develop a methodology to obtain an order-of-magnitude relationship between the return period of storm surge at the open coast and storm surge within semi-enclosed bays.

The model couples meteorological forcing with hydrodynamic response and provides a first-estimate of storm surge within semi-enclosed bays. Hindcasts of historical storms indicate the model performs reasonably well. On average, the simulated storm surge is within ± 0.5 meter of the observed peak-surge.

Storm surge within the bay is estimated by simulating local wind set-up and inflow. Inflow is assumed quasi-steady in relation to wind set-up, which implies an instantaneous distribution of influx over the bay. As a result, the model over-estimates inflow and under-estimates wind set-up around landfall. The extensive low-lying areas around the bay will flood during a storm and depending on the inflow the windward side of the basin may become exposed. The model employs a "bathtub" approach with fixed vertical boundaries, and ignores local geography. In reality, many basins have time-dependent moving boundaries while inflow does not spread instantaneous and local geographic features enhance or decrease surge.

Because of abovementioned constraints, the simplified model does not provide a satisfactory description of time-dependent water motion within the bay. Hindcasts did show that the model provides a reasonable estimate of peak-surge within the bay. In addition, closer analysis reveals that the error caused by neglecting alongshore flow tends to counteract the error resulting from overestimating the hydraulic head. The obtained peak surface elevations are accurate enough for an order-of-magnitude safety level analysis. A higher degree of accuracy and thereby increased confidence in model results can be achieved by (in order of importance);

1) Adopting a 2-dimensional method to estimate surge within the bay.
2) Adopting an improved method do convert gradient to surface wind velocity.
3) Adopting a 2-dimensional method to estimate surge at the open coast.

7.2 Conclusions

The second objective of this thesis was to derive the preferred strategy for Galveston Bay given a financial budget or desired level of risk reduction.

Hurricane surge in coastal bays is highly sensitive to storm path and landfall location. Landfall west of Galveston Bay tends to result in the highest surges as Galveston Bay encounters the strongest winds in on-shore direction. Model results indicate that storm surge within Galveston Bay is a delicate balance between inflow and local wind set-up. Depending on landfall location and storm intensity, local wind set-up contributes up to 50% to surge within the bay.

The direct effect of wind is to pile up water at the leeward side of the bay. Southerly winds increase the surge at the northern end of the bay. Northerly winds decrease the surge at the northern end of the bay though will not overcome the effect of inflow. In general, a shallow coastal bay will serve to amplify surge for hurricanes making landfall west of the bay. Observed bay behavior is specific to storm surge in shallow wind governed coastal basins.

The influence of local wind set-up on storm surge within shallow semi-enclosed bays is significant. The probabilistic simulations indicate that surge within the bay exceeds surge at the open coast at least once per 50 year. The 1/1,000 yr^{-1} and 1/10,000 yr^{-1} surge elevation at the northern bay end exceeds the 1/1,000 yr^{-1} and 1/10,000 yr^{-1} surge elevation at the open coast by, respectively, about 0.5 and 1.0 meter.

In terms of surge barrier cost, a 0.5 to 1.0 meter increase in barrier height results in a 10% to 30% rise in cost. The magnitude of other factors including length, existing safety level and local geography is similar. There is no indication that the additional barrier height, required for local solutions, plays a crucial role in strategy selection.

The preliminary flood risk assessment confirms our hypothesis that the Galveston Bay Area is vulnerable to flooding. The 1/100 $year^{-1}$ inundation pattern suggests that most industrial areas are well protected, while residential exposure is significant. By analyzing the 1/10,000 yr^{-1} inundation pattern, we find that industrial exposure significantly outweighs residential exposure. Results indicate Texas City remains highly vulnerable to flooding despite its existing flood risk reduction structure.

Flood exposure is, among other factors, dependent on the extent of flooding. Within a semi-enclosed system, a lower probability surge event results in a significantly larger extent of flooding. Both exposure and expected damage increases non-linear with a decreasing probability of occurrence, encouraging high safety levels.

We assessed the benefits in terms of risk reduction of a coastal spine, a ship channel gate and an upgrade of the Texas City levee system. Each of the three risk reduction strategies provides a positive rate of return within the 1/1,000 yr^{-1} to 1/10,000 yr^{-1} range. Preliminary results indicate that a coastal spine significantly reduces storm surge within the bay and yields the highest benefits in terms of risk reduction. The ship channel gate and the Texas City levee upgrade yield a similar rate of return but achieve considerably less benefits in terms of risk reduction.

7.3 Recommendations

The following is a set of recommendations drawn from the findings of this study;

- **Compare model results to other models.** Historical observations are limited and do not allow extensive calibration and validation of results. To gain more confidence in model results one should verify the model with existing models.

- **Quantify climatologic uncertainty.** The model assumes a stationary climate consistent with historical records. The finite number of observed hurricanes introduces a large source of epistemic uncertainty because the future population of hurricanes might profoundly differ from the present day population. Quantifying this source of uncertainty will benefit the interpretation of results.

- **Address parametric uncertainty.** Limited information on the actual value or distribution of several model parameters introduces a significant source of uncertainty. It is recommended to reduce parametric uncertainty by performing in-situ tests or additional studies.

- **Verify hurricane population.** The 1/10,000 yr^{-1} storm event is a very rare and severe storm event. Between 1900 and 2013, only three category 5 hurricanes made landfall on the US continent. More research is required to assess whether such events are physically possible within the area of interest. In addition, the applied statistical window neglects long-term (decadal) variability in hurricane intensity such as the Atlantic Multi-decadal Oscillation (AMO). By optimizing the statistical window, one can improve the hurricane sample set.

- **Include a Planet Boundary Layer model.** The sensitivity analysis indicated that the conversion from gradient wind velocity to surface wind velocity introduces the largest source of uncertainty. Incorporating a dynamic location and time dependent conversion parameter is relatively simple and comes at little computational cost.

- **Improve flood risk assessment accuracy.** The first-estimate flood risk assessment provides insight into flood risk vulnerabilities. The applied method has limited applicability because the constructed flood maps did not capture the hydrodynamics of storm surge. In addition, a storm surge barrier does not prevent windstorm damage. To obtain the true benefits of a surge barrier one should use a more sophisticated method to determine the inundation area and include windstorm in the cost benefit analysis.

- **Investigate nonstructural risk reduction measures.** In this thesis we mainly addressed structural risk reduction measures. Reduction of flood vulnerability may also be achieved by optimizing spatial patterns, enforcing stricter building codes or reducing the amount of structures on the floodplain.

Bibliography

Admiraal, J., 2011. *Flood damage to port industry,* Amsterdam: Vrije Universiteit Amsterdam.

Arcadis US, 2011. *ADCIRC based storm surge analysis of sea level rise in the Galveston Bay and Jefferson County area in Texas,* Colorado: Arcadis US.

Bedient, P., 2012. *Lessons from Hurricane Ike.* 1st ed. Houston: Texas A&M University Press.

Bijker, W., 2007. American and Dutch coastal engineering: differences in risk conception and differences in technological culture. *Social Studies of Science,* 37(1), pp. 143-151.

Blain, C., Westerink, J. & Luettich, R., 1998. Grid convergence studies for the prediction of hurricane storm surge. *International journal for numerical methods in fluids,* Issue 26, pp. 369-401.

Bodine, B., 1969. *Hurricane Surge Frequency Estimated For The Gulf Coast Of Texas.* Washington, DC: U.S. Army Coastal Engineering Research Center.

Bodine, B., 1971. *Storm Surge on the Open Coast: Fundamentals and Simplified Prediction,* Washington, DC: U.S. Army Corps of Engineers Coastal Engineering Research Center.

Bunpapong, M., Reid, R. & Whittaker, R., 1985. *An Investigation of Hurricane-Induced Forerunner Surge in the Gulf of Mexico",* Vicksburg: Coastal Engineering Research Center.

Census, 2010. *United States Census 2010,* Washington, DC: U.S. Census Bureau.

Chouinard, L., Liu, C. & Cooper, C., 1997. A model for the severity of hurricanes in the Gulf of Mexico. *Journal of Waterways and Harbours,* Volume 123, pp. 113-119.

CND, 1984. *Hurricane Alicia Galveston and Houston, Texas,* Washington, DC: National Acedemy Press.

CoreLogic, 2013. *2013 Storm Surge Report,* Austin: CoreLogic.

CPRA, 2007. *Integrated Ecosystem Restoration and Hurricane Protection: Louisiana's Comprehensive Master Plan for a Sustainable Coast,* Baton Rouge: State of Louisiana.

Crawford, K., 1979. Hurricane Surge Potentials Over Southeast Louisiana as Revealed by a Storm-Surge Forecast Model: A Preliminary Study. *Bulletin of the American Meteorological Society,* pp. 423-429.

Czajkowsky, J., Kunreuther, H. & Michel-Kerjan, E., 2013. *Catastrophe Model Based Quentification of Riverine and Storm Surge Flood Risk in Texas,* Philadelphia: Wharton University.

Davis, A., 1966. *Design of Hurricane flood protection works on the upper Texas coast,* Galveston, TX: USACE.

Dean, R., Chiu, T. & Wang, S., 1994. *Combined total storm tide frequency analysis for Bay County, Florida,* Tallahassee: Florida State University.

Dean, R. & Dalrymple, R., 1991. *Water Wave Mechanics for Engineers and Scientists.* s.l.:World Scientific.

Dean, R. & Dalrymple, R., 2001. *Coastal Processes with Engineering Applications.* 2 ed. s.l.:World Scientific Pub Co Inc.

Dorn, v., 1953. Wind stress on an artificial pond. *Journal of Marine Research.*

Dorst, N., 2007. *What is the average forward speed of a hurricane?.* [Online]
Available at: http://www.aoml.noaa.gov/hrd/tcfaq/G16.html
[Accessed 7 2 2013].

East, J., Turco, M. & Mason, R., 2008. *Monitoring Inland Storm Surge and Flooding from Hurricane Ike in Texas and Louisiana,* United States: US Geological Survey.

Eastman, J., Kyem, P., Toledano, J. & Jin, W., 1993. *GIS and decision making.* 1 ed. Geneva: United Nations.

EIA, 2013. *Refiners' Total Operable Atmospheric Crude Oil Distillation Capacity.* [Online]
Available at:
http://www.eia.gov/pub/oil_gas/petroleum/data_publications/refinery_capacity_data/current/table5.pdf
[Accessed 8 8 2013].

Emanuel, K., 1987. The dependence of hurricane intensity on climate. *Nature,* pp. 483-485.

Emanuel, K. & Jagger, T., 2010. On Estimating Hurricane Return Periods. *Journal of Applied Meteorology and Climatology,* Volume 49, pp. 837-844.

ESRI, 2011. *ArcGIS Desktop: Release 10.* Redlands, CA: Environmental Systems Research Institute.

Farrer, L., 1958. *Wind Tide on Lake Okeechobee.* Jacksonville, USACE.

FEMA, 2008. *Hurricane Ike Impact Report,* Washington, DC: FEMA.

FEMA, 2009. *Hurricane Ike in Texas and Louisiana,* Washington DC: NHC.

FEMA, 2011. *Hazus 2.0 Technical and User's Manuals,* Washington, DC: FEMA.

FEMA, 2013a. *flood-zones.* [Online]
Available at: http://www.fema.gov/national-flood-insurance-program-2/flood-zones

Gilmore, R. & Englebretson, R., 1997. *Hurricane haven evaluation,* Monetery: US Naval Research Labaratory.

Gonnert, G., Dube, S., Murty, T. & Siefert, W., 2001. *Global Storm Surges: Theory, Observations and Applications.* 1st ed. Heide: Boyens & Co.

Grigg, N. S. & Helweg, O. J., 1975. State of the art of estimating flood damage in urban areas. *Water Resources Bulletin,* 11(12), pp. 379-390.

Hallegatte, S., 2006. A cost-benefit analysis of the New Orleans Flood Protection System. *AEI-Brookings Joint Center. Regulatory Analysis,* 12975(12975), pp. 1-18.

Handwerk, G., 2001. *Petroleum Refining.,* s.l.: CRC Press.

Harris, D., 1957. *The Hurricane Surge.* Washington, DC, Coastal Engineering Proceedings.

Holland, G. J., 1980. An analytic model of the wind and pressure profiles in hurricanes. *Monthly Weather Review,* Volume 108, pp. 1212-1218.

Hurricane Central, 2013. *Hurricane Central.* [Online]
Available at: http://hurricanecentral.freeservers.com/
[Accessed 05 06 2013].

IPET, 2009. *Interagency performance evaluation taskforce vol 8: Engineering and operational risk and reliability analysis.,* New Orleans: IPET.

Irish, J. & Canizares, R., 2009. Storm-Wave Flow through Tidal Inlets and Its Influence on Bay Flooding. *Journal of Waterway, Port, Coastal and Ocean engineering,* Volume 135, pp. 52-60.

Irish, J. L., Resio, D. T. & Ratcliff, J. J., 2008. The influence of storm size on Hurricane Surge. *Journal of Physical Oceanography,* pp. 2003-2013.

Jin, C. et al., 2012. *Site Specific Wave Parameters for Texas Coastal Bridges: Final Report,* College Station: Texas A&M.

Jonkman, S. et al., 2013. Cost of Adapting Coastal Defences to Sea-Level Rise. *Journal of Coastal Research,* 29(5), pp. 1212-1226.

Jonkman, S. & Kok, M., 2008. Risk-based design of flood defence systems-a preliminary analysis for the New Orleans metropolitan area. *International Journal on Flood Defence,* pp. 1-9.

Keim, B. & Muller, R., 2007. Spatiotemporal Patterns and Return Periods of Tropical Storm and Hurricane Strikes from Texas to Maine. *Journal of Climate,* 20(3509), pp. 3498-.

Kennedy, A. et al., 2011a. Inundation and destruction on the Bolivar Peninsula during hurricane Ike. *Journal of Waterway Port Coastal and Ocean Engineering,* 127(132), pp. 132-141.

Kennedy, A. et al., 2011b. Origin of the Hurricane Ike forerunner surge. *Geophysical Research Letters,* 38(8), p. 5.

Keulegan, G., 1967. *Tidal Flow in Entrances: Water Level Fluctuations of Basins in Communication with the Seas,* Vicksburg: U.S. Army Engineers Waterways Experiment Station.

Kraus, N., 2007. *Coastal Inlets of Texas, USA.* Reston, ASCE Press.

Laing, A. & Evans, J., 2011. *Introduction to Tropical Meteorology.* 2nd ed. Boulder, CO: MetEd COMET program.

Ledden, M. v., 2013. *Personal Communication.* Rotterdam: s.n.

Lester and Gonzales, 2005. *Briefing Paper on Galveston Bay Plan Action Items Freshwater Inflow and Bay Circulation,* Houston: Houston Advanced Research Center.

Lester; Gonzales, 2002. *The State of The Bay, Galveston Bay Estuary Program,* Houston: Environmental institute of Houston.

Martin Associates, 2011. *The Local and Regional Economic Impacts of The Port of Houston,* Lancaster: Martin Associates.

Merrell, W., 2010. *Let's Build the Ike Dike.* Galveston, TX: Texas A&M Galveston.

Moretzsohn, F., Sanchez Chavez, J. & Tunnell , J., 2002. *Galveston Bay.* [Online]
Available at: http://www.gulfbase.org/bay/view.php?bi
[Accessed 05 03 2013].

Needham, H. F. & Keim, B. D., 2012. A Storm Surge Database for the U.S. Gulf Coast. *International Journal of Climatology,* 32(14), pp. 2108-2123.

Needham, H. & Keim, B., 2012. *SurgeDAT.* [Online]
Available at: http://surge.srcc.lsu.edu/data.html
[Accessed 10 04 2013].

NGDC, 2007. *National Geophysical Data Center; Galveston, TX 1/3 arc-second MHW DEM,* Galveston, TX: NOAA.

NHC, 2012. *Storm Surge Scales and Storm Surge Forecasting.* [Online]
Available at: http://www.nhc.noaa.gov/pdf/sshws_statement.pdf

NOAA HRD, 2013c. *http://www.aoml.noaa.gov/hrd/Storm_pages.* [Online]
Available at: http://www.aoml.noaa.gov/hrd/Storm_pages
[Accessed 10 4 2013].

NOAA, 2013a. *Tides and Currents.* [Online]
Available at: http://tidesandcurrents.noaa.gov/
[Accessed 1 1 2013].

NOAA, 2013b. *Storm Surge Overview.* [Online]
Available at: http://www.nhc.noaa.gov/surge/

NOAA, 2013d. *Hurricane Climatology 1980s.* [Online]
Available at: http://www.srh.noaa.gov/hgx/?n=hurricanes_climatology_1980s
[Accessed 06 05 2013].

NRC, 2005. *Re-Engineering Water Storage in the Everglades.* 1 ed. Washington, DC: The National Academic Press.

Parisi, P. & Lund, R., 2008. Return Periods of Continental U.S. Hurricanes. *American Metrological Society - Notes and Correspondence,* pp. 403-411.

Pearce, B., 1972. *Numerical calculation of the response of coastal waters to storm systems,* s.l.: University of Florida.

Perry, R., Eckels, R. & Newby, B., 2008. *Texas Rebounds,* Austin: State of Texas.

Phillips, J., 2004. *A sediment budget for Galveston Bay,* Kentucky: Department of Geography, University of Kentucky.

Pielke, R. et al., 2008. Normalized Hurricane Damage in the United States 1900 - 2005. *Natural Hazards,* Issue February, pp. 29-48.

Platzman, G. W., 1971. Ocean tides and related Waves. *Mathematical Problems in the Geophysical Sciences.,* pp. 239-291.

Poke, A., 1960. Chesapeake Bay hurricane surge. *Chesapeake Science,* pp. 178-186.

Powell, M., 2012. *Note on using H*Wind fields for storm surge and wave modeling.* [Online]
Available at: http://www.aoml.noaa.gov/hrd/data_sub/HwindOceanModel.html
[Accessed 16 5 2013].

Powell, M. et al., 2010. Reconstruction of Hurricane Katrina's wind fields for storm surge and wave hindcasting. *Ocean Engineering,* Volume 37, pp. 26-36.

Reed, C. & Sanches, A., 2010. *CIRP.* [Online]
Available at: http://cirp.usace.army.mil/wiki/Weirs
[Accessed 03 06 2013].

Rego, J. & Li, C., 2010. Storm surge propagation in Galveston Bay during Hurricane Ike. *Journal of Marine Systems,* 82(4), pp. 265-279.

Reid, R. & Bodine, B., 1968. *Numerical model for storm surges in Galveston Bay,* Galveston: Journal of Wtaterways and Harbors Division.

Resio, D., Irish, J., Westerink, J. & Powell, N., 2012. The effect of uncertainty on estimates of hurricane surge hazzards. *Natural Hazards.*

Resio, D. T., Irish, J. L. & Cialone, M., 2009. A surge response function approach to coastal hazard assesment - part 1: basic concepts. *Nat Hazards,* pp. 163-182.

Resio, D. T. & Westerink, J. J., 2008. Modeling the physics of storm surges. *Physics Today,* pp. 33-38.

Roth, D., 2010. *Texas Hurricane History,* Camp Springs: National Weather Service.

Ruijs, M., 2011. *The effects of the "Ike Dike" barriers on Galveston Bay,* Delft: TU Delft.

Schiller, A., 2010. The impact of a storm surge on business establishments in the Houston MSA. *Natural Hazards,* pp. 331-346.

Schloemer, R. W., 1954. *Analysis and synthesis of hurricane wind patterns over lake Okeechobee, Florida,* Washington, D.C: United States Weather Bureau.

Shaw, E., 1983. *Hydrology in Practice.* first ed. London: Imperial College.

Shen, J., Wang, H., Sisson, M. & Gong, W., 2006. Storm tide simulation in the Chesapeake Bay using an unstructured grid model. *Estuarine, Coastal and SHalf Science,* Issue 68, pp. 1-16.

Smith, K., 1998. *Floods: Physical Processes and Human Impacts.* 1st ed. s.l.:Wiley.

Sobey, R., Harper, B. & Mitchell, G., 1980. Numerical modelling of tropical cyclone storm surge. *Coastal Engineering,* Volume 1980, pp. 725-745.

SSPEED, 2011. *SSPEED center phase 1 report,* Houston: Severe Storm Prediction, Education and Evacuation from disasters Center .

Stoeten, K., 2012. *Applying best practices from the Dutch Delta Works and New Orleans to Galveston Bay.* Galveston: Texas A&M University.

TNRIS, 2013. *Texas Natural Resources Information System.* [Online]
Available at: http://www.tnris.org/
[Accessed 03 06 2013].

Toorn, A. v., 2013. *Personal communcation.* Delft: s.n.

TUD, 2009. *Open Channel Flow Lecture Notes.* Delft: Delft University of Technology.

TWDB, 2010. *Estuary Monitoring Program.* Houston: s.n.

USACE, 1981. *Hydraulics and stability of Five Texas Inlets,* Fort Belvoir: USACE.

USACE, 1984. *Shore protection manual,* Vicksburg: US Corps of Engineers.

USCG, 2013. *US Army.* [Online]
Available at:
http://www.army.mil/article/89077/Texas_Coastal_Study___Corps_to_partner_with_state___federal_agencies_to_protect___restore_coast/
[Accessed 03 05 2013].

USNRC, 2012. *The Estimation of Very-Low Probability Hurricane Storm Surges for Design and Licensing of Nuclear Power Plants in Coastal Areas,* Vicksburg: U.S. Army Engineer Research and Development Center.

Valle-Levinson, A., Wong, K. & Thompson-Bosley, K., 2002. Response of the lower Chesapeake Bay to forcing from Hurricane Floyd. *Continental Shelf Research,* Issue 22, pp. 1715-1729.

Vickery, P., 2005. Simple Empirical Models for Estimating the Increase in the Central Pressure of Tropical Cyclones after Landfall along the Coastline of the United States. *American Meteorological Society,* Issue 44, pp. 1807-1827.

Vickery, P., Masters, J., Powell, M. & Wadhera, D., 2009b. Hurricane hazard modeling: The past, present and future. *Journal of Wind Engineering and Industrial Aerodynamics,* pp. 392-405.

Vickery, P., Wadhera, D., Powell, M. & Chen, Y., 2009a. A Hurricane Boundary Layer and Wind Field Model for Use in Engineering Applications. *American Meteorological Society,* Volume 48, pp. 381-405.

Villemonte, J., 1947. Submerged Weir Discharge Studies. *Engineering News Record,* Issue dec 25, pp. 866-869.

Weisberg, R. & Zheng, L., 2006. Hurricane storm surge simulation for Tampa Bay. *Estuarine and Coasts,* Issue 29, pp. 899-913.

Willoughby, H. & Rahn, M., 2004. Parametric Representation of the Primary Hurricane Vortex. Part I: Observations and Evaluation of the Holland (1980) Model. *International Hurricane Research Center,* Volume 132, pp. 3033-3048.

Wu, J., 1969. Wind Stress and Surface Roughness at Sea Interface. *Journal of Geophysical Research,,* pp. 444-453.

Zdunkowski, W. & Bott, A., 2003. *Dynamics of the Atmosphere: A Course in Theoretical Meteorology.* 1st ed. s.l.:Camebridge University Press.

Glossary

BFE	Base Flood Elevation
CBA	Cost-Benefit Analysis
Coastal Spine	Delta Works type of coastal barrier
DEM	Digital Elevation Model
dFIRM	Digital Flood Insurance Rate Map
DTM	Digital Terrain Model
EAD	Expected Annual Damage
FEMA	Federal Emergency Management Agency
Fetch	Length over which a given wind blows
GIS	Geospatial Information System
GIS	Geospatial Information Systems
GMSL	Geodetic Mean Sea Level
Gradient Height	Height above the ground where surface friction has negligible influence
HAT	Highest Astronomical Tide
LAT	Lowest Astronomical Tide
Hazard	Situation that poses a threat to humans or assets
Intangible loss	Losses that are not monetizable
JPDF	Joint Probability Density Function
MEOW	Maximum Envelope of Water
MSL	Mean Sea Level
NAVD88	North American Vertical Datum of 1988
NFIP	National Flood Insurance Policy
NHC	National Hurricane Center
NOAA	National Oceanographic and Atmospheric Association
NPV	Net Present Value
PBL	Planet Boundary Layer
Risk	Probability of a hazard multiplied by its consequences
RMW	Radius to Maximum Winds
SLOSH	Sea, Lake and Overland Surges from Hurricanes
Storm Surge	Wave of water produced by approaching storm
Tangible loss	Losses that are monetizable
USACE	United States Corps of Engineers
Wind set-up	Wind-stress induced difference in still-water level between the windward and leeward sides of a water body
WSG84	World Geodetic System '84

List of Figures

List of Tables

Appendix A Map of Galveston Bay

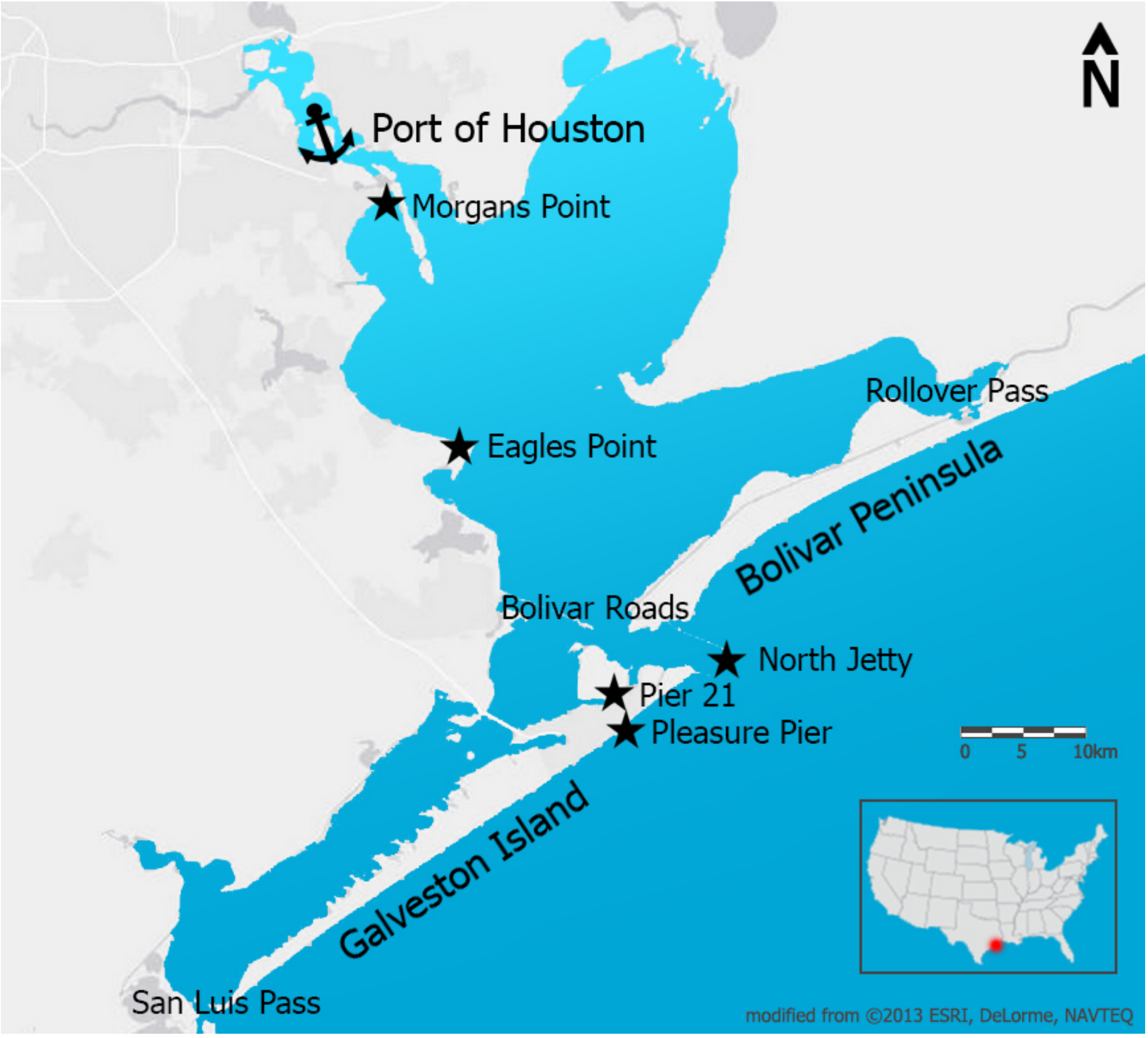

Figure A-1: Map of Galveston Bay. Modified from ESRI, DeLorme, NAVTEQ (2013).

Appendix B Hurricane Climatology

This Appendix presents the derivation of Hurricane Climatology on the Upper Texas Coast. The statistical analysis of historical storms relies on the Peak Over Threshold (POT) method. The temporal timeframe of the statistical analysis is limited to the period of 1900 and onwards because the historic description of storms prior to 1900 do not suffice for storm surge modelling (NOAA, 1987).

The optimal spatial sample size relies on the method by Chouinard et. al. (1997) as discussed in (IPET, 2009). The dataset contains storm events with a core pressure below 990hPa that made landfall within a 200-kilometers radius around Galveston. A total of 110 seasons and 28 storms are available for the statistical analysis.

Figure B-1a gives an overview of the hurricane population. Figure B-1b presents recurrence intervals for the population, following Gringorten (1963). The 1/10,000 yr^{-1} hurricane approaches the Maximum Potential Intensity of 880hPa (Emmanuel, 1987)

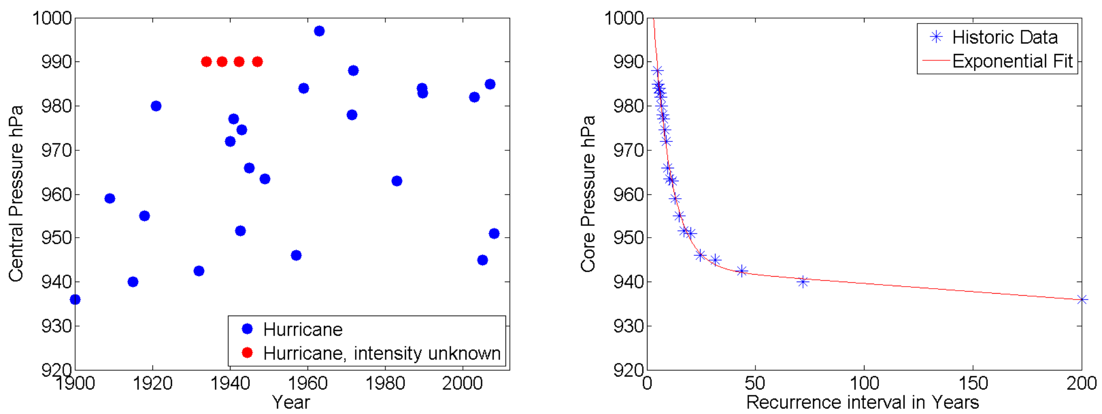

Figure B-1 – Hurricanes on the Upper Texas Coast 1900 – 2010.

Table B-1 - Return periods for landfall central pressures at 400km coastal segment

Return Period 1/yr	Central Pressure (hPa)
20	949
100	939
500	923
1,000	902
10,000	880 (MPI)

Table B-2 – List of historical storms used in statistical analysis.

Name	Year	Cat	Pressure	Vf	RMW	Direction	Wind	Source
	-	-	hPa	ms^{-1}	km	degree	kmh^{-1}	-
Ike	2008	2	951	6.7	85	325	175	a
Humberto	2007	1	985	5.5	20	25	150	a
Rita	2005	2	945	6	34	325	185	a
Claudette	2003	1	982	11.5	34	295	140	a
Jerry	1989	1	983	5.5	21	340	140	a
Chantal	1989	1	984	5.5	-	320	130	a
Bonnie	1986	1	995	5.2	-	320	140	a
Alicia	1983	3	963	4.6	48	340	185	a
Fern	1971	1	988	3.5	19	320	120	a
Edit	1971	5	978	8.7	-	50	160	a
Cindy	1963	1	997	2.1	-	340	120	a,b
Debra	1959	1	984	2.1	-	0	130	a,b
Audrey	1957	4	946	7.1	32	0	230	a,b
-	1949	4	963	5.7	37	5	215	b
-	1947	1	-	2.5	-	295	130	b
-	1945	4	966	2	33	10	220	b
"surprise"	1943	1	975	4.1	30	290	140	b
-	1942	2	952	7.2	33	320	175	b
-	1942	1		2.5	-	305	120	b
-	1941	1	977	6.7	39	0	130	b
-	1940	1	972	4.1	20	295	130	b
-	1938	2	-	7.4	-	350	120	b
-	1934	1	-	-	-	270	130	b
-	1932	4	942	7.7	22	320	230	b
-	1921	1	980	4.8	-	350	150	b
-	1918	3	955	-	-	330	195	b
Galveston	1915	4	940	5.7	54	310	215	b
-	1909	3	959	6.1	35	295	165	b
Great Galveston	1900	4	936	5.2	26	305	230	b

a) NOAA HRD (2013)

b) NOAA Technical Report NWS38 (1987)

Appendix B.1 Correlation between historical parameters

Potential sources of correlation between hurricane parameters need to be assessed before performing a Monte Carlo analysis. Table B-3 lists the correlation coefficients of storm parameters.

Table B-3 – Correlation coefficients of simulation parameters

Parameter 1	**Parameter 2**	**Correlation Coefficient**
Central Pressure	Observed Storm Surge	- 0.7
Central Pressure	RMW	- 0.35
Central Pressure	Forward Speed	+ 0.11
Forward Speed	Angle of Approach	+ 0.1

Storm Surge and Central Pressure are, as expected, negatively correlated. A storm with a lower central pressure brings a larger surge when other system parameters are assumed constant. Storm surge is a complex phenomenon that is influenced by many factors including storm intensity. The Saffir-Simpson scale solely classifies Hurricanes based on sustained wind velocity, it excludes many phenomenon's that impact storm surge does not depict storm surge potential very well.

The magnitude of the Radius to Mean Winds (RMW) and core pressure are negatively correlated (Vickery, et al., 2009b). Stronger hurricanes tend to have a smaller RMW although the correlation is weak. The RMW does not affect maximum wind velocity in the Holland B model.

The forward velocity of hurricanes does not seem to relate to the central pressure or angle of approach.

The Holland B parameter is an artificial parameter that is derived from storm parameters. The Holland B parameter tends to decrease with an increasing RMW and is not dependent on the central pressure (Vickery et al. (2009a); Powell et al. (2005)). Simulations with a single value of Holland B are sufficient in most cases (Vickery, et al., 2009b). Resio et al. (2009) found an average value of 1.27 in the Gulf of Mexico.

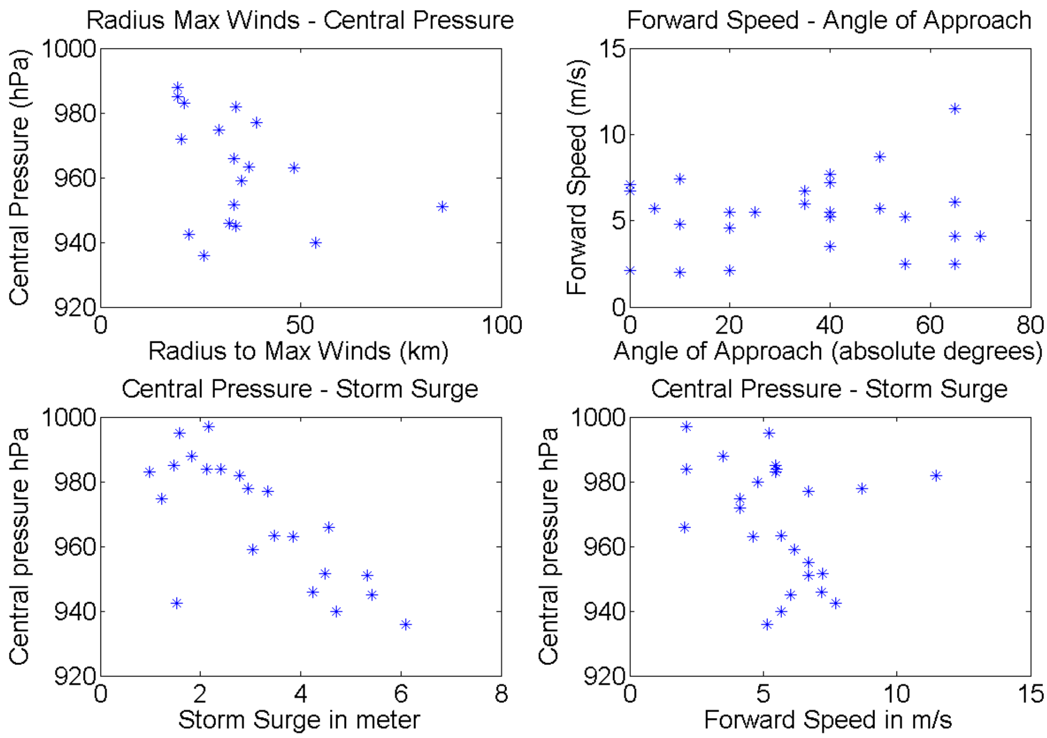

Figure B-2 - Correlation between storm parameters

Appendix B.2 Statistical analysis of historical storms

The Generalized Extreme Value theorem, or GEV, is a method to estimate the mathematical form near the tail of long-tailed distributions. The extreme value parameters of each distribution has been determined with the Maximum Likelihood function available in Matlab.

Table B-4– Hurricane distribution parameters.

Parameter	**Distribution**	**Sigma (scale)**	**Mu (location)**	**k (shape)**
Core Pressure	GEV	19.5	964	- 0.79
RMW	Lognormal	0.38	3.46	-
Forward Velocity	GEV	1.6	3.6	- 0.01
Landfall Location	Uniform	-	0	-

Hurricane intensity, or core pressure, is truncated between a region specific Maximum Potential Intensity (Emanuel, 1987) and 990 hPa, the assumed minimum intensity of a category 1 hurricane. The Radius to Maximum Winds is related to the core pressure following IPET (2009). The velocity of hurricanes that make landfall on the Upper Texas is truncated to the boundaries according to Dorst (2007). The probability of landfall location is assumed uniform along the entire Upper Texas Coast.

Table B-5 - Truncation boundaries of probability density functions.

Parameter	Distribution	Lower Limit	Upper Limit
Core Pressure	Gumbel	990 hPa	880 hPa
RMW	Gumbel	25 km	25 + 0.3(110 - Δp) km
Forward Velocity	Gumbel	2 ms^{-1}	15 ms^{-1}
Landfall Location	Uniform	- 100 km	+ 100 km

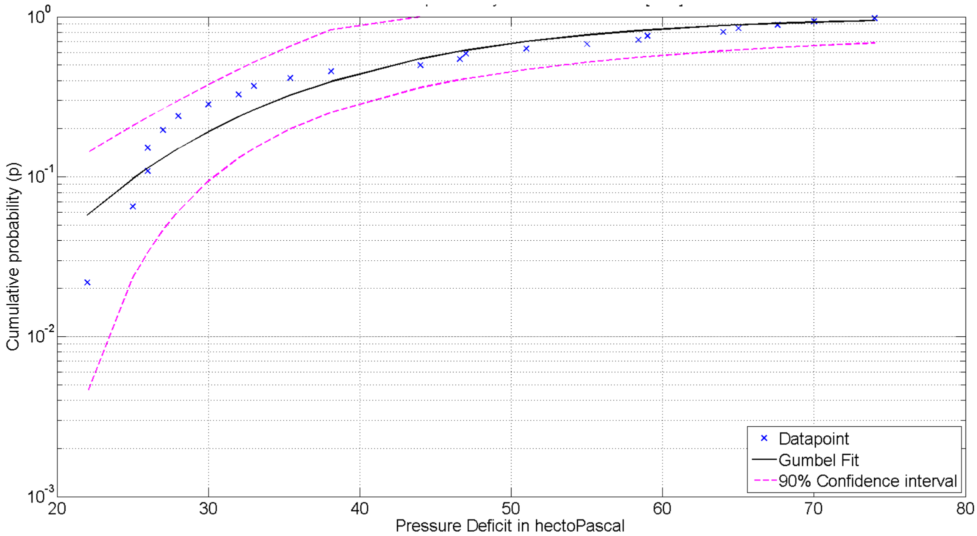

Figure B-3 - Cumulative probability of the Pressure Deficit [hPa].

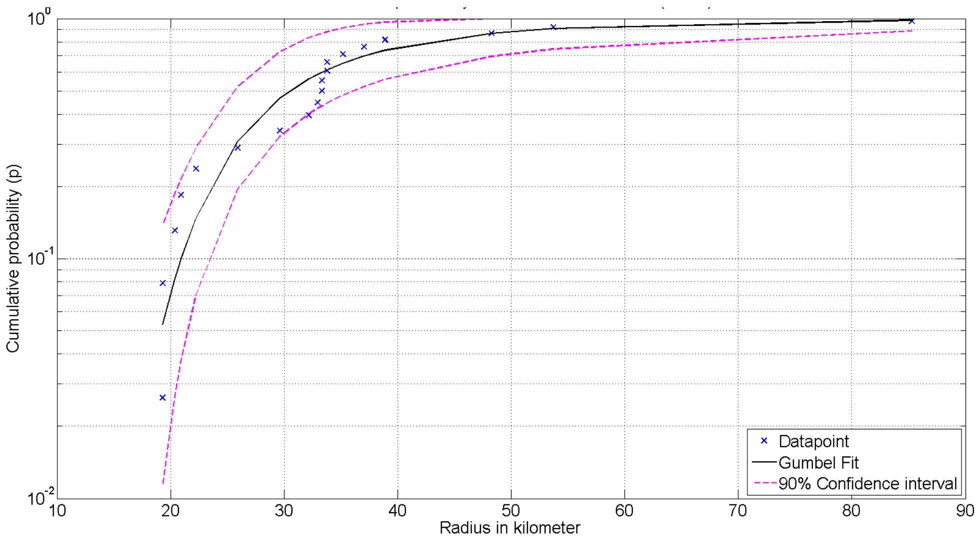

Figure B-4 - Cumulative probability of the Radius to Maximum Wind [km].

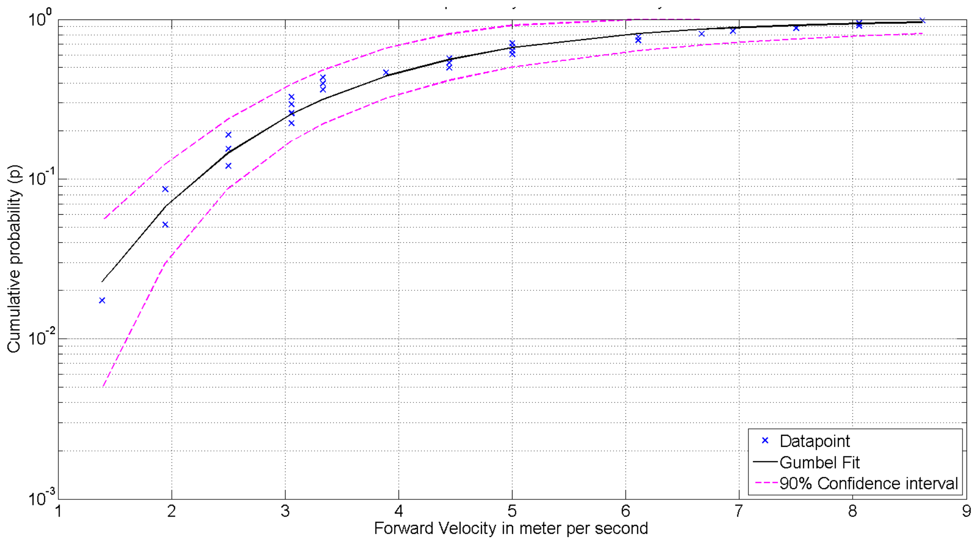

Figure B-5 - Cumulative probability of the Translation Speed [ms-1].

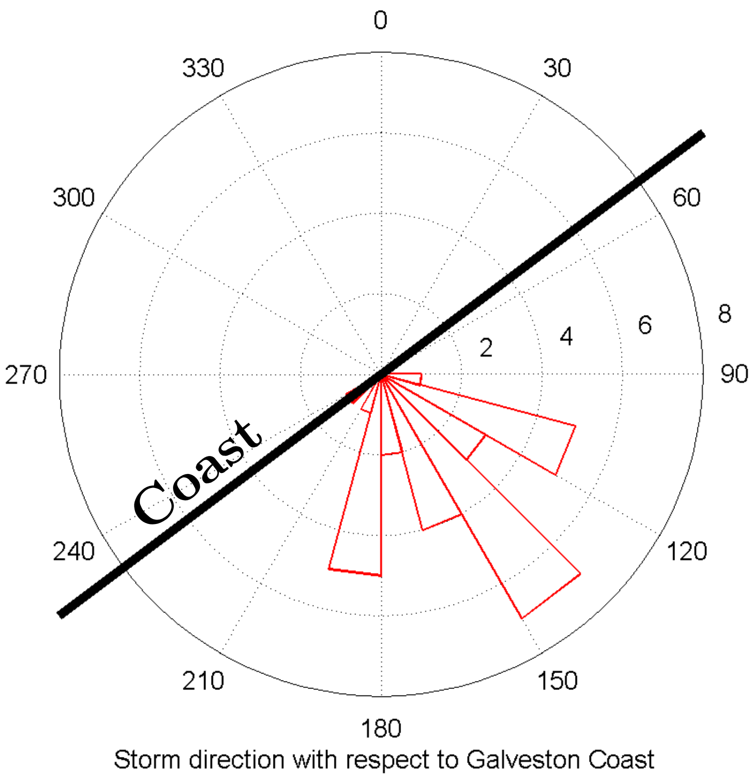

Figure B-6 - Angle of Approach of Historic Storms.

Bibliography

Chouinard, L., Liu, C. & Cooper, C., 1997. A model for the severity of hurricanes in the Gulf of Mexico. Journal of Waterways and Harbours, Volume 123, pp. 113-119.

Dorst, N., 2007. What is the average forward speed of a hurricane? [Online]
Available at: http://www.aoml.noaa.gov/hrd/tcfaq/G16.html
[Accessed 7 2 2013].

Emanuel, K., 1987. The dependence of hurricane intensity on climate. Nature, pp. 483-485.

Gringorten, I., 1963. A plotting rule for extreme probability paper. Journal of Geophysical Research, 68(3), pp. 813-814.

NOAA HRD, 2013. http://www.aoml.noaa.gov/hrd/Storm_pages. [Online]
Available at: http://www.aoml.noaa.gov/hrd/Storm_pages
[Accessed 10 4 2013].

Appendix C Data Processing

Appendix C.1 Digital Elevation Model

Digital elevation data is obtained from the National Geophysical Data Center catalog. The spatial resolution of the dataset varies between 1/3 and 1/9 arc second. The majority of the dataset is available in 1/9 arc second. The average vertical Root Mean Squared Error (RMSE) equals about 10 cm.

Appendix C.2 Bathymetry

Bathymetric data is obtained from the National Geophysical Data Center Coastal Relief Model. The spatial resolution of the bathymetric grid is 3 arc-second, about 90 meters. The vertical accuracy of each grid tile is approximately 1/10th of a meter. A one dimensional shore-normal bathymetric transect is obtained using ESRI® ArcMap® (2013) (Figure C-1). Dimensions of the inlet (Figure C-2) are obtained in a similar way.

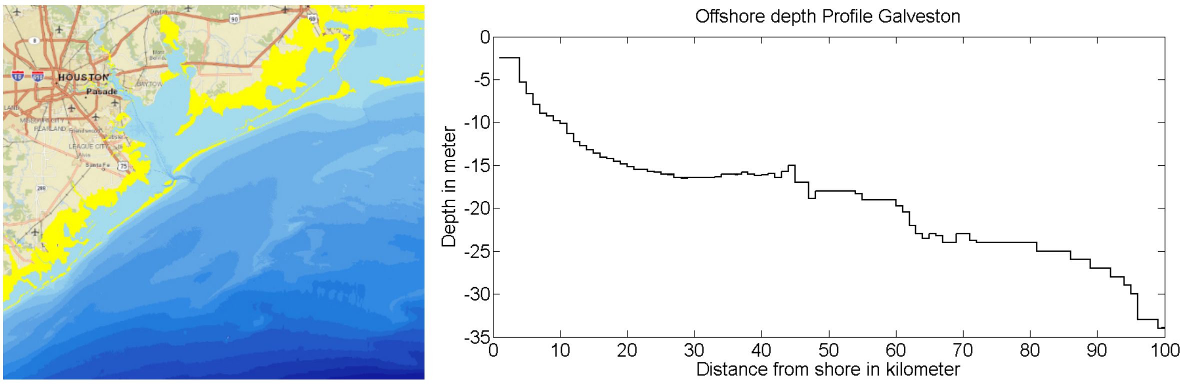

Figure C-1 – NOAA Coastal Relief Model (left) and discretized shore-normal transect (right).

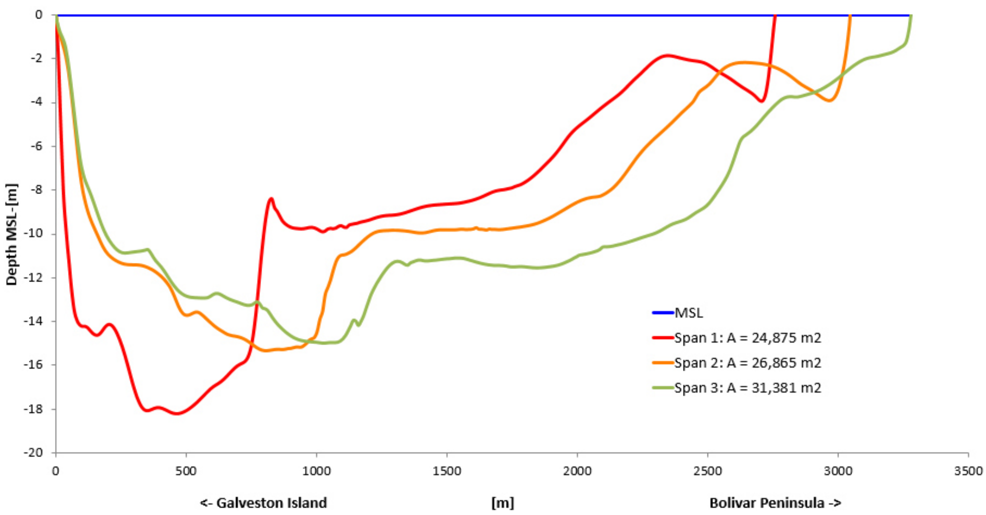

Figure C-2 –Depth transect of Bolivar Roads inlet (Vries, unpublished).

Appendix C.3 Property Value

Data on property value was obtained through the 2007-2011 American Community Survey (Census, 2010). The data were provided in TIGER/Line shapefiles that provide a geographic and cartographic representation of the US Census data on block group level.

TIGER/Line shapefiles provide the estimated number of residential properties within a certain value interval. The average value of the homes in a certain category is unknown. To prevent overestimation of flood damage the lower limit was used in the flood risk assessment.

Table C-6 – Excerpt from TIGER file.

Category	**Home Value**	**Area 7260**	**Area 7261**
DP4_HC_286	$25,000 - $50,000	16	0
DP4_HC_290	$50,000 - $100,000	74	159
DP4_HC_294	$100,000 - $150,000	77	167
DP4_HC_298	$150,000 - $200,000	100	115
DP4_HC_302	$200,000 - $300,000	194	270
DP4_HC_306	$300,000 – $500,000	38	183
DP4_HC_310	$500,000 - $1,000,000	14	149

Appendix C.4 Harmonic Constituents

Harmonic constituents at the Galveston Bay entrance are available at the NOAA tides and currents website (NOAA, 2013a). Tidal constituents with an amplitude smaller than 0.01 meter have been neglected. The tidal amplitude ζ of a single constituent at time T can be computed with;

$$\zeta = A \cdot \cos(v \cdot T - \varphi) \qquad \text{Eq. C.3.1}$$

where A [m] is the constituent amplitude, T [hour] is the time in hours, v [degrees/hour] is the propagation speed of the tidal constituent and φ [degrees] is the phase difference in degrees.

Table C-1 - Harmonic Constituents at the Galveston Bay Entrance (NOAA, 2013a).

Constituent	**Amplitude in meter**	**Phase in degrees**	**Speed in degrees/hour**
M2	0.116	282.1	28.9841
S2	0.029	297.5	30
N2	0.032	257.7	28.43973
K1	0.142	37.3	15.04107
O1	0.128	36.9	13.94304
M1	0.009	37.1	14.49669
J1	0.01	37.5	15.58544
SSA	0.086	55.6	0.082137
SA	0.066	155.7	0.041069
Q1	0.025	36.7	13.39866
P1	0.047	37.3	14.95893

Appendix C.5 Depth Damage Curves

The following depth-damage curves were used in the flood risk assessment.

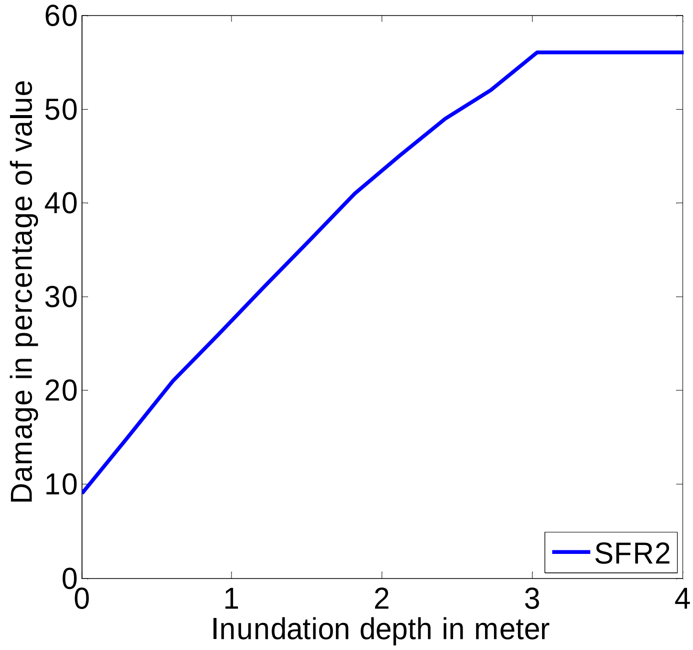

Figure C-3 – Generic depth-damage curve for residential property (FEMA, 2011).

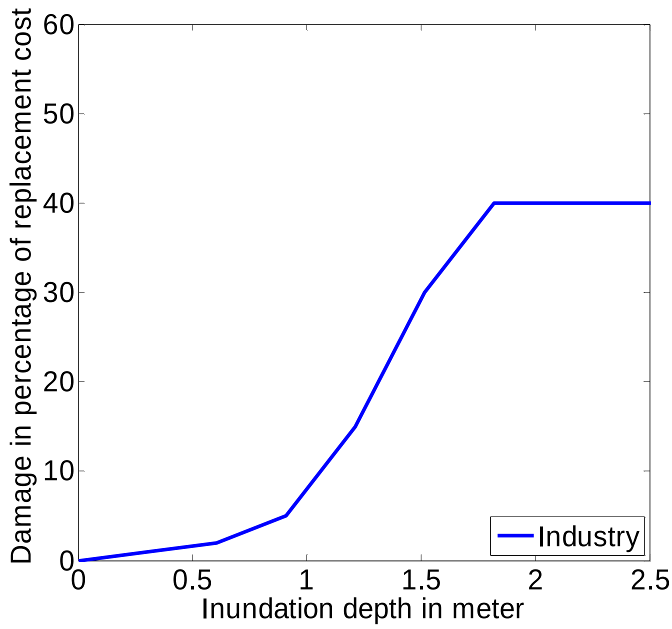

Figure C-4 – Generic depth-damage curve for industrial complexes (FEMA, 2011).

Bibliography

ESRI 2013. ArcGIS Desktop: Release 10.1. Redlands, CA: Environmental Systems Research Institute.

NGDC, 2007. *National Geophysical Data Center; Galveston, TX 1/3 arc-second MHW DEM,* Galveston: NOAA.

NOAA National Geophysical Data Center, U.S. Coastal Relief Model, 2013, http://www.ngdc.noaa.gov/mgg/coastal/crm.html

FEMA, 2011. *Hazus 2.0 Technical and User's Manuals,* Washington: FEMA.

Appendix D Storm Surge Model

Appendix D.1 Probabilistic Application

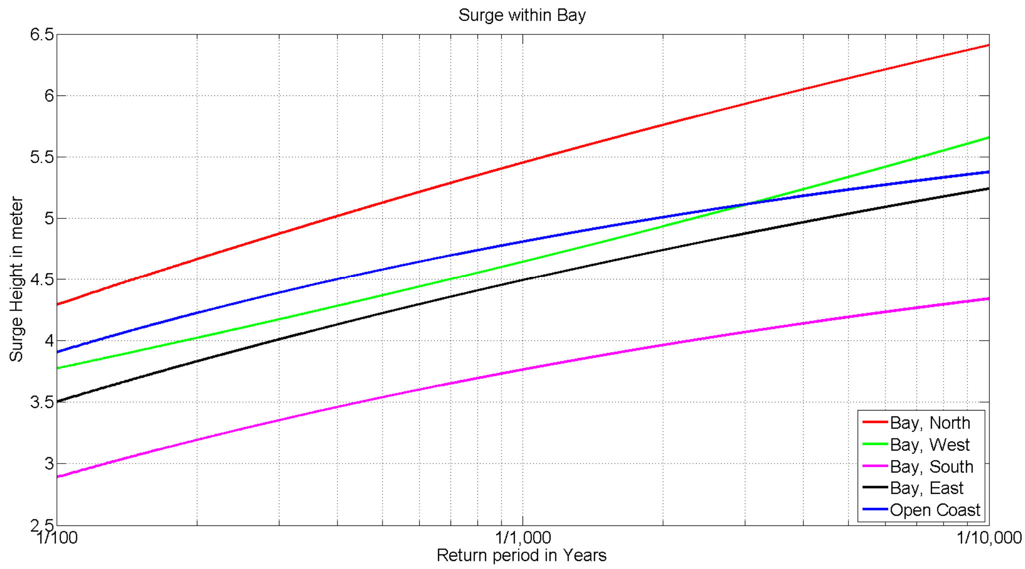

Figure D-1 – Storm Surge within simplified basin. Baseline Simulation.

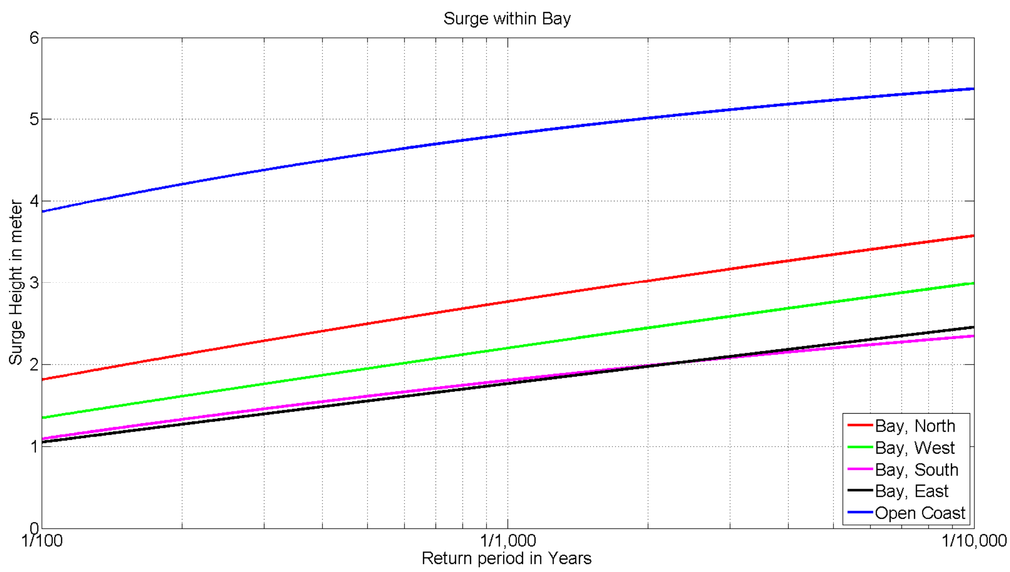

Figure D-2 – Storm Surge within Basin. Coastal Spine.

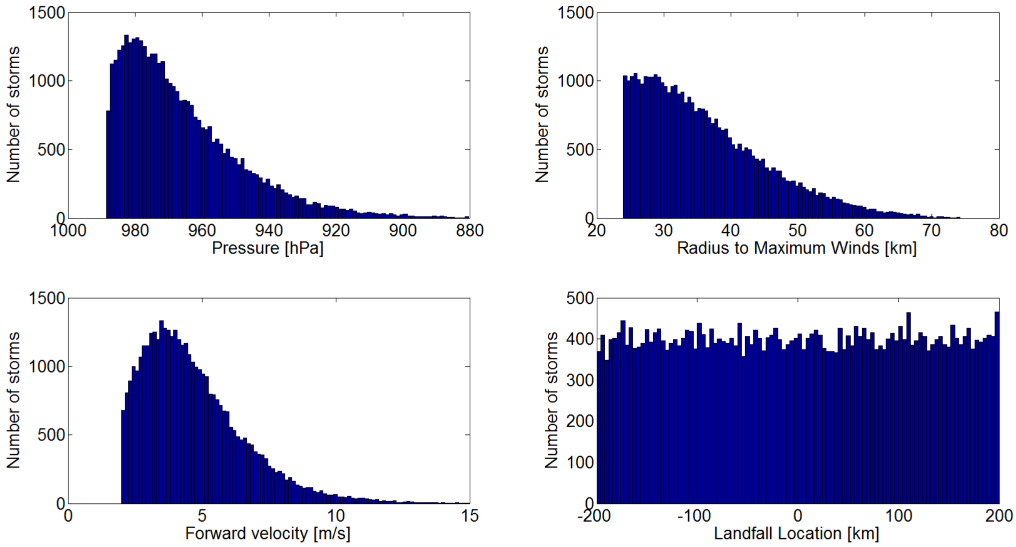

Figure D-3 – Synthetic dataset of 40,000 storms.

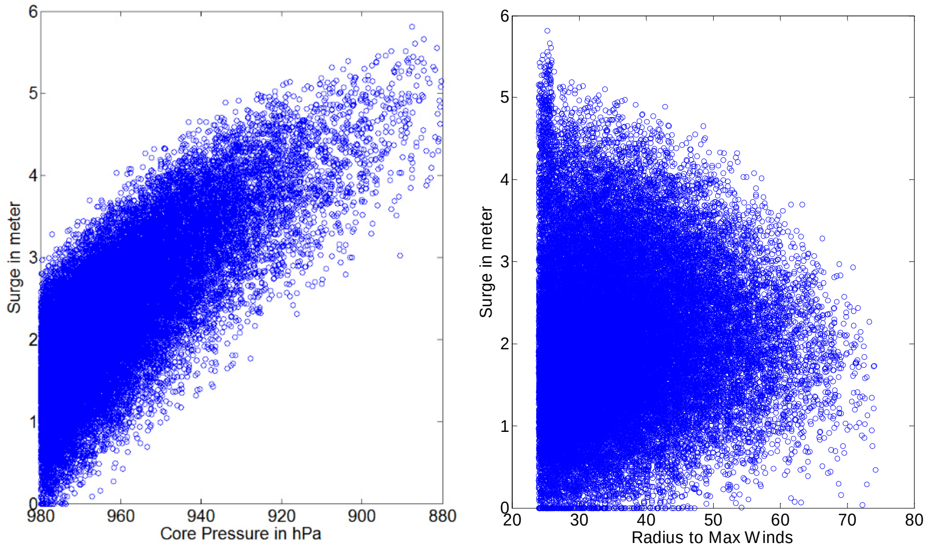

Figure D-4 – Relation between Core Pressure, Radius to Maximum Winds and Storm Surge

Appendix D.2 Model Parameters

Tabel D-1 – List of model parameters

Parameter	Value	Unit
Density air	1.15	kg/m3
Density sea water	1025	kg/m3
Gravitational acceleration	9.81	m/s^2
Latitude	0.5111	radian
HURRICANE MODEL		
Far field pressure	1015	hPa
Holland B offshore	1.27	-
Holland B overland	1.0	-
Coriolis parameter	7.14 e^{-5}	radian/second
Surface/Gradient ocean	0.73	-
Surface/Gradient land	0.68	-
Track Length	1500	km
Density air	1.15	Kg/m^3
STORM SURGE MODEL		
Cell size	150	meter
Time step	75	seconds
Pressure Set-up Coefficient	0.01	m/hPa
Wave Set-up Factor	1.1 – 1.15	-
Density water	1025	Kg/m^3
Friction Factor (Manning)	0.02	$m^{1/3}s^{-1}$
STORM SURGE BAY		
Initial depth bay	3.0	meter
Surface Area	1399	km^2
Fetch	30	kilometers
INLET		
Average Width	2800	meter
Average Depth	9.0	meter MSL
Length	10000	meter
Chezy number	40 (Manning ~0.035)	$m^{1/2}s^{-1}$
BARRIER ISLANDS		
Height	1.5	meter above MSL
Length	28000	meter

Appendix E Risk Reduction Strategies

To assess the influence of flood risk reduction strategies on flood risk within the Galvston Bay Area three flood risk reduction strategies were developed. The following Risk Reduction Strategies are assessed in the flood vulnerability analysis;

1) Protect all of Galveston Bay with a coastal spine.
2) Protect the Houston Ship Channel.
3) Upgrade of the Texas City Hurricane Protection Structure.

A strategy that protected most of Galveston Bay by local levees was included but not worked out into detail as the projected investment cost significantly exceeded the investment cost of the Coastal Spine. Figure E-1 presents the three risk reduction strategies.

Figure E-1 – Flood Risk Reduction Strategies

A first estimate indicative investment cost of barriers is obtained by;

$$C = H_l \cdot U_l \cdot L_l + U_b(L_b \cdot H_b \cdot RH_b) \qquad \text{Eq. E.1}$$

Where H_l [m] is the height of the levee, U_l [$] is the unit cost of one meter levee, L_l [m] is the length of the levee, U_b [$] is the unit cost of one meter barrier, L_b [m] is the length of the barrier, H_b [m] is the height of the barrier and RH_b [m] is the retaining height of the barrier.

The unit cost of levees and barriers are obtained by assessing the present day replacement value of existing barriers (Toorn, 2013). The estimated cost of a barrier per meter, per meter height, per meter retaining height is $U_b = \$40,000$ [$/m^3] for a navigable sector or hinge gate, and $U_b = \$25,000$ [$/m^3] for an environmental-flow gated barrier. The estimated united cost per meter levee, per meter heightening, is $U_l = \$5,000$ [$/m^2] (adopted from: Jonkman et al., 2013). The minimum levee upgrade height was set at 1 meter.

Appendix E.1 Coastal Spine

The Coastal Spine (Figure E-1) is inspired by the Ike Dike (Merrell, 2010), a proposal for a coastal barrier that protects Galveston Bay by keeping the surge at the coast. The proposal encompasses closure of the 2400-meter wide Bolivar Roads, complemented by about 80 kilometers of levees on the Bolivar Peninsula and Galveston Island. Figure E-2 presents an overview of the Bolivar Roads inlet including a cross section of the channel.

Figure E-1 – Coastal Spine.

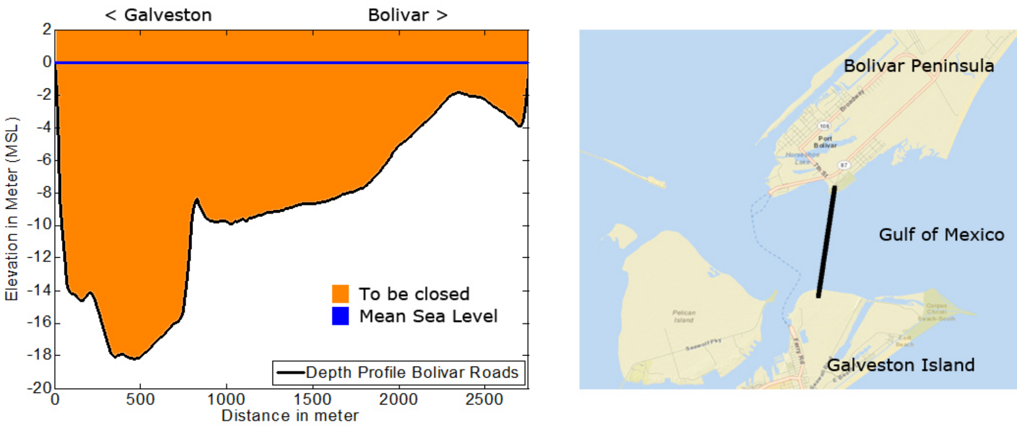

Figure E-2 –Bolivar Roads Closure.

Shipping requires a navigable span of at least 220 meter in the Bolivar Roads Barrier. Table E-1 presents the estimated dimensions of the required elements. Table E-2 presents a first estimate cost figure of a coastal spine.

Table E-1 – Coastal Spine.

Element	**Length [m]**	**Surge [m] / Average Barrier Height [m]**			
		1/100	1/1,000	1/5,000	1/10,000
Bolivar Roads Navigable Gate	220	3.9 / 17.9	4.8 / 18.8	5.2 / 19.2	5.4 / 19.4
Bolivar Roads Gate	2,000	3.9 / 10.9	4.8 / 11.8	5.2 / 12.2	5.4 / 12.4
Levees	80,000	3.9 / 2.9*	4.8 / 3.8*	5.2 / 4.2*	5.4 / 4.4*

*benefits from existing barrier island height.

Table E-2 – Estimated cost of a coastal spine as a function of the safety level.

Return Frequency [1/year]	**1/100**	**1/1,000**	**1/5,000**	**1/10,000**
Retaining Height [meter]	MSL + 3.9 m	MSL + 4.8 m	MSL + 5.2 m	MSL + 5.4 m
Estimated Cost [billion $]	3.9	5.1	5.7	6.0

Appendix E.2 Ship Channel Gate

The Ship Channel Gate is inspired by the Centennial Gate (SSPEED, 2011), a surge barrier concept proposed by the SSPEED center at Rice University. The proposal encompasses a sector or hinged gate, complemented with levees, located at the entrance of the Houston Ship Channel (Figure E-3, right).

The sole purpose of the Ship Channel Gate is to reduce the risk of flooding within the Houston Ship Channel. Figure E-3 (left) presents an overview of the proposed closure area including a cross section of the channel. The Ship Channel Gate requires a large sector gate with a span of 220 meter, approximately 8 kilometers of levees and 100 to 200 meter of common flow gates.

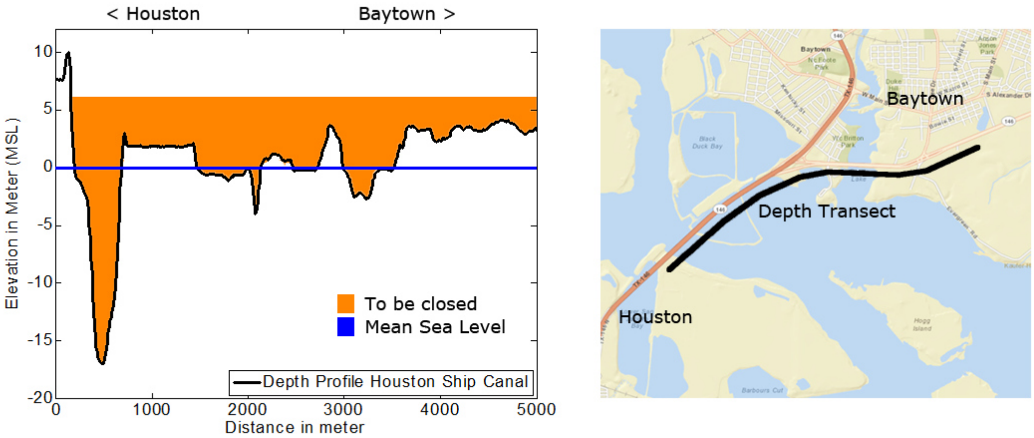

Figure E-3 – Ship Channel Gate.

Table E-3 presents the estimated dimensions of the required elements. Table E-4 presents the estimated required investment as a function of the safety level for the Ship Channel Gate.

Table E-3 – Ship channel gate.

Element	**Length [m]**	**Surge [m] / Average Barrier Height [m]**			
		1/100	1/1,000	1/5,000	1/10,000
Navigable Gate	220	4.2 / 15.2	5.5 / 16.5	6.2 / 17.2	6.5 / 17.5
Flow Gates / Goose Creek	200	4.2 / 8.2	5.5 / 9.5	6.2 / 10.2	6.5 / 10.5
Levees	8,000	4.2 / 1.7*	5.5 / 3*	6.2 / 3.7*	6.5 / 4.0*

*benefits from existing surface elevation.

Table E-4 - Estimated cost of the Ship Channel Gate as a function of the safety level.

Return Frequency [1/year]	**1/100**	**1/1,000**	**1/5,000**	**1/10,000**
Retaining Height [meter]	4.2 m	5.5 m	6.2 m	6.5 m
Estimated Cost [billion $]	1.0	1.3	1.5	1.6

Appendix E.3 Texas City Upgrade

The preliminary flood vulnerability analysis indicates that Texas City is highly susceptible to floods despite of the existing Hurricane Protection Structure (Figure E-4). The existing 1/100 yr^{-1} Texas City Protection Structure includes a small vertical lift gate and approximately 30 kilometers of levee.

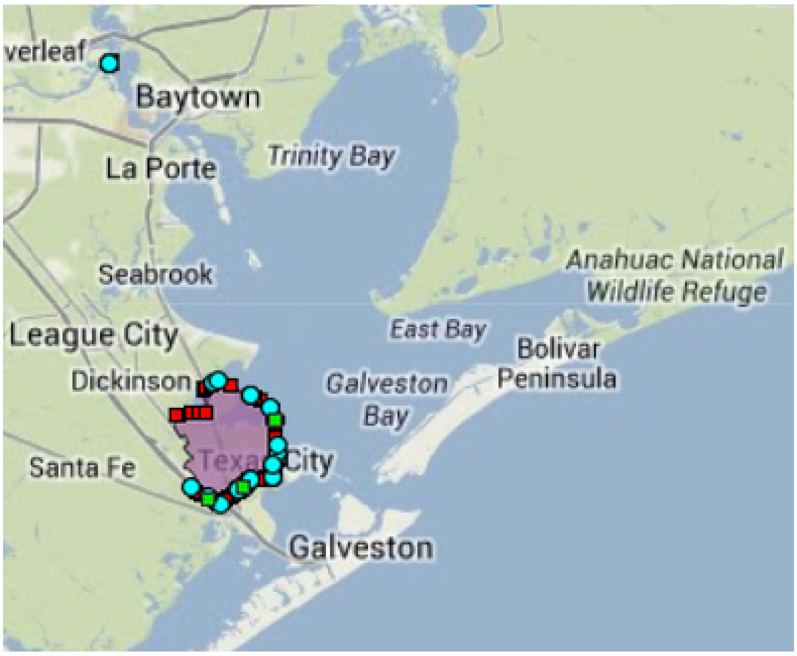

Figure E-4 – Existing Texas City Hurricane Protection Structure (USACE NLDB, 2013).

Table E-5 presents the estimated dimensions of the required elements. Table E-6 presents the estimated required investment as a function of the safety level.

Table E-5 – Texas City Levee Upgrade

Element	**Length [m]**	**Heightening [m]**			
		1/100	1/1,000	1/5,000	1/10,000
Levee Upgrade	30,000	n/a	1.1	1.8	2.2

Table E-6 – Estimated cost of the Texas City Levee Upgrade as a function of the safety level.

Return Frequency [1/year]	**1/100**	**1/1,000**	**1/5,000**	**1/10,000**
Estimated Cost [billion $]	0	0.5	0.8	1.0

References

Jonkman, S. et al., 2013. Coast of Adapting Coastal Defences to Sea-Level Rise. *Journal of Coastal Research.*

Vries, P., unpublished. *Thesis,* Delft: Delft University of Technology.

USACE, 2013. National Levee Database. [Online]
Available at: http://nld.usace.army.mil
[Accessed 03 06 2013].